

Lidar-assisted wake redirection control

A thesis accepted by the Faculty of Aerospace Engineering and Geodesy of the
University of Stuttgart in partial fulfillment of the requirements for the degree of
Doctor of Engineering Sciences (Dr.-Ing.)

by

Steffen H. Raach

born in Reutlingen, Germany

Main referee: Prof. Dr. Po Wen Cheng

Co-referee: Prof. Dr. Lucy Pao

Date of defense: 21.09.2018

Institute of Aircraft Design

University of Stuttgart

2019

Scripture quotations taken from The Holy Bible, New International Version[®] NIV[®] Copyright © 1973 1978 1984 2011 by Biblica, Inc. TM. Used by permission. All rights reserved worldwide.

If I speak in the tongues of men or of angels, but do not have love, I am only a resounding gong or a clanging cymbal. If I have the gift of prophecy and can fathom all mysteries and all knowledge, and if I have a faith that can move mountains, but do not have love, I am nothing. If I give all I possess to the poor and give over my body to hardship that I may boast, but do not have love, I gain nothing. [...]

When I was a child, I talked like a child, I thought like a child, I reasoned like a child. When I became a man, I put the ways of childhood behind me. For now we see only a reflection as in a mirror; then we shall see face to face. Now I know in part; then I shall know fully, even as I am fully known.

And now these three remain: faith, hope and love. But the greatest of these is love.

— 1 Corinthians 13 *The Bible*

Acknowledgments

Doing a PhD at Stuttgart Wind Energy (SWE) at University of Stuttgart was an incredible experience and a very good journey for me. During my oral PhD examination the representative of the faculty asked me the final question what it meant to me doing a PhD. For me, doing a PhD means finding your own challenges, it means finding your own style, and it means finding your own way. Saying this I would like to thank my colleagues at SWE for having such a fruitful environment and for having such a familial team, a special thanks to Ines, Florian, Frank, David, Sarah, Birger, Friedemann, Kolja, Matthias, Andy. Thanks to Po Wen for giving freedom in topic and research, and giving me the opportunity to develop myself. During my PhD I got the chance to meet a lot of interesting people. A special thanks goes to people at NREL, especially I want to acknowledge Paul, Andy, Jen, Lucy and Katie with their lovely families. Beside working with you, which I always enjoyed, I really appreciate your hospitality. Driving down to Boulder already felt a little bit like driving home. I got the opportunity to become work package leader in the European H2020 project CL-Windcon where I again met fantastic people, thanks to Ervin from DNV GL, Mikel and Irene from CENER, and Carlo, Johannes, and Filippo from TUM. In the second half of my PhD the cooperation with Jan-Willem and his group became of importance for me. With them I found partners who encouraged me, challenged me, and moreover supported me in my work, thanks Sjoerd, Bart, Jan-Willem. Beside that I enjoyed several trips with Jan-Willem and I assume we are still missing a solution to the “moose-elk-problem”. Thank you, Jan-Willem, for your support and your friendship.

Professional life is just one side in doing a PhD. Everybody who accompanied me is important to me and has his or her portion in my life. A special thanks to my family and close friends. They are the most important part in my life, Matthias, Matthias, die Bebel Kommune, Anne, Gerd. Having you in my life means a lot to me. I want to acknowledge my parents Hans, Evi, and my sister Anja, you are very special and role models for me. And in the end, the most important person in my life, my wife Carina. Sharing life with you is so beautiful. Since we have got to know each other I have learned so much from you and I am looking forward to continuing our wonderful journey.

Table of contents

Abstract	xi
Kurzfassung	xiii
Abbreviations	xv
List of symbols	xvii
1 Introduction	1
1.1 Motivation	3
1.2 Related work	4
1.3 Research objectives and methodology	5
2 Background	9
2.1 Wind	10
2.1.1 Wind power	11
2.1.2 Inertial and wind coordinate system	12
2.1.3 Linear reduced-order wind field models	13
2.1.4 Nonlinear reduced order wind field models	14
2.1.5 Nonlinear wind models	15
2.2 Modeling wind turbines	15
2.2.1 Aero-elastic wind turbine model	16
2.2.2 Control-oriented wind turbine model	16
2.2.3 Static wind turbine model	17
2.2.4 Wind turbine specification	17
2.3 Modeling wind turbine-flow interactions	17
2.3.1 Engineering wake models	18
2.3.2 Reduced-order computational fluid dynamics	19
2.3.3 The Large Eddy Simulation model PALM	22
2.4 Lidar systems	22
2.4.1 Technology	23
2.4.2 Lidar coordinate system	23
2.4.3 Lidar point measurement model	24
2.4.4 Lidar volume measurement model	24

2.5	Wind field reconstruction	25
2.5.1	Concept of model-based wind field reconstruction	25
2.5.2	Example of model-based wind field reconstruction	25
2.6	Wind turbine control	27
2.6.1	Baseline wind turbine controller	27
2.6.2	Yaw controller	29
2.7	Wind farm control	29
2.7.1	Objectives	30
2.7.2	Axial induction control	31
2.7.3	Wake steering	32
3	Wake steering field experiment	35
3.1	Objectives	36
3.2	Experimental setup of the field testing	36
3.2.1	General setup of field testing	37
3.2.2	Test procedure	37
3.2.3	Scanning lidar system	38
3.2.4	Considered time periods and data processing	40
3.3	Wake steering results	40
3.4	Conclusions	43
4	Concept of lidar-based closed-loop wake redirection	45
4.1	Objectives of closed-loop wake redirection	46
4.2	General concept	47
4.2.1	Estimation task	48
4.2.2	Control task	48
4.3	Challenges and conclusions	49
4.3.1	Challenges of the concept	49
4.3.2	Challenges of the estimation task	50
4.3.3	Challenges of the control task	50
4.3.4	Conclusion	50
5	Wake modeling	53
5.1	Objectives and assumptions	54
5.2	Wake deficit and wake evolution model	55
5.3	Wake deflection model	57
5.4	Wake modeling for controller design	58
5.4.1	Static wake deflection model	58
5.4.2	Dynamic wake deflection model with time delay	59
5.4.3	Linear dynamic wake deflection models	62
5.4.4	Model parametrization	62
5.4.5	Linear parameter-varying wake deflection model	67
5.5	Conclusions and recommendations	69

6	Lidar-based wake tracking	73
6.1	Objectives and assumptions	74
6.2	Classification of lidar-based wake tracking methods	75
6.3	Model-based wake tracking	76
6.3.1	Methodology	76
6.3.2	Model formulation	77
6.3.3	Model-based wake tracking algorithm	78
6.4	Results	79
6.4.1	Setup and considered measurement data	79
6.4.2	Results of model-based wake tracking	80
6.5	Conclusions and possible extensions	80
7	Wake redirection controller design	83
7.1	Objectives and assumptions	84
7.2	Internal model wake redirection control	85
7.2.1	Controller design	86
7.2.2	Controller analysis	90
7.2.3	Simulation results with a medium-fidelity CFD model	91
7.2.4	Summary and possible extensions	93
7.3	\mathcal{H}_∞ wake redirection control	94
7.3.1	Generalized plant	94
7.3.2	Controller design	95
7.3.3	Controller analysis	97
7.3.4	Simulation results using a medium-fidelity CFD model	99
7.3.5	Simulation results with the LES model PALM	101
7.3.6	Summary and possible extensions	106
7.4	Robust wake redirection control	106
7.4.1	Uncertain plant	107
7.4.2	Controller design	112
7.4.3	Controller analysis	112
7.4.4	Simulation results using a medium-fidelity CFD model	116
7.4.5	Summary and possible extensions	118
7.5	Conclusions and possible extensions	119
8	Conclusions	123
8.1	Summary	124
8.2	Future research	127
8.2.1	General concept of lidar-based closed-loop wake redirection	127
8.2.2	Estimation task	127
8.2.3	Control task	128
8.2.4	Field experiments	128
8.3	Outlook	128

Bibliography 133
Curriculum vitae 143

Abstract

Wind energy has developed to a competitive energy source and is intended to play an important role in the world-wide sustainable energy supply. The size of wind turbines has tremendously increased and turbines have been clustered to wind farms in order to share infrastructure and moreover reach energy production capacities of conventional power plants. However, the operation of wind turbines in a wind farm hasn't changed compared to single turbine operation. Possible interactions between wind turbines through the wind are not considered in the operation strategy of the turbines. The wake of a wind turbine can negatively influence the operation of a downwind turbine because the wind speed is reduced and the turbulence intensity is increased in the wake. Currently, each wind turbine is maximizing its power output independently of the other wind turbines. In a total consideration this may result in a suboptimal power output due to the interaction of wind turbines. In the case a wake impinges a second wind turbine, that turbine produces less power and the structural loads may increase. Both effects negatively impact the operation of the wind turbine and therefore it makes sense to avoid wake interactions. This task demands new wind park control concepts which take wind turbine interactions into account.

In current research activities the wind farm is treated as the total system. Different investigations in wind farm control have identified two promising operation concepts: axial induction control and wake redirection control.

Whereas the concept of induction control tries to minimize the impact of wakes on other wind turbines, the basic idea of wake redirection control is to redirect the wake of a wind turbine by yawing the wind turbine and therefore forcing a misalignment to the wind direction. Using this technique, interactions between wind turbines can be minimized. The current concept is based on an open-loop methodology in which a reduced-order wake model is used to pre-calculate the optimal yaw angles. This results in two disadvantages: The uncertainty which a simplified model introduces and the missing possibility to react to disturbances. This work introduces the concept of lidar-based closed-loop wake redirection control which can

adapt to uncertainties and react on disturbances. Therefore it extends the concept of wake redirection control with a new closed-loop methodology.

This work contributes various aspects to enable a lidar-based closed-loop wake redirection control. It first presents the general concept. Then it is separated in two subtasks: the measurement and the control tasks. This separation helps to focus on the specific questions of each task.

First the measurement task is addressed and solutions are provided to process lidar measurement data to a useful signal for the wake redirection controller. Different methodologies are presented to track the wake position using lidar measurement data and the concept of model-based wake tracking is described in detail.

Afterwards the control task is considered. Three different controller synthesis concepts are applied to wake redirection and controllers are synthesized. The different controllers are analyzed and the performances are assessed. Then the controllers are verified in different simulation tools. Mainly simulations are performed with a medium-fidelity computational fluid dynamics simulation tool. In addition the concept is implemented in a Large-Eddy simulation tool to demonstrate the adaption to disturbances and model uncertainties.

Altogether the work introduces lidar-based closed-loop wake redirection control. It demonstrates the feasibility of the concept as well as the adaptivity of the controller to model uncertainties and disturbances. The different aspects of the concept are considered and methodologies for wake position estimation are provided and controllers are designed. Finally, recommendations are given to realize the concept in reality, and open questions are highlighted which require deeper investigations.

Kurzfassung

Die Windenergie hat sich über die Jahre als konkurrenzfähige Energiequelle entwickelt und spielt in der Planung der weltweiten nachhaltigen Energieversorgung eine wichtige Rolle. Durch den Zusammenschluss von Windenergieanlagen zu Windparks mit mehreren hundert Anlagen werden Einspeisekapazitäten in der Größenordnung von konventionellen Kraftwerken erreicht. Der Betrieb einzelner Anlagen im Windpark unterscheidet sich bisher noch nicht zu dem von freistehenden Einzelanlagen. Das bedeutet, dass Interaktionen durch den Wind zwischen Windenergieanlagen nicht im Betrieb berücksichtigt werden. Eine Windenergieanlage kann durch ihren Nachlauf eine andere Anlage beeinflussen, da in ihrem Nachlauf die Windgeschwindigkeit reduziert und das Turbulenzniveau erhöht ist. In aktuellen Betriebsstrategien maximiert jede Windenergieanlage ihre Leistung. Dies kann in der Gesamtbetrachtung, falls Anlagen interagieren, zu einem suboptimalen Ergebnis führen. Im Falle einer Interaktion, wenn also der Nachlauf einer Anlage eine andere trifft, reduziert sich die Stromproduktion der Anlage und zusätzlich kann sich die strukturelle Belastung der Anlage erhöhen. Da beide Effekte negativ für den Betrieb der Anlage bzw. ihre Stromproduktion sind, ist es sinnvoll, solche Interaktionen zu verhindern. Diese Aufgabe stellt neue Herausforderungen an die Regelung von Windparks, Interaktionen einzubeziehen.

Aktuelle Methoden zur Regelung von Windparks betrachten den Windpark als Gesamtsystem. Forschungsergebnisse dazu haben zwei Betriebskonzepte als vielversprechend bewertet, Induktionsregelung und Nachlaufablenkung. Während die Induktionsregelung die Nachläufe der Anlagen aufeinander abstimmt, zielt die Nachlaufablenkung darauf ab, durch eine gewollte Schräganströmung den Nachlauf einer Windenergieanlage so abzulenken, dass Interaktionen zwischen Anlagen minimiert werden. Das bisherige Konzept bringt aber auch Nachteile und Unsicherheiten mit sich. Es basiert hauptsächlich auf den Berechnungen von reduzierten Modellen und nutzt eine Vorsteuerung um den Winkel der Schräganströmung einzustellen. Daraus ergeben sich zwei Nachteile: Die Unsicherheit die vereinfachte Modelle beinhalten und die fehlende Möglichkeit, auf Störungen zu reagieren. Diese Arbeit stellt das Konzept der Lidar-basierten geregelten Nachlaufablenkung vor, welches sich an Unsicherheiten anpasst

und Störungen kompensiert. Dadurch wird das bisherige Konzept der Nachlaufablenkung durch eine neue Methodik erweitert.

Diese Arbeit trägt mehrere Aspekte dazu bei das Konzept der Lidar-basierten geregelten Nachlaufablenkung zu realisieren. Es wird als Gesamtkonzept eingeführt und in zwei Teilbereiche aufgeteilt, einen messtechnischen und einen regelungstechnischen Bereich. Die Aufteilung in messtechnischen und regelungstechnischen Bereich erleichtert die getrennte Betrachtung der spezifischen Fragestellungen der Bereiche.

Zuerst wird die messtechnische Fragestellung betrachtet und untersucht, wie Lidar Messdaten verarbeitet werden können, um sie für die Regelung des Nachlaufs nutzbar zu machen. Verschiedene Methoden werden vorgestellt und das Konzept des modellbasierten Nachlaufverfolgens im Detail eingeführt.

Anschließend wird die regelungstechnische Fragestellung betrachtet. Drei Ansätze des Reglerentwurfs werden auf das Problem angewandt und Regler zur Nachlaufablenkung entworfen. Die Regelgüte der verschiedenen Regler wird analysiert und anschließend werden die Regler in verschiedenen Simulationsumgebungen verifiziert. Dabei werden hauptsächlich die Simulationen in einem numerischen Strömungssimulationsmodell mittlerer Komplexität durchgeführt. Zusätzlich wurde das Konzept in einer Large Eddy Simulationsumgebung umgesetzt, um die Anpassungsfähigkeit des Konzepts zu demonstrieren.

Zusammengefasst stellt diese Arbeit die Lidar-basierte geregelte Nachlaufablenkung vor. Die prinzipielle Machbarkeit des Konzepts sowie die Anpassungsfähigkeit werden gezeigt. Die unterschiedlichen Aspekte des Konzepts werden beleuchtet, es werden Methoden zur Positionsbestimmung des Nachlaufs vorgestellt und Regler entworfen. Abschließend werden Empfehlungen zur praktischen Umsetzung und offene Fragestellungen aufgeführt, die weiterführende Untersuchungen benötigen.

Abbreviations

APC	active power control
CFD	Computational Fluid Dynamics
DOE	U.S. Department of Energy
DOF	Degree Of Freedom
EAWWE	European Academy of Wind Energy
FAST	An aeroelastic computer-aided engineering (CAE) tool for horizontal axis wind turbines
FLORIS	FLOW Redirection and Induction in Steady-state
IFB	Institut für Flugzeugbau (Institute of Aircraft Design)
IMC	Internal Model Controller
IPC	Individual Pitch Control
LCOE	levelized cost of energy
LES	Large Eddy Simulation
lidar	light detection and ranging
LPV	Linear parameter-varying
NREL	National Renewable Energy Laboratory
NS	Navier Stokes equations
NWTC	National Wind Technology Center
PALM	Parallelized Large-Eddy Simulation Model
PI	Proportional-Integral
SLOW	Simplified Low Order Wind turbine
SOWFA	Simulator fOr Wind Farm Applications
SWE	Stuttgart Wind Energy
WFSim	the dynamic Wind Farm SIMulator

List of symbols

Greek letters

α_V	vertical flow angle
α_H	horizontal flow angle
β	wake model parameter for tuning the sensitivity of wake redirection
δ_V	linear vertical shear
δ_H	linear horizontal shear
δ_{yaw}	wake deflection from yaw misalignment
ϵ	wake dissipation coefficient
γ	yaw angle
Γ	Prandtl's root and tip losses function
Υ_{wind}	summary of wind field characteristics
Υ_{wake}	summary of wake characteristics
λ	tip speed ratio
λ_*	optimal tip speed ratio
$\Lambda_{\tau_{profile},n}$	Padé approximation of order n of the time delay based on the wake profile
μ	viscosity
Ω	rotor speed
ω	a frequency parameter
ω_{CL}	closed-loop bandwidth
ω_c	filter cut-off frequency
ϕ	wind direction angle at the rotor
ψ_L	rotation around z -axis by the yaw angle
ϕ_L	rotation around x -axis by the roll angle
$\Psi_{initial}$	initial wake deficit
Ψ	wake deficit
ρ	air density

θ_L	rotation around y -axis by the pitch angle
τ	delay time
τ_{Taylor}	delay time based on Taylor's hypothesis
τ_{profile}	delay time based on the wake profile
Ξ	two-dimensional Gaussian shape filter
ξ	angle of the wake with respect to the main direction
ξ_{init}	initial angle of the wake with respect to the main direction

Roman letters

A	rotor cross-section
a	axial induction
c_p	power coefficient
$c_{p,\text{max}}$	maximum power coefficient
c_T	thrust coefficient
D	rotor diameter
d	downwind distance from the rotor
f	focus distance
F_T	thrust force
G	the plant model
G_*	the uncertain plant model
G_p	dynamic transfer function of the wake deflection at setpoint p
H_p	proportional gain
H_i	integral gain
i	imaginary number
J_{rot}	inertia of the rotor
k	time step
$K(\gamma)$	yaw dependent gain
K	controller
K_Ω	feedback gain for the generator torque controller
K_p	static gain of wake deflection at setpoint p
l_y	wake lateral offset
M_{aero}	aerodynamic torque
M_g	generator torque
N_x	number of grid points in x -direction
N_y	number of grid points in y -direction

n_{pi}	number of grid points inside of the rotor
n_p	number of poles
n_z	number of zeros
p	pressure
P_{el}	electrical power
q_T	tower top position
R	rotor radius
S	sensitivity
s	a complex number frequency parameter
t	time
T_i	turbulence intensity
$T_{i,bin}$	turbulence intensity of binned data
\mathcal{T}	complementary sensitivity
U	flow velocity
u	flow component in x -direction
v	flow component in y -direction
w	flow component in z -direction
\bar{u}	mean wind speed in the u -component
u_∞	inflow wind speed
\mathcal{U}	controller sensitivity
v_0	rotor effective wind speed
v_{los}	line-of-sight wind speed
\tilde{v}	time varying crosswind perturbation
$\Delta(s)$	complex uncertainty
W	range weighting function
$W_S(s)$	performance weight on the sensitivity
$W_T(s)$	performance weight on the complementary sensitivity
$W_U(s)$	performance weight on the controller sensitivity
x	x -coordinate
x_L	x -position of the lidar
y	y -coordinate
y_L	y -position of the lidar
y_W	wake position
$y_{W,des}$	desired wake position

$y_{W,model}$	wake position predicted by the wake model
$\tilde{y}_{W,model}$	undelayed wake position predicted by the wake model
z	z -coordinate
z_L	z -position of the lidar

Subscripts

$(\cdot)_I$	inertial coordinate system
$(\cdot)_W$	wind coordinate system
$(\cdot)_L$	lidar coordinate system
$(\cdot)_\infty$	refers to inflow conditions
$(\cdot)_R$	refers to conditions at the rotor
$(\cdot)_W$	refers to conditions in the wake

Operators

$\ \cdot\ _\infty$	infinity norm
lft	linear fractional transformation
\max	maximization
\min	minimization
$(\cdot)^\dagger$	Moore-Penrose pseudoinverse
∇	differential operator

1

Introduction

*Und jedem Anfang wohnt ein Zauber inne,
der uns beschützt und der uns hilft, zu leben.*

— Hermann Hesse, *Stufen*

1.1	Motivation	3
1.2	Related work	4
1.3	Research objectives and methodology	5

Sustainable energy supply is named as one of the main goals that transforms our world in the new sustainable development agenda of the United Nations in 2015, see [1]. In their goals by 2030, the share of renewable energy in the global energy mix is aimed to be increased significantly. In past decades, wind energy has developed from a niche to a reliable technology for power production. Nowadays, wind energy is even seen to be one of the key technologies to meet future renewable energy goals. With the increasing amount of installed capacity, the responsibilities for grid services and availability gets more and more important and therefore, new challenges appear. Furthermore, the challenges in wind energy have changed from pioneering the technology to making it competitive and mature. In energy production, the minimization of the levelized cost of energy (LCOE) is the overall objective because it quantifies the profitability.

In wind energy, there have been different evolutions to minimize the LCOE, like design optimization, change in operation, or share of infrastructure. Examples for design optimizations are the increase in hub height, because of the increased mean wind speed at higher elevation, or the increase in rotor diameter, because of the bigger swept area the rotor is harvesting, see figure 1.1. An example of change in operation was the introduction of variable speed wind turbines by blade pitch control and a decoupling of the generator from the grid. The clustering of wind turbines to a wind farm enables a share of common infrastructure, such as the grid connection point with converters. Most of the evolutions have advantages but aggressive LCOE goals often generate new challenges, *e.g.*, the need for new materials for the blades, new manufacturing technologies for the tower and blades, more stable wind turbine designs, or analysis techniques to simulate multi-body systems, or the quantifying of the flow interactions in a wind farm.

While wind turbine technology has developed, the operation of wind turbines in a wind farm hasn't changed from the general concept of operating a single wind turbine. Current research in wind farm control is addressing these issues, see [3, 4, 5, 6]. Wind turbines can interact through their wakes if a wake of a wind turbine impinges a downwind turbine. The flow interactions of the wind turbines negatively impact the operation of the wind farm because in a wake the wind speed is reduced and the turbulence intensity is increased. From an operational point of view, wakes challenge the operational strategy because flow interactions often result in a decrease in power yield and an increase in structural loads of the wind turbines in a wind farm. In particular, higher structural loads increase the operational and maintenance costs which play a significant role (20 % to 25 % according to [7]) in the LCOE. At different levels, these issues have been addressed using methods such as considering flow

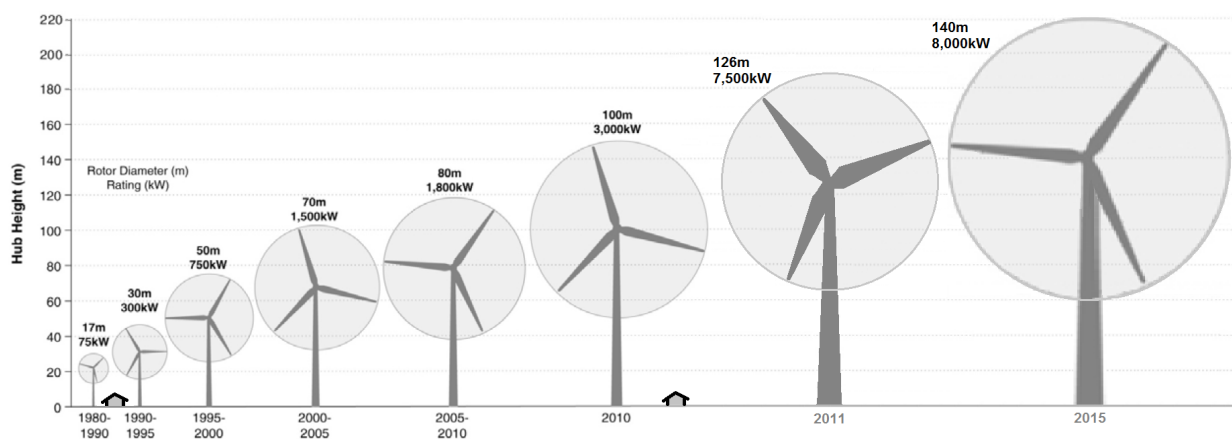


Figure 1.1: Technology development in wind energy has led to increasing wind turbine sizes from 1980 to 2015 [2].

interactions in the layout design process, or new control strategies for wind farms. However current wind farm control strategies rely on a local maximization of the produced power, the so called “locally greedy” control. The structural loads are eventually also considered locally in the turbine controller.

In current investigations, wind turbines are often included as a part of the whole control problem, and control solutions are sought for the complete wind farm. This can result in minimizing the LCOE on wind farm level but can lead to operation strategies which are sub-optimal on the turbine level.

This work contributes to the field of wind farm control by providing methodologies for lidar-based wake characterization and closed-loop wake redirection control. Both fields enable further development in realizing new wind farm control concepts that consider the complete wind farm. The specific use and applications are described detail in the following sections.

1.1 Motivation

New technologies and concepts in wind farm control treat the wind farm as a global system and aim at operating it in an optimized way. Flow interactions caused by the wakes of the wind turbines represent the main disadvantages in a wind farm: the decrease in power yield and the increase in structural loads influenced by the flow interactions.

The European Academy of Wind Energy (EAWE) has published their view on the main research questions in the next years in [3]. They emphasize specifically that new operation

strategies are needed to operate the wind turbines of a plant in an optimized way. Further, they point out the need to develop control oriented models which describe the main effects of interactions and on using those models to design wind farm controllers that fulfill overall wind farm performance measures. Another important point that the EAWE points out is the controller synthesis for wind turbines in a wind farm. For this task, new degrees of freedom to control the wind farm need to be taken into account as well as new sensing technologies.

Control-oriented wake models for wind farm control have gained importance in recent years. The main reason is that the flow interactions in the wind farm are very complex and need a high computational power to be calculated. For controller design, such a high order model complexity is not suitable. Control-oriented wake modeling deals with providing wake models which suit the need of controller design or which can be used in model-based controllers. This means that they need to represent dominant and relevant effects of the wake and furthermore, the computational complexity should be low when being applied in a model-based controller.

Future wind farm controllers will provide capabilities to manipulate the flow interactions in the wind farm. This implies that in the controller design process the interactions need to be taken into account. As already stated, while this can lead to locally suboptimal operation, the overall farm wide performance is higher.

This work contributes to those research questions by providing new methodologies for wind farm control and wake characterization, and the development and usage of control-oriented wake models in those methods.

1.2 Related work

The related research topics and work are subdivided into control-oriented wake modeling, wake measurements, and wind farm control.

The beginnings of control-oriented wake modeling originated from the first engineering wake models, [8] and [9]. They used static engineering models to describe the wake deficit and its evolution. However, because of their simplicity and model characterization, they are not suitable for controller design, and moreover, they did not consider wake redirection through yaw misalignment. In recent years, the work of [10] made a significant contribution to wake redirection as a control technique for wind farm control. Newer contributions improve or develop engineering models like [11], or approach the task with a reduced modeling of the Navier Stokes equations [12, 13].

The topic of flow measurements in wind farms has been of interest for years, however, the measurement capabilities haven't been available yet. With the introduction of remote sensing techniques like light detection and ranging (lidar), new possibilities have arisen. Although the measurement principle imposes some limitations on the direct use of the measurement data, new approaches for wind field reconstruction have been investigated, see [14, 15, 16, 17]. The achievements of these investigations motivate adapting the concept to estimate wake flow properties.

Recent activities in the field of wind farm control include optimizing the wind farm operation, see [18, 19, 20, 21], which has been the main focus for several years. In the last couple years, the focus has shifted to investigating power reference tracking and power curtailment with minimal wind turbine loading, see [22, 13, 23].

1.3 Research objectives and methodology

This work contributes to the field of wind farm control. More precisely, the usage of the remote sensing device lidar is investigated to develop a closed-loop wake redirection controller. The main research questions of this work are the following:

- First, the question is investigated of how a lidar device can be used to provide wake information for wind farm control. This includes a review of the first utility-scale wake redirection field-testing experiment at the National Renewable Energy Laboratory (NREL).
- Second, the usage of wake position information in a closed-loop controller for wake redirection control is investigated.
- And lastly, the controller design process for closed-loop wake redirection control is investigated.

For each topic, the specific questions and objectives are stated and assumptions are given. This helps to integrate the contributions into the current state of knowledge in the different fields and to highlight the character of the work. Analyses of the field-testing campaign mainly include experiences and main results, and motivates to proceed with the closed-loop concept. Whereas the concept of lidar-based closed-loop wake redirection control and the controller design are studied with a conceptual and theoretical focus, the verification of the feasibility is ultimately of interest. Especially for the conceptual and theoretical work, assumptions have been made to highlight the main points, and moreover, to demonstrate the main effects. Furthermore, economical aspects as well as some of the practical aspects have been neglected to

emphasize the goals and capabilities of the concept. Additionally, not all effects and phenomena in the flow are considered, however, it is assumed that this simplification is tolerable and that it only has a minor impact on the system. To emphasize the adaptivity of the concept, it is implemented in the Large Eddy Simulation (LES) code Parallelized Large-Eddy Simulation Model (PALM) and a demonstration case is simulated.

In summary, this thesis aims to investigate the following topics:

- First, the concept and framework of lidar-based closed-loop wake redirection control,
- Second, an approach for model-based wake tracking to estimate wake parameters,
- Third, different approaches to obtain controller design models for closed-loop wake redirection control,
- And fourth, different wake redirection controllers, including an internal model controller, a \mathcal{H}_∞ controller, and a robust \mathcal{H}_∞ controller, and their design process.

After this introduction (chapter 1), the thesis continues in chapter 2 with providing background information about relevant topics related to the thesis. First, the necessary models to describe a wind farm are presented, the description of the wind, the wind turbines, and the wake flow interactions. Then, the lidar measurement principle and the methodology of wind field reconstruction are introduced. The chapter ends with an overview on wind turbine and wind farm control. The next chapter, chapter 3, presents the utility-scale wake steering experiment at NREL and gives an overview on the main results of it. In this experiment, the feasibility of wake redirection in reality is investigated. The objectives of the experiment and the setup of the field-testing are described. Then the results are presented and discussed. They further point out the necessity of closed-loop techniques for wake redirection control. Chapter 4 introduces the concept of lidar-based closed-loop wake redirection. It starts with the definition of the objectives of closed-loop wake redirection. Afterwards, the general concept is presented and divided into two subtasks which are further specified. These subtasks are: the control task and the estimation task. Both form the framework of lidar-based closed-loop wake redirection. In the next part the necessary wake models for the realization of the closed-loop wake redirection concept are described and derived in chapter 5. First, an engineering model for the lidar-based wake tracking approach in the estimation task is derived. The necessary model parts are then adapted to the needs of the controller design process. The next chapter focuses on solutions for lidar-based estimation techniques. The general idea is to use lidar measurements in the wake to estimate the position of the wake. First, the objectives of

the task are stated, a classification of different methodologies is provided, and finally, a model-based wake tracking approach is derived and applied. This provides the basis for the controller design process because the estimation results are used as input in the controller. In chapter 7, different controller design methodologies are applied to closed-loop wake redirection. The objectives of the controller design task are stated and three different control strategies are derived, analyzed, and applied. An overall summary is given in chapter 8 which provides overall conclusions, recommendations on future research, and an outlook on how this concept can be transferred to industrial wind farm applications.

2

Background

*Allein ist der Mensch ein unvollkommenes Ding;
er muss einen zweiten finden, um glücklich zu sein.*

— Blaise Pascal

2.1	Wind	10
2.2	Modeling wind turbines	15
2.3	Modeling wind turbine-flow interactions	17
2.4	Lidar systems	22
2.5	Wind field reconstruction	25
2.6	Wind turbine control	27
2.7	Wind farm control	29

Wind energy research is a highly multi-disciplinary field. Different experts from different fields have developed the technology in the last century. In the development that has led to today's wind turbines, design and aerodynamic questions have been the main focus. Nowadays, experts from aerodynamic, structural dynamics, material science, industrial design, electrical engineering, control engineering as well as physicists are studying different aspects of wind turbines and working together on the further development of this technology.

This chapter provides necessary background and side information to the general topics of this work. It serves to assist in understanding the concept and further outlines relevant concepts which have enabled this work. In section 2.1 an introduction to wind field models is given. A summary of modeling wind turbines is given in section 2.2. The different approaches of modeling the wake of a wind turbine in a wind farm are presented and discussed in section 2.3. The different approaches are ordered with increasing model complexity. The remote sensing technology lidar is introduced in section 2.4 and its application areas are reviewed. The concept of lidar-based wind field reconstruction is then presented in section 2.5. Its main idea is to retrieve wind field information from lidar measurement data. As examples, the application of two wind field models for wind field reconstruction are described. Having described basic knowledge and measurement background information, the last sections provide background information about control in wind energy. First, in section 2.6, a baseline control-oriented wind turbine model and a baseline turbine controller as well as supporting control concepts for wind farm control are presented. Then, in the end, in section 2.7, the state-of-the-art of wind farm flow control is presented and discussed.

2.1 Wind

The main goal of a wind turbine is to convert kinetic energy of the wind flow into electrical energy. As a side effect, the wind turbine is continuously loaded by the wind. Hence, the wind is the energy source and natural power that stresses the turbine. Therefore, different applications in wind energy are dominated by either trying to maximize the electrical energy produced or minimize the structural loading on the wind turbine.

2.1.1 Wind power

The rotor of a wind turbine can be approximated by assuming the swept rotor area as a rotor disk. Then the continuity equation of fluid mechanics defines the kinetic power of the wind flow at the rotor disk area A that depends on the air density ρ and the flow velocity U as

$$P_{\text{Wind}} = \frac{1}{2} \rho A U^3. \quad (2.1)$$

As already mentioned, the basic idea of a wind turbine is to extract kinetic energy from the wind flow and to convert it to electrical energy. The extracted energy can be described in terms of the free stream energy and the remaining energy of the wake, which is the flow behind a wind turbine. The actuator disk concept describes the relation between the wind speeds by assuming a constant mass flow rate:

$$\rho A_{\infty} U_{\infty} = \rho A_{\text{R}} U_{\text{R}} = \rho A_{\text{W}} U_{\text{W}} \quad (2.2)$$

with A the cross-section-area, U the flow velocity and ρ the air density. The different indices refer to different locations, where ∞ refers to the conditions in front of the wind turbine, R refers to the conditions at the rotor, and W refers to the conditions in the wake. Following the rotor disk theory (see e.g. [24] for a detailed derivation), the relation between the wind velocity at the rotor disk and the free-stream velocity is

$$U_{\text{R}} = (1 - a) U_{\infty} \quad (2.3)$$

with the induction factor a . The velocity difference between the free-stream and the wind velocity in the wake is $U_{\infty} - U_{\text{W}}$. Having assumed conservation of mass and applying Bernoulli's equation to both sides yields the relation between the free stream velocity and the velocity in the wake (see e.g. [24])

$$U_{\text{W}} = (1 - 2a) U_{\infty}. \quad (2.4)$$

The energy extraction is limited to the Betz limit (see e.g. [24]) since the wind flow can not be fully stopped and the wind turbine can not extract all kinetic energy of the wind flow.

The extracted power at the rotor disk follows from (2.3) and the force which causes the change of momentum to $F U_{\text{R}}$. The force is caused by the drop in pressure at the disk and is calculated to

$$F = 2\rho A_{\text{R}} U_{\infty}^2 a(1 - a). \quad (2.5)$$

Then, the extracted power is

$$P = F U_R = 2\rho A_R U_\infty^3 a(1-a)^2. \quad (2.6)$$

Together with (2.1), the available wind power, the ratio between extracted power P and available P_{Wind} defines the power coefficient:

$$c_P = \frac{P}{P_{\text{Wind}}} = \frac{2\rho A_R U_\infty^3 a(1-a)^2}{\frac{1}{2}\rho U_\infty^3 A_R} = 4a(1-a)^2. \quad (2.7)$$

The maximal power extraction, the Betz limit, can be calculated from (2.7), which gives $a = \frac{1}{3}$ and $c_{P,\text{max}} = \frac{16}{27} = 0.593$. According to the power coefficient, a similar coefficient for the thrust force is defined, the thrust coefficient c_T , (see e.g. [24]):

$$c_T = 4a(1-a). \quad (2.8)$$

Then, the thrust force is expressed as

$$F_T = \frac{1}{2}\rho A_R c_T U^2. \quad (2.9)$$

In [25], an adaption of (2.8) is proposed which is later used in the two dimensional flow model, the dynamic Wind Farm SIMulator (WFSim):

$$c_T(a) = \begin{cases} 4aQ(1-a), & \text{if } 0 \leq a \leq 0.4 \\ \left(\frac{8}{9} + \frac{36Q-40}{9}a + \frac{50-36Q}{9}a^2\right) & \text{if } 0.4 < a < 1 \end{cases} \quad (2.10)$$

where Q is the Glauert correction factor which needs to be tuned.

As a next step, these aspects of wind power are put in the framework of wind farm control. The coordinate systems used in this work are described first and different wind field models are briefly recapitulated before moving to the main modeling aspects of a wind farm.

2.1.2 Inertial and wind coordinate system

Generally, the wind field can be described as a system. The wind speed at a specific point can be mathematically described by a three dimensional wind speed vector $[u, v, w]^T$ aligned with a given coordinate system. In the following, the orientation of the system with respect to a global inertial system is introduced and different modeling approaches for the wind field are

described. The complexity of the models progressively increase, starting with linear and non-linear engineering models to Computational Fluid Dynamics (CFD) models. The engineering models are briefly explained, see [26] for more details.

In the following, a wind coordinate system is introduced to describe the location and the orientation of the wind system. In this work, the wind coordinate system is denoted with W . It is used to locate and orientate the wind model in the inertial coordinate system. The inertial coordinate system is denoted with I . The wind coordinate system is aligned with the mean wind direction. The direction is expressed with the horizontal flow angle α_H and the vertical flow angle α_V . It can be assumed that the origin of the wind coordinate system is at the same point as the inertial coordinate system. Then, the transformation matrix from wind to inertial coordinate system is

$$T_{IW} = \begin{bmatrix} \cos \alpha_H & -\sin \alpha_H & 0 \\ \sin \alpha_H & \cos \alpha_H & 0 \\ 0 & 0 & 1 \end{bmatrix} \begin{bmatrix} \cos \alpha_V & 0 & \sin \alpha_V \\ 0 & 1 & 0 \\ -\sin \alpha_V & 0 & \cos \alpha_V \end{bmatrix} \quad (2.11)$$

and the transformation from inertial to wind coordinates to

$$T_{WI} = T_{IW}^{-1}. \quad (2.12)$$

Thus, the wind vector at a specific point in the wind field coordinate system is

$$\begin{bmatrix} u_i \\ v_i \\ w_i \end{bmatrix}_I = T_{WI} \begin{bmatrix} u_i \\ v_i \\ w_i \end{bmatrix}_W \quad (2.13)$$

in inertial coordinates. In this work, the coordinate center is assumed at the center of the inertial coordinate system and the flow is assumed to be vertically aligned. Thus, the vertical flow angle is assumed to be zero, $\alpha_V = 0$.

In the following, different wind field models are described starting with linear and nonlinear engineering models, to partial differential equations.

2.1.3 Linear reduced-order wind field models

The idea of linear wind field models is to describe the wind field linearly in terms of wind properties, e.g., rotor effective wind speed ν_0 , vertical shear δ_V , or horizontal shear δ_H . By

collecting them in Υ the linear wind field is written in the form

$$\begin{bmatrix} u_i \\ v_i \\ w_i \end{bmatrix}_w = A_i \Upsilon. \quad (2.14)$$

The matrix A_i depends on the location of the considered point i . For a lot of applications $v = 0$ and $w = 0$ are assumed which means the second and third rows of A_i are set to zero.

The simplest linear description is to only consider the rotor effective wind speed $\Upsilon = v_0$ which makes the A_i matrix independent of the grid:

$$\begin{bmatrix} u_i \\ v_i \\ w_i \end{bmatrix}_w = \begin{bmatrix} 1 \\ 0 \\ 0 \end{bmatrix} [v_0] \quad \forall i. \quad (2.15)$$

By further adding linear vertical and horizontal shear, $\Upsilon = [v_0, \delta_H, \delta_V]^T$, the matrix A_i depends on the grid. Thus, at point $[x_i, y_i, z_i]_w$ the wind vector yields

$$\begin{bmatrix} u_i \\ v_i \\ w_i \end{bmatrix}_w = \begin{bmatrix} 1 & y_i & z_i \\ 0 & 0 & 0 \\ 0 & 0 & 0 \end{bmatrix} \begin{bmatrix} v_0 \\ \delta_H \\ \delta_V \end{bmatrix}. \quad (2.16)$$

To remark, the assumption $v = w = 0$ is made in the wind coordinate system. Transforming a linear wind field model into the inertial coordinate system, the components can be nonzero, $v_{i,I} \neq w_{i,I} \neq 0$.

2.1.4 Nonlinear reduced order wind field models

Nonlinear wind field models can be described as follows:

$$\begin{bmatrix} u_i \\ v_i \\ w_i \end{bmatrix}_w = F(\Upsilon, x_i, y_i, z_i). \quad (2.17)$$

F is a nonlinear function which maps specific quantities (e.g., v_0 , δ_H , or δ_V) which are summarized in Υ and grid information onto the wind vector. Examples for this type of model are

the dynamic wind field introduced in [17] or [27]. Later in this work, a nonlinear wind field model is used in section 6.3 for model-based wake tracking.

2.1.5 Nonlinear wind models

In contrast to the above nonlinear wind field model, in reality the wind depends on several physical quantities. Therefore, not only wind speed information influences the behavior, but also pressure, temperature, air density, surface properties, and others. The main flow behaviour can be expressed by the Navier Stokes equations (NS) equations, see [28]. For high-fidelity wind farm simulations, LES models have become the state-of-the art. Examples of different LES models are Simulator fOr Wind Farm Applications (SOWFA) [29], SP-Wind [30], and PALM [31]. The latter is used in a case study to demonstrate closed-loop wake redirection in this work. These high-fidelity models describe the wind flow in a three-dimensional complex model where the wind farm is spatially discretized to resolve the flow. The resolution of smaller eddies is included by additional models, and these adjustments make the model more computationally feasible. Nevertheless, the computation time of LES models is very high and high performance computation clusters are needed to perform simulations.

2.2 Modeling wind turbines

Modeling a wind turbine involves different fields. A wind turbine is a coupled system of aerodynamics, structural dynamics, and servo dynamics. Furthermore, the control system describes the reaction of the wind turbine to disturbances and determines its operation. Wind turbine simulation models are widely used to assess operational information in simulation, *e.g.*, to analyze a design early in the design phase, to assess the structural loads in a life time analysis, to study specific components, or to design the control system. Therefore, depending on the application, different model fidelity is needed to describe the wind turbine. Since for this work, the wind turbine is not of primary interest, different model fidelities are highlighted and examples are given. First, aero-elastic simulation tools are shortly recapped, then a reduced order wind turbine model that is used for controller design is given, and finally a static wind turbine model is described. The wind turbine flow interactions are considered in the dedicated wind model descriptions. Finally, in section 2.2.4, the NREL 5 MW reference wind turbine is specified as that is the wind turbine model used throughout this work.

2.2.1 Aero-elastic wind turbine model

To describe a wind turbine as a dynamical system it can be formulated as a coupled and interacting model. Besides the aerodynamics, there are the structural dynamics, the servo dynamics, and the control system that influence the overall dynamics of the system. Examples of simulation tools are the open source aero-elastic simulation code An aeroelastic computer-aided engineering (CAE) tool for horizontal axis wind turbines (FAST) (see [32]) or the commercial simulation tool Bladed by DNV GL [33]. The aero-elastic simulation code is used to evaluate the structural loads and the performance of the wind turbine.

2.2.2 Control-oriented wind turbine model

A control-oriented model description of a wind turbine covers the main dynamics of the wind turbine. In the following, the Simplified Low Order Wind turbine (SLOW) model is briefly recapped that is described in detail in [26].

The main focus of the model is the orientation towards controller design and evaluation, and therefore only the main and dominant structural dynamics are considered. The rotational dynamics are described by the angular momentum equation and approximating the rotor and the rotational parts as a disk with mass and inertia J_{rot} yields

$$J_{\text{rot}}\dot{\Omega} = M_{\text{aero}} - M_{\text{g}} \quad (2.18)$$

with $\dot{\Omega}$ the rotor acceleration, M_{aero} the aerodynamic torque, and M_{g} the generator torque. The rotor dynamics equation is a linear differential equation, however, nonlinearity is introduced with the aerodynamic coupling through M_{aero} , which will be described later.

Additionally, the tower foreaft motion is modeled, since this motion directly interacts with the rotor motion through the aerodynamic thrust F_T . The tower top motion is modeled using a mass-spring-damper system with a stiffness k_T , the equivalent mass m_T (see [26]), and the damping d_T as

$$m_T\ddot{q}_T + d_T\dot{q}_T + k_Tq_T = F_T. \quad (2.19)$$

The tower dynamics also becomes nonlinear because the aerodynamics is nonlinear.

The dynamics of a wind turbine are controlled using the blade pitch angle, the yaw actuator, which describes the orientation with respect to the wind direction, and the generator torque. Both the pitch and the yaw actuator dynamics are either modeled as dynamic linear differential equations or are approximated with rate limiters.

Table 2.1: Turbine specification of the NREL 5 MW reference wind turbine.

Hub height	(m)	90
Rotor diameter	(m)	126
Rated power	(MW)	5
Rated rotor speed	(rpm)	12.1
Rated wind speed	(ms ⁻¹)	11.4

In modern wind turbines, the yaw actuator is much slower than the pitch actuator because of the large inertia of the rotor. In this work it is modeled with the maximum yaw rate limited to 1 degs⁻¹. The yaw controller which aligns the wind turbine with respect to the wind direction is later described in section 2.6.2.

2.2.3 Static wind turbine model

Depending on the application, the wind turbine can be represented as a static model without structural dynamics. For example, in flow simulations, the turbines are usually modeled using the actuator disk assumption. This yields a thrust force (2.9) that is distributed over the rotor disk and acts on the flow. In the medium-fidelity CFD simulation tool WFSim, this approach is further reduced to a two dimensional line, since the wind turbines are assumed to have infinite height. In the LES simulation tool PALM a rotating actuator disk approach is used, see [34], however, the wind turbines are modeled with structural dynamics similar to aero-elastic simulation tools, see [31].

2.2.4 Wind turbine specification

In this work, the NREL 5 MW reference wind turbine is used as it is a generic wind turbine design widely used in research. A detailed description of the turbine can be found in [35]. In table 2.1 the key specifications for this work are summarized.

2.3 Modeling wind turbine–flow interactions

As already pointed out in section 2.1.1 the wind turbine extracts energy from the wind flow. Because of the power extraction, the wind speed is changed behind the wind turbine. The effect that results from the energy extraction of a wind turbine is called a wake. It mainly depends on atmospheric conditions and on the operational condition of the wind turbine, however,

other aspects like terrain aspects also have impacts on wakes but are neglected here. After the wind turbine's energy extraction, the wake starts to interact with the undisturbed flow and is being mixed depending on the atmospheric conditions. Since the atmospheric condition and the wind turbine operation continuously change, the wake behavior is space- and time-dependent. There are different models which describe the wake dynamics, ranging from high fidelity CFD models to engineering models. The high fidelity models mostly use the Navier Stokes equations, see [28, 36, 29, 37, 38], to describe the wake in the flow. Other models use approximations like condensing the flow in a two dimensional model. Engineering models mostly focus on dedicated wake effects and combine them to an overall model representation.

In the following, a short overview on engineering models is given in section 2.3.1. The two dimensional flow model WFSim is presented, which is used as the simulation model in this work, in section 2.3.2. Finally, in section 2.3.3, a short remark on higher fidelity CFD models is given.

2.3.1 Engineering wake models

Engineering wake models describe the different wake effects and combine them to an overall wake description. The modeling is mainly driven by the application of the models, *e.g.*, layout optimization or steady state wake redirection. The main effects are the wake deficit and its decay (wake recovery), the increase of turbulence intensity, wake meandering, the wake shape and its expansion, and wake deflection. One of the main reasons why engineering models have been developed is the complexity of the flow models. The models need to be computational efficient and fast in its evaluation, however the domain and the resolution claim huge model dimensions with millions of states. Since some applications are only interested in steady state solutions or even only in single wake properties, there have been a lot of different approaches to model the different wake effects.

Samples of engineering wake models are the Jensen model [8, 9], the Frandsen model [39], the FLOW Redirection and Induction in Steady-state (FLORIS) model [18] that has extended the Jensen model with different wake zones and wake deflection, and more recently [40]. They all use different approaches for describing several wake effects and combine them to a total wake model. Furthermore, the model in [41] presents a full wind farm simulation framework with an included engineering wake model.

The models have been widely used in different investigations. An example shall highlight the importance of the model choice. Axial induction based wind farm control for power op-

timization was investigated in the past. Different model fidelities have been used to obtain the results. The studies in [19, 42, 43] used engineering wake models for optimized axial induction control. Having investigated the results using high-fidelity CFD simulation models, the results range from a high power increase to no increase, see [4, 44]. Thus, the assumptions and the model fidelity seem to be crucial for some investigations, although the Jensen type wake model FLORIS has been able to predict wake losses in some cases, see [18].

2.3.2 Reduced-order computational fluid dynamics

Instead of modeling the wake effects and combining them in an engineering model, the Navier Stokes equations can be used to describe the flow, as mentioned in section 2.1.5. In order to keep the computational effort low, only two dimensions are modeled and the wind turbines are modeled as infinitely tall wind turbines. This leads to assumptions on the flow behavior, however, the computational effort makes those models attractive for wind farm control applications.

In this work the two-dimensional Navier-Stokes model WFSim is used as the simulation model. The following section summarizes the flow model, the implementation of the turbines and the boundary conditions. A full description can be found in [12, 45].

WFSim is a two-dimensional flow model that can compute flow fields for a given wind farm topology. The model includes the momentum equation in the x - and y -directions:

$$\frac{\partial \mathbf{u}}{\partial t} + (\mathbf{u} \cdot \nabla) \mathbf{u} + \frac{1}{\rho} \nabla p - \frac{\mu}{\rho} \nabla^2 \mathbf{u} = \mathbf{f}, \quad (2.20)$$

as well as the continuity equation in x - and y -directions:

$$\mathbf{u} \cdot \nabla = 0, \quad (2.21)$$

with the vector differential operator ∇ defined as

$$\nabla = \left[\frac{\partial}{\partial x} \quad \frac{\partial}{\partial y} \right]^T \quad (2.22)$$

and

$$\nabla^2 = \frac{\partial^2}{\partial x^2} + \frac{\partial^2}{\partial y^2}. \quad (2.23)$$

The term \mathbf{f} represents the turbines while $\mathbf{u} = [u \ v]^T$ and \mathbf{p} represent the flow velocities and pressure, respectively. The air density ρ and the viscosity μ are considered to be constant. Under the boundary conditions and the forcing terms defined later, no analytic solution of the equations exists yet. Hence, the governing equations are resolved numerically using a spatial and temporal discretization scheme. In WFSim, the state variables u_k , v_k and p_k at time step k are defined as:

$$\mathbf{u}_k = \begin{bmatrix} u_{3,2} \\ \vdots \\ u_{3,N_y-1} \\ u_{4,2} \\ \vdots \\ u_{4,N_y-1} \\ \vdots \\ u_{N_x-1,2} \\ \vdots \\ u_{N_x-1,N_y-1} \end{bmatrix}, \quad \mathbf{v}_k = \begin{bmatrix} v_{2,3} \\ \vdots \\ v_{2,N_y-1} \\ v_{3,3} \\ \vdots \\ v_{3,N_y-1} \\ \vdots \\ v_{N_x-1,3} \\ \vdots \\ v_{N_x-1,N_y-1} \end{bmatrix}, \quad \mathbf{p}_k = \begin{bmatrix} p_{2,2} \\ \vdots \\ p_{2,N_y-1} \\ p_{3,2} \\ \vdots \\ p_{3,N_y-1} \\ \vdots \\ p_{N_x-1,2} \\ \vdots \\ p_{N_x-1,N_y-1} \end{bmatrix}. \quad (2.24)$$

The constants N_x and N_y are the number of grid points in the x - and y -direction, respectively. The finite volume and an implicit method are applied resulting in the following set of nonlinear algebraic difference equations:

$$\underbrace{\begin{bmatrix} A_x(\mathbf{u}_k, \mathbf{v}_k) & \mathbf{0} & B_1 \\ \mathbf{0} & A_y(\mathbf{u}_k, \mathbf{v}_k) & B_2 \\ B_1^T & B_2^T & \mathbf{0} \end{bmatrix}}_{A(x_k) \in \mathbb{R}^{m \times m}} \underbrace{\begin{bmatrix} \mathbf{u}_{k+1} \\ \mathbf{v}_{k+1} \\ \mathbf{p}_{k+1} \end{bmatrix}}_{x_{k+1}} = \underbrace{\begin{bmatrix} b_1(\mathbf{u}_k, \mathbf{v}_k) + S_k^x(\mathbf{u}_k, \mathbf{v}_k) \\ b_2(\mathbf{u}_k, \mathbf{v}_k) + S_k^y(\mathbf{u}_k, \mathbf{v}_k) \\ b_3 \end{bmatrix}}_{b(x_k) \in \mathbb{R}^{m \times 1}}, \quad (2.25)$$

with $m = n_u + n_v + n_p$ and $\mathbf{u}_k \in \mathbb{R}^{n_u}$, $\mathbf{v}_k \in \mathbb{R}^{n_v}$, $\mathbf{p}_k \in \mathbb{R}^{n_p}$ the velocity vectors in the x -direction, y -direction and the pressure vector at time k , respectively. Each component of \mathbf{u}_k , \mathbf{v}_k , and \mathbf{p}_k represents at time k a velocity and pressure at a grid point in the field defined by its subscript. The computational cost for solving this set of equations is kept low by exploiting sparsity and by applying the reverse Cuthill-McKee algorithm. The terms $b_1(\mathbf{u}_k, \mathbf{v}_k)$, $b_2(\mathbf{u}_k, \mathbf{v}_k)$ and b_3 represent the boundary conditions and the terms $S_k^x(\mathbf{u}_k, \mathbf{v}_k)$ and $S_k^y(\mathbf{u}_k, \mathbf{v}_k)$ the turbines.

Boundary conditions

For the u and v velocities, first order conditions are prescribed on one side of the grid related to the ambient inflow defined by u_b and v_b . Zero stress boundary conditions are imposed on the other boundaries. For the initial conditions, all u and v velocity components in the field are defined as u_b and v_b respectively, the boundary velocity components. The initial pressure field is set to zero. Furthermore, the inflow velocity can be changed to realize variable inflow conditions.

Turbine modeling

According to momentum theory (see [28]), the following force term is defined:

$$F_T = c_T(a) \frac{1}{2} \rho A U_\infty^2, \quad (2.26)$$

with thrust coefficient $c_T(a)$ depending on the axial induction factor a . U_∞ is the rotor upwind velocity and A is the rotor swept area. The Glauert correction factor Q is set to 1.75, see (2.10). Since U_∞ is difficult to measure in a wind farm, it is helpful to write the force in terms of the flow velocity at the rotor. The following relations are defined:

$$\beta = \frac{a}{1-a}, \quad U_\infty = \frac{U_R \cos(\gamma - \phi)}{1-a}, \quad U_R = \sqrt{u_r^2 + v_r^2}, \quad (2.27)$$

with U_R the flow velocity vector at the rotor with direction defined by the wind direction angle ϕ and the yaw angle γ of the turbine (figure. 2.1). Substituting these relations in (2.26) yields the force expression F_T :

$$F_T = \frac{1}{2} \rho A c_T(\beta) [U_R \cos(\gamma - \phi)(\beta + 1)]^2. \quad (2.28)$$

The forces in the x - and y -directions are now defined as:

$$S_k^x(u_k, v_k) = -F_T \cos(\gamma), \quad S_k^y(u_k, v_k) = F_T \sin(\gamma). \quad (2.29)$$

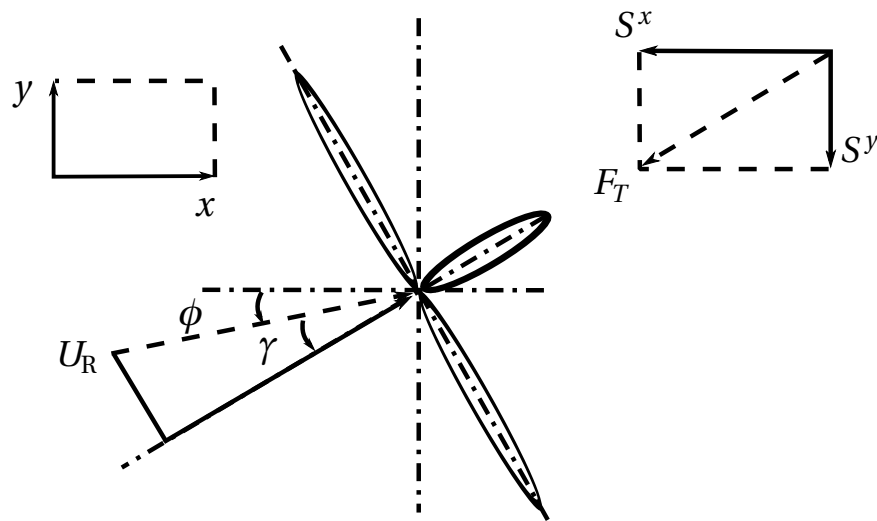


Figure 2.1: Schematic representation of a turbine with yaw angle γ , wind direction angle at the rotor ϕ and flow velocity U_R at the rotor. Figure taken and adapted from [46].

2.3.3 The Large Eddy Simulation model PALM

The LES model PALM is later used in a case study to realize closed-loop wake redirection in a high-fidelity CFD simulation model. PALM can be used to simulate wind turbines in a three-dimensional flow model using LES based on the filtered, incompressible Navier Stokes equations. The wind turbines are represented by the rotating actuator disk model (ADM-R) [34]. The PALM model calculates the flow velocities in the x - y - and z -directions (u , v , w) on a staggered grid. In the case study, non-cyclic boundary conditions are imposed and time-dependent turbulent inflow data is generated by using a turbulence recycling method. More information on PALM can be found in [31].

2.4 Lidar systems

Lidar is a remote sensing technology that is used to measure wind speed. A laser is used to estimate wind speed remotely. The system has opened new possibilities in measuring wind speed without using a meteorological tower. Additionally, new applications like lidar-assisted control or forecasting have been enabled through the usage of lidar systems.

There are different types of lidar systems. Most commercial and available devices are specialized for a specific usage like site assessment and wind profiling, or long range scanning at different elevation angles.

2.4.1 Technology

Lidar uses a laser source and the backscattered light to estimate the wind speed. Nowadays two concepts have been commercially established: a pulsed and a continuous measurement principle. The advantage of a continuous lidar system is the high measurement frequency. The advantage of the pulsed system is the ability to measure wind speed information along the laser beam at several distances simultaneously.

Both concepts use the Doppler principle between the emitted laser light and the one backscattered from aerosols in the air. The Doppler principle gives a relationship between frequency shift and velocity, see [47, 48, 49, 50]. For wind speed measurements, it is assumed that aerosols are moving with the wind flow. Because of using the laser only the projection of the wind flow on the laser is measured, the line-of-sight wind speed, v_{los} .

In the following sections, the measurement principle is assessed in detail and the resulting limitations are discussed.

2.4.2 Lidar coordinate system

To enable a simplified description of the laser beam and the measurement at a certain position, a lidar coordinate system is introduced. According to [26], the origin of the lidar coordinate system is located at the origin of the laser beam; that means the lidar system is located at a specific position $[x_L, y_L, z_L]_{\text{I}}$ in the inertial coordinate system with a defined orientation. Related to the wind coordinate system, there is also a transformation from the lidar to the inertial coordinate system. All six Degrees of Freedom (DOFs) are considered: the three translational DOFs and the three rotational DOFs. The rotation is performed as follows: first, rotation around the z -axis by the yaw angle ψ_L , second, around the rotated y -axis by the pitch angle θ_L and finally around the rotated x -axis by the roll angle ϕ_L . This yields the rotational transformation

$$T_{\text{IL}} = \begin{bmatrix} \cos \psi_L & -\sin \psi_L & 0 \\ \sin \psi_L & \cos \psi_L & 0 \\ 0 & 0 & 1 \end{bmatrix} \begin{bmatrix} \cos \theta_L & 0 & \sin \theta_L \\ 0 & 1 & 0 \\ -\sin \theta_L & 0 & \cos \theta_L \end{bmatrix} \begin{bmatrix} 1 & 0 & 0 \\ 0 & \cos \phi_L & -\sin \phi_L \\ 0 & \sin \phi_L & \cos \phi_L \end{bmatrix}. \quad (2.30)$$

Thus, the transformation from lidar coordinate system to the inertial coordinate system is

$$\begin{bmatrix} x \\ y \\ z \end{bmatrix}_I = T_{IL} \begin{bmatrix} x \\ y \\ z \end{bmatrix}_L + \begin{bmatrix} x_L \\ y_L \\ z_L \end{bmatrix}_I. \quad (2.31)$$

2.4.3 Lidar point measurement model

The measurement of a lidar can be idealized as a point measurement. Thus, the line-of-sight wind speed measured at a point $[x, y, z]_{i,I}$ with focus distance

$$f_i = \sqrt{x_{i,I}^2 + y_{i,I}^2 + z_{i,I}^2} \quad (2.32)$$

is

$$v_{\text{los}} = \frac{1}{f_i} \left(x_{i,I} u_{i,I} + y_{i,I} v_{i,I} + z_{i,I} w_{i,I} \right), \quad (2.33)$$

with $[u, v, w]_{i,I}$ the wind vector at the measurement point. This assumption is very practical since it gives a linear relation between the wind vector components and the measurement value. Therefore, it is widely used in processing the measurement data and retrieving wind field information as presented in section 2.5.

2.4.4 Lidar volume measurement model

Real lidar systems can not measure at a dedicated point in space as the idealized measurement equation (2.33) imposes, however, they measure in a certain volume around the measurement position along the laser beam. This yields the volume measurement equation of a lidar:

$$v_{\text{los}} = \frac{1}{f_i} \int_{-\infty}^{\infty} (x_{a,i,I} u_{a,I} + y_{a,i,I} v_{a,I} + z_{a,i,I} w_{a,I}) W(a) da \quad (2.34)$$

at point $[x, y, z]_{i,I}$ in the inertial coordinate system I with the range weighting function $W(a)$, that depends on the lidar system, see [26]. The wind vector used in (2.34) is evaluated at

$$\begin{bmatrix} x_{a,i,I} \\ y_{a,i,I} \\ z_{a,i,I} \end{bmatrix} = \begin{bmatrix} x_{i,I} \\ y_{i,I} \\ z_{i,I} \end{bmatrix} + a \begin{bmatrix} x_{n,i,I} \\ y_{n,i,I} \\ z_{n,i,I} \end{bmatrix} \quad (2.35)$$

according to [26].

2.5 Wind field reconstruction

The lidar technology has opened new possibilities of getting insight in the wind flow. A lidar system can measure at different positions in space and provides v_{los} measurements. The measurement principle of the system, described in section 2.4.4, imposes limitations in assessing the flow since it is not possible to determine all three wind components at a point with one lidar system. By introducing assumptions on the flow and the measurement principle, however, the problem can be simplified and flow quantities can be assessed.

For all applications, where lidar measurements are used, two main points are important, 1) the measurement setup and 2) the quantities of interest. They determine the assumptions which have to be made to further use the lidar measurement data. [26, 14, 51], and others, have pointed out possible assumptions, like homogeneous flow, inflow angle, linearity in shear, or the validity of Taylor's Frozen Turbulence. These assumptions expressed in the wind field models enable to either directly calculate or estimate the wind field model.

In the following, an example of wind field reconstruction is given. A model-based reconstruction of the wind speed and linear wind shear is explained. The background information and a detailed description of the method can be found in [26].

2.5.1 Concept of model-based wind field reconstruction

Model-based wind field reconstruction is a model fitting technique for the measurement data. It uses a model of the lidar and a reduced order wind field model, which includes the assumption on the wind field, to fit them to the measured line-of-sight velocities measured with the lidar system. Figure 2.2 shows the general concept of model-based wind field reconstruction.

2.5.2 Example of model-based wind field reconstruction

As indicated in the introduction, assumptions on the wind field and the measurement data are necessary to reconstruct wind field characteristics from lidar measurement data. The model-based wind field reconstruction methodology uses assumptions on the wind field and the point measurement lidar model to reconstruct wind field characteristics.

In this example, the rotor effective wind speed v_0 and the linear vertical shear δ_V is reconstructed from lidar measurements.

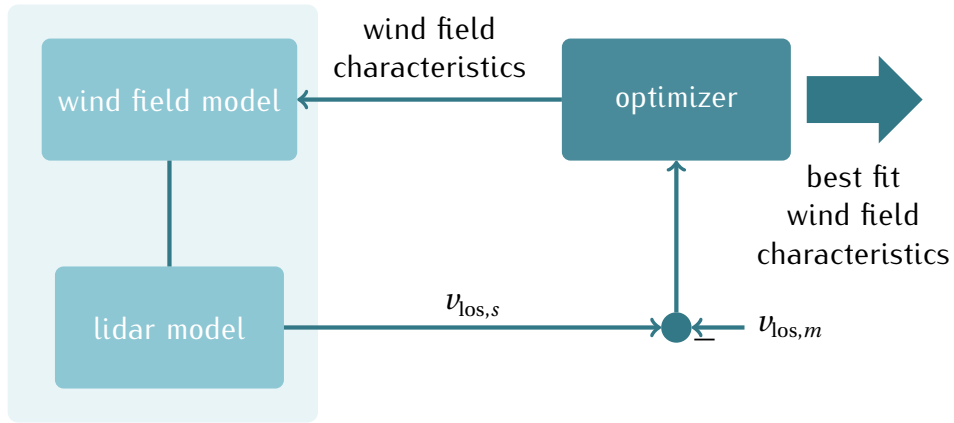


Figure 2.2: The general concept of model-based wind field reconstruction.

The wind field model is described in the wind coordinate system W introduced in section 2.1.2. Since the flow components $[u, v, w]_W^T$ depend linearly on the wind characteristics v_0 and δ_V , a wind field formulation as presented in (2.16), neglecting the horizontal shear component, is chosen. Thus, the linear wind field model is

$$\begin{bmatrix} u_i \\ v_i \\ w_i \end{bmatrix}_W = A_i \Upsilon = \begin{bmatrix} 1 & z_{i,W} \\ 0 & 0 \\ 0 & 0 \end{bmatrix} \begin{bmatrix} v_0 \\ \delta_V \end{bmatrix} \quad (2.36)$$

where $z_{i,W}$ is the z coordinate of point i in the wind coordinate system. Together with the lidar point measurement model description of (2.33), the system description is completed. Hence, a lidar measurement at point $[x_i, y_i, z_i]^T$ can be written as

$$v_{\text{los},i} = \frac{x_i}{f_i} (v_0 + z_i \delta_V). \quad (2.37)$$

Reconstructing wind field characteristics from lidar line-of-sight measurement data, v_{los} , results in the inversion of the system. Because of the two wind field characteristics v_0 and δ_V , at least two independent measurements are necessary to perform the reconstruction. Thus, with two measurements $v_{\text{los},1}$ and $v_{\text{los},2}$ at two independent points $[x_1, y_1, z_1]^T$ and $[x_2, y_2, z_2]^T$, the wind field reconstruction is

$$\begin{bmatrix} v_0 \\ \delta_V \end{bmatrix} = M^{-1} \begin{bmatrix} v_{\text{los},1} \\ v_{\text{los},2} \end{bmatrix} \quad (2.38)$$

with

$$M = \begin{bmatrix} \frac{x_1}{f_1} & \frac{x_1 z_1}{f_1} \\ \frac{x_2}{f_2} & \frac{x_2 z_2}{f_2} \end{bmatrix}. \quad (2.39)$$

In general M is a $m \times x$ matrix with m the number of independent measurements and n the number of wind field characteristics. When the number of wind field characteristics and the number of independent measurements are equal, $m = n$, a unique solution exists.

However, in case of more measurements than unknown wind field characteristics, $m > n$, no unique solution exists. A least squares solution can be calculated by using the Moore-Penrose pseudoinverse M^\dagger .

2.6 Wind turbine control

A wind turbine converts wind power into electrical energy. The wind turbine controller maintains the wind turbine to operate in its desired way. In wind turbine control, a trade-off between maximizing the power output and minimizing the structural loads of the wind turbine has to be made. These two goals also define the different operation regions of a wind turbine which are partial load and full load operation. In partial load operation, the main goal is maximizing power since the wind speed has not reached its nominal value; in full load operation, mitigating structural loads while keeping constant rotor speed is the main control goal. The wind turbine produces its nominal power output in full load operation. An overview of the different control regions is given in Figure 2.3.

In the following, the control inputs of a wind turbine are described and a baseline controller is presented in section 2.6.1.

2.6.1 Baseline wind turbine controller

This section presents briefly a standard controller for wind turbines consisting of a partial load controller and a full load controller.

Partial load control

As mentioned before, in partial load operation maximizing the power output is the main control goal. This is achieved by maintaining the optimal tip speed ratio λ_* . The tip-speed-ratio is defined as

$$\lambda = \frac{\Omega R}{v_0}, \quad (2.40)$$

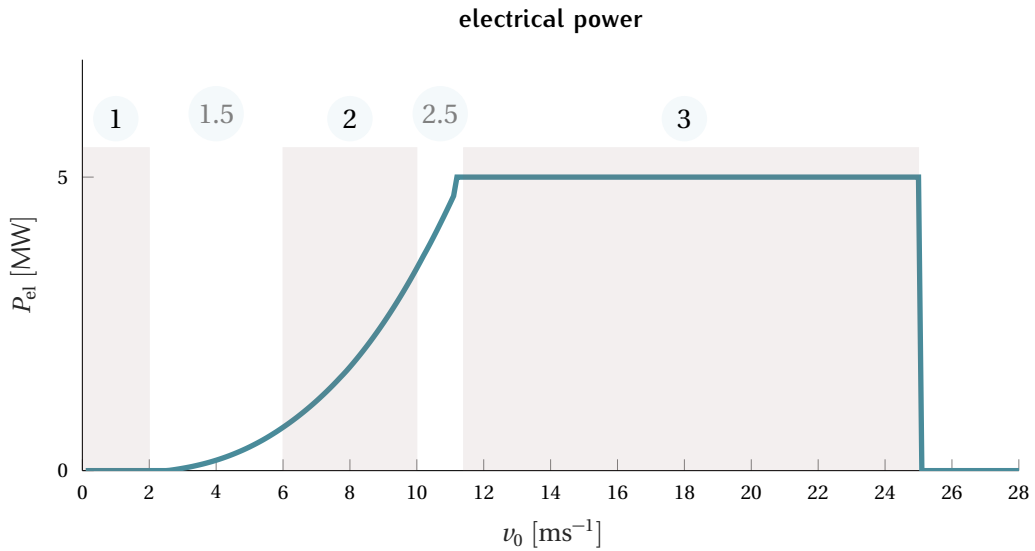


Figure 2.3: The different control regions of a 5 MW wind turbine.

with Ω the rotor speed, R the rotor radius and v_0 the rotor effective wind speed. Thus, the wind turbine can gain maximum power because of operating at its optimal operation point. The partial load controller uses the generator torque input and a nonlinear feedback of the rotor speed

$$M_g = K_\Omega \Omega^2 \quad (2.41)$$

as described in [24]. The constant K is well chosen as

$$K_\Omega = \frac{1}{2} \rho \pi R^5 \frac{c_{P,\max}}{\lambda_*^3}, \quad (2.42)$$

with ρ the air density and $c_{P,\max}$ the maximum power coefficient. For more information on partial load control, see [24].

Full load control

In full load operation, maintaining constant rotor speed and mitigating disturbances to minimize structural loads of the wind turbine are the main focus of the controller. The blades are pitched to reduce the aerodynamic torque and suppress effects due to changes in the wind speed. In constant power operation, the generator torque is set using the current rotor speed

measurement to produce nominal power to

$$M_g = \frac{P_{\text{rated}}}{\Omega}. \quad (2.43)$$

In constant torque control (an alternative operation mode to constant power), the torque is set constant to rated torque.

The pitch controller is then used to realize constant rotor speed. Therefore, very often a gain-scheduled Proportional-Integral (PI) controller is used. For the design of the controller, see *e.g.* [24].

2.6.2 Yaw controller

Assessing the wind direction is a challenging task since on current wind turbines the wind vane on the nacelle is used to obtain the wind direction. There are two main disadvantages of this concept: 1) the wind direction measurement is heavily disturbed by the rotor, and 2) the wind direction is assessed at one point, however, the rotor area is a much larger area and the mean wind direction might be different from the measured one. To overcome those disadvantages, the signal of the wind vane is corrected and heavily filtered with a low-pass filter, see [24]. Nevertheless, the measurement is very imprecise. Recent work, such as in [52, 53, 54], use lidar measurements to get a more precise estimation of the misalignment of the wind turbine.

The yaw controller uses the estimated wind direction from the wind vane to correct for misalignment. However, to avoid too much actuator action a threshold on the misalignment is applied and a control action is only allowed if the absolute error is above the threshold.

Because of the high rotor inertia, the actuation speed is designed to be very slow. In this work a maximum yaw rate of 1 degs^{-1} is assumed. However, no threshold behavior is used because of the direct control of the yaw angle and the assumption that the rotor is generally aligned with the main wind direction.

2.7 Wind farm control

Wind farm control deals with control concepts that improve the overall performance of a wind farm. A wind farm is a closely clustered array of wind turbines. Clustering wind turbines to a wind farm reduces the infrastructural costs and further minimizes the used area. Because of closer distances between the wind turbines, they can interact through their wakes. This leads to less energy yield of the wind turbines in the wakes and increased structural loads due

to the higher turbulence intensities in the wakes. Wind farm control addresses these issues by aiming to reduce interactions and mitigate the impacts of them, see [55], [10], [4]. The same two goals are valid for both wind turbine and wind farm control: 1) maximization of the total power and 2) reduction of the structural loads. Currently, wind turbines are mainly operated independently of the layout and wind farm interactions. Farm-wide operation is only considered in derating the wind turbines equally in case of less energy demand of the grid. Current research in wind farm control deals with realizing the goals on a farm level and therefore minimizing the cost of energy on a farm level. On the wind farm level a third task is valid active power control (APC). APC provides grid services like primary control, secondary control, or tertiary control.

Altogether, two main actuation concepts have been introduced for wind farm control: 1) axial induction control and 2) wake redirection control. As pointed out in the introduction, this work is in the field of wake redirection, however, a brief overview on the axial induction concept is given.

In the following, first, the objectives of wind farm control are described, then, the two main concepts axial induction control and wake redirection control are described.

2.7.1 Objectives

There are three objectives for wind farm control: power maximization, minimization of structural loads, and providing grid services like APC. The overall goal of them are to reduce the LCOE of wind energy and to make wind energy more competitive against other energy resources.

Power maximization

Power maximization gives a direct financial return. A gain in energy yield directly results in a financial gain and makes the wind farm more profitable. However, power maximization always needs to be balanced with structural load considerations, since the design constraints in terms of load envelope limits the achievable margin. Because of the wake deficit, power maximization can be stated as avoidance of wake interactions or mitigating of wake effects. This can be realized by wake redirection. A remarkable power maximization has been achieved, see [10, 18]. The benefit of axial induction control on power maximization is questionable, see [44].

Minimization of structural loads

Quantifying the financial benefit of load reduction depends on the design and turbine type. However, modern control technologies have enabled a less conservative or larger design. Load minimization on the turbine level is often achieved by additional control loops, like tower damper or individual pitch control. On a broader perspective, wake impingements on the rotor causes higher structural loads due to the turbulent asymmetric characteristic of the wake. Therefore, the avoidance of wake impingements lead to less structural loads. Further, by minimizing the wake effects (less wake deficit), due to axial induction control, the loads might also be decreased. However, this field is still a research topic and the overall conclusions haven't been stated.

Active power control

Active power control belongs to the field of grid service applications. It involves providing frequency regulation, or power reserve, as well as power reference tracking. The goal of these applications is to provide services for the energy grid and to improve the energy quality provided by wind turbines. Active power control is not considered in this work, but the actuation concepts, described in the next section, might also be used for active power control, e.g., axial induction control in the case of power reference tracking and power curtailment among the wind turbines.

2.7.2 Axial induction control

Axial induction control aims to achieve a better performance in the sense of the control goals by intelligently curtailing the wind turbines. By manipulating the axial induction with the blade pitch or torque actuator and operating the wind turbine at a lower production level a reduced impact on downwind turbines is sought. A lower axial induction results in a lower wake deficit, however, it also results in less turbulent mixing in the wake, see [56]. It seems that this would minimize the impact of the wake on structural loads, however, more investigations are necessary to conclude this. Regarding the goal of maximizing overall energy yield by preserving energy in the flow, results obtained with the high-fidelity CFD simulation tool SOWFA (see [29]) illustrate that performance increase seems hardly achievable, see [44]. However, axial induction control again becomes more important when a global power demand from the grid operator is intelligently distributed. This might lead to a high reduction of structural loads

and an increased lifetime operation. Consider [5] for a more precise summary and current research questions on axial induction wind farm control.

2.7.3 Wake steering

In contrast to axial induction control, wake steering aims at redirecting the wake to avoid wake interactions with downstream wind turbines. The general idea of wake redirection is to deflect the wake by either yawing the wind turbine or by cyclic blade pitching, see [11, 46, 57]. This concept has mainly been investigated for maximizing energy yield, however, avoiding partial wake overlaps seems also a promising field.

Several publications have shown promising results in increasing the performance of downwind turbines by using wake redirection techniques, see [10, 18, 19, 58, 20]. [22] further includes wind turbine loads in the optimization procedure to perform a multi-objective wake redirection. An overview on the field of wind farm control with a detailed summary of different methodologies is given in [5].

Current investigations focus on wind tunnel (see, [59, 60, 61]) and field testing experiments (see, [62]) to strengthen the results of previous simulation studies and demonstrate the applicability on industrial wind turbines and commercial wind farms.

Furthermore, when designing new wind farms, having the ability to deflect the wake gives an additional degree of freedom in operation. This might lead to different layouts in which wind turbines are positioned denser and therefore, the consumed area is used more efficiently. The operational strategy of these wind farms will include wake redirection to avoid partial wake overlaps and the total power output will be increased compared to conventional operation. [58] makes use of this approach and redesigns a wind farm using system engineering techniques.

3

Wake steering field experiment

*Wir standen Hand in Hand und schwiegen, und deine
Augen träumten hell.*

*Schon kam die Nacht auf stillen Stiegen, ins
abendeinsame Castell.*

— R. M. Rilke, *Arco*

3.1 Objectives	36
3.2 Experimental setup of the field testing	36
3.3 Wake steering results	40
3.4 Conclusions	43

With the different investigations on wake redirection in which an increase in energy yield of wind farms have been shown in simulations, the question of being able to transfer the results into reality hasn't been answered. Therefore, field-testing is necessary to investigate the different aspects of the concept. From September 2016 until May 2017, a dedicated field testing campaign was conducted at the National Wind Technology Center (NWTC) of NREL to investigate wake steering on a utility-scale wind turbine. The focus of the field testing campaign was to demonstrate wake steering in reality.

This chapter presents some of the main results and gives a motivation for the closed-loop wake redirection concept. It is mainly based on the results of [62] and [63], however, both contain much more information on their specific topics. The chapter is structured as follows: First, the objectives of the field testing are stated in section 3.1, then in section 3.2 the experimental setup is described. In section 3.3 some relevant results are presented, and finally in section 3.4 a conclusion and a motivation for the closed-loop wake redirection concept are given.

3.1 Objectives

The field experiment was conducted in order to provide a data set for model validation of wake models and to demonstrate wake steering in reality. More precisely, one main goal was to gain more confidence in the prediction capabilities of control-oriented wake models. They have been mainly used, as mentioned in section 2.7.3, for open-loop wind farm control. By using them in an optimization framework, optimal yaw offsets are computed which were applied to the wind turbines in high fidelity simulations. However, under real field testing conditions, the models haven't been validated. Furthermore, the impact of different atmospheric conditions on the wake shape and redirection have been of interest in this campaign.

3.2 Experimental setup of the field testing

The field testing was conducted at the NWTC of NREL. The U.S. Department of Energy (DOE) 1.5 MW turbine was run with a scanning lidar system on the nacelle that faced downwind and continually scanned the wake. The yaw misalignment angles were changed continually to different offsets. The campaign started in September 2016 and ended in May 2017.

In the following, first, the general setup is described. Then the test procedure is presented and finally the lidar system is briefly described.



Figure 3.1: The DOE 1.5 MW turbine at the NWTC is shown with the Stuttgart Wind Energy (SWE) scanning lidar being installed. Photo by Dennis Schroeder, NREL 38271

3.2.1 General setup of field testing

As already mentioned, the field testing took place at the NWTC which is located south of Boulder, Colorado in the US. Because of its location close to the Rocky Mountains, the site is dominated by winds from the mountains. The site is equipped with different turbines and meteorological masts. For this field testing, a meteorological mast was available a distance of 161 m upstream in the dominant wind direction. The measurement data of the meteorological mast provided basic meteorological information that was also used in evaluating the experiment. Additionally, turbine measurement data was recorded and time synced with all other measurement data.

The wind turbine is the DOE 1.5, see figure 3.1. The main turbine properties are listed in Table 3.1. The wind turbine was operated normally, however, different yaw misalignment offsets were applied.

3.2.2 Test procedure

The DOE 1.5 was operated with its normal controller. To realize the yaw offsets, an auxiliary controller was built around the normal baseline controller which applies yaw offset positions.

Table 3.1: Turbine specifications of the test turbine DOE 1.5 at the NWTC.

Rated power	(kW)	1500
Hub height	(m)	80
Rotor diameter	(m)	77
Rated wind speed	(ms^{-1})	14

**Figure 3.2:** The SWE scanning lidar being installed on a rotating frame on the DOE 1.5 turbine. Photo by Andrew Scholbrock, NREL

These offset positions were changed every hour and always included the baseline of zero offset in regular rotation. This practice helped ensure that for post-processing, each offset position could be compared with baseline operation in almost similar inflow conditions. Additionally, the lidar system was mounted on a rotating frame which counter rotates the measurement system in order to maintain the same measurement position while yawing the turbine, see figure 3.2. Thus, the lidar always pointed downwind while the turbine was misaligned.

3.2.3 Scanning lidar system

For the field-testing experiment, the Stuttgart scanning lidar system was used. It was developed in 2008 for nacelle-based lidar measurement campaigns to redirect the laser beam of a standard Windcube lidar system, see [64]. The complete system consists of two parts: a Windcube V1 from Leosphere and a scanner unit developed at SWE at the University of Stuttgart. A

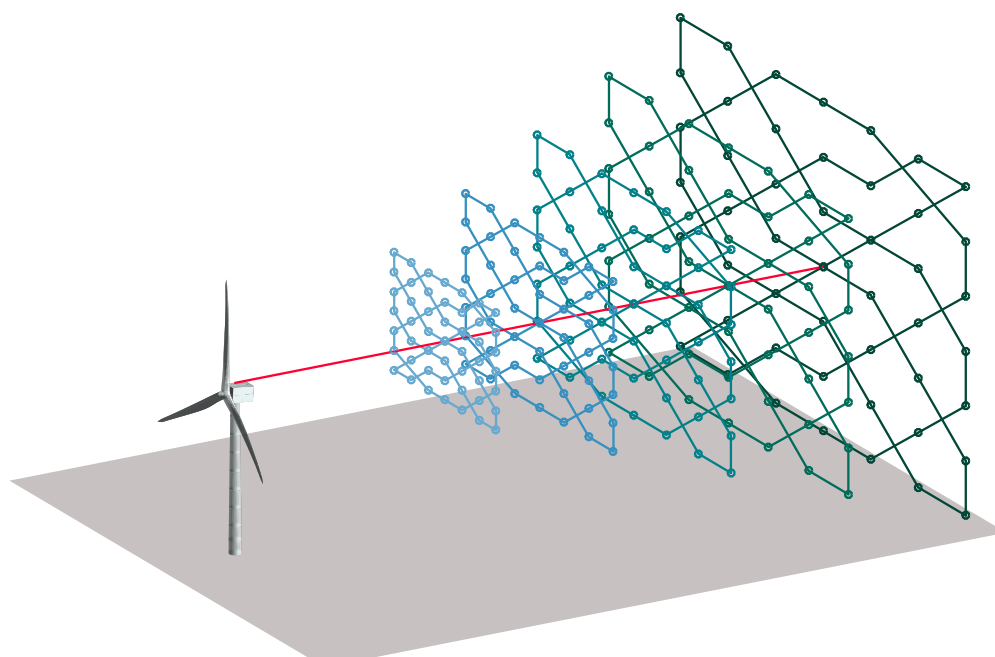


Figure 3.3: Visualization of the lidar scan pattern that is used to measure the wake behind the wind turbine. A grid of 49 points is used with a sampling frequency of 1 Hz to scan the wake in five different distances from 1 to 2.8 times the rotor diameter (D).

picture of the lidar from the University of Stuttgart is shown in figure 3.2. Because the original Windcube was designed for site assessment with its beam pointing upwards, a two-degree-of-freedom mirror for redirecting the beam in any position within the mirror's range was installed in a second casing. The accessible area is a $0.75 D$ -by- $0.75 D$ square in $1 D$ distance, where D is the rotor diameter. The modified software allows up to 49 measurement positions and 5 scan distances to be used. Further, the scan rate depends on the number of pulses used for each measurement position. In this case 10,000 pulses have been used and thus the measurement frequency is approximately 1 Hz. The lidar system has been successfully used for numerous measurement campaigns as well as inflow measurements for lidar-assisted control and wake measurements, see [65, 66, 67, 68, 69, 70, 26]. In this campaign, the lidar performs a grid measurement pattern to record the wake in five different distances ($1 D$ to $2.8 D$) as shown in figure 3.3). At each measurement point, the lidar measures the line-of-sight wind speed, v_{los} , that is a projection of the three wind vector components $[u, v, w]$ onto the laser beam (see section 2.4.4). The complete scan pattern consists of 49 points in each scan plane, and the five planes are measured simultaneously. One scan takes an average of 48 s to complete.

3.2.4 Considered time periods and data processing

The data set was limited to undisturbed inflow sections. Since there are other wind turbines in the surroundings of the DOE 1.5, only situations are considered where the wind turbine is in undisturbed inflow conditions. Further, situations were excluded in which the lidar might hit the wiring of the meteorological tower with its laser beam.

Data processing is of high importance to obtain a useful data set for the evaluation. Therefore, first the recorded lidar measurement data are processed to filter out implausible data. Several methods are applied to check for hard target measurements, filter out lidar data with a bad carrier-to-noise ratio, and check for plausibility of the measurement data. Then, depending on the analysis, the data is treated differently to obtain the final data set for analysis. All processed lidar data are grouped into scans, and combined with statistics of turbine and met mast sensor data, such as mean and standard deviation, over the period in which the scan is collected. Altogether, a data set was generated that is used in the following to show some of the main results of the field-testing.

3.3 Wake steering results

As elaborated before, the main objectives of the campaign are to demonstrate the possibility of wake redirection and to gain confidence in the predictability of the redirection. Therefore, averaged analyses are performed which depict the flow and covers only static phenomena.

For the analysis, the data set is binned by wind speed and turbulence intensity. The data are filtered to include only certain conditions. A threshold of 100kW on the produced power ensures that only normal operation data is included and faults, idling and other conditions are removed. Furthermore, as indicated before, only periods are included in which the met tower is nominally upwind of the turbine and the target and realized yaw offset are close. The main results of the campaign are presented in [62], where the general setup and test procedure are described, as well as preliminary results. [63] gives a more detailed analysis on wake steering, moreover, the predictability of the wake by different wake models is investigated.

Figure 3.4 shows the median analysis at 181 m downstream for 8 ms^{-1} and stable atmospheric conditions and low turbulence intensity. With increasing yaw offset the intensity of the wake deficit is reduced and the wake is curved. The wake redirection is visible although the shape changes significantly with increasing yaw offset. Circles indicate the size of the wind turbine rotor in the flow plots. The circles are displaced by the predicted wake deflection which is calculated by the FLORIS model. In the calculations the actual atmospheric condi-

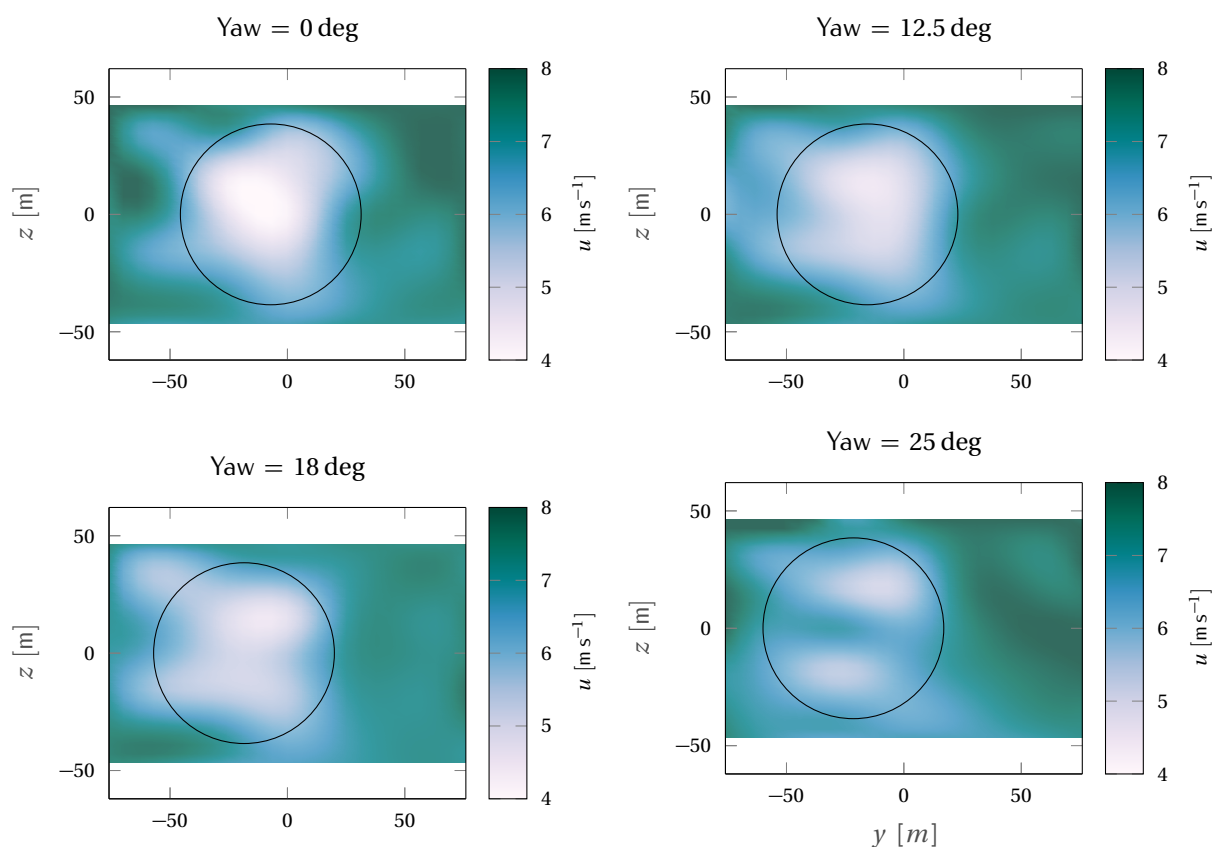


Figure 3.4: Median scans of lidar measurements at 181 m distance downstream at 8 ms^{-1} for 0 deg, 12.5 deg, 18 deg and 25 deg yaw offset at low turbulence intensity ($T_{i,\text{bin}} = 6.25\%$). The circles indicate the size of the rotor and show the wake deflection predicted by the FLORIS model.

tions have been used. The accordance between measurement data and engineering model is visible especially for stable atmospheric conditions. Thus, the results strengthen the wake redirection concept at stable conditions and low turbulence intensity. However, for higher turbulence intensity, the median analysis shows a faster wake recovery and a less strong wake deficit as shown in figure 3.5. Altogether, the results show that wake steering is possible in reality, although the atmospheric conditions have a high influence on the wake and the ability to steer it.

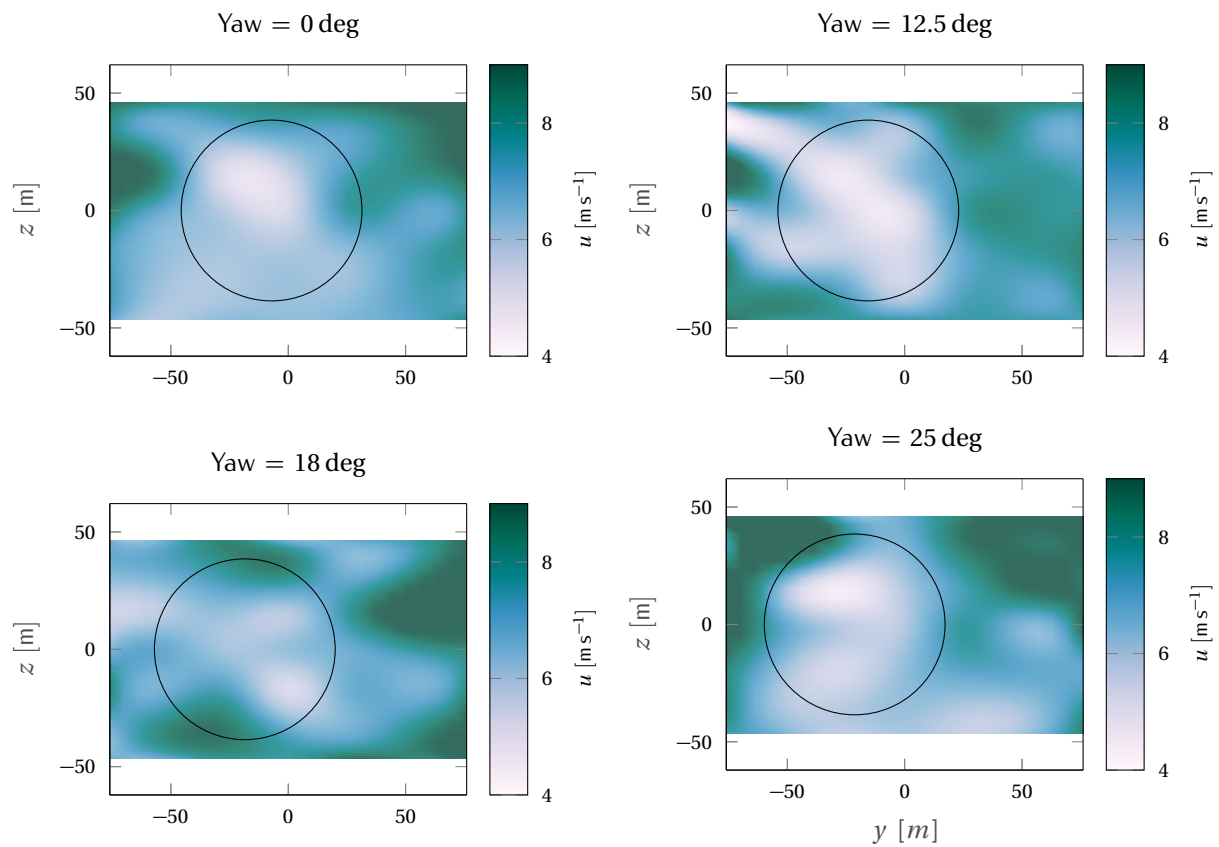


Figure 3.5: Median scans of lidar measurements at 181 m distance downstream at 8 ms^{-1} for 0 deg, 12.5 deg, 18 deg and 25 deg yaw offset at high turbulence intensity ($T_{i,\text{bin}} = 15\%$). The circles indicate the size of the rotor and show the wake deflection predicted by the FLORIS model.

3.4 Conclusions

The results of this first field-testing investigation have shown promising analyses in terms of the feasibility of wake steering. A redirection of the wake is possible, although the first investigations have shown that atmospheric conditions highly influence the wake steering. Such behavior has been already observed in simulations, see [71]. Altogether, the campaign gives a first proof of concept of the open-loop wake redirection approach. The averaged results show good agreement with the steady state FLORIS model and its modifications, see [63]. This strengthens the concept of wake redirection.

The following points have turned out to be important in the planning of the campaign and its execution. The choice of measurement setup, the choice of lidar system as well as its availability, and a repetitive testing procedure that enables a comparability of different atmospheric conditions. The use of a nacelle-based lidar system enabled the measurements behind the wind turbine without inclination angle. Other measurement configurations that use ground-based long range lidar systems may face difficulties in analyzing the data due to the volume averaging of the lidar system and the spacial resolution of the measurements. However, because of the yawing of the wind turbine and the redirection in the opposite direction, the rotational mounting of the measurement system was necessary. Altogether, the field-testing with a nacelle-based lidar system has led to a data set that will be publicly available and can be used for further analysis and investigation.

In the next chapter the lidar-based closed-loop wake redirection concept is introduced. The goal of this new concept is to maintain the benefits of open-loop wake redirection control and to improve the weaknesses of the concept which are the wake model uncertainty and the sensitivity against disturbances.

4

Concept of lidar-based closed-loop wake redirection

Le cœur a ses raisons que la raison ne connaît pas.

— Blaise Pascal

4.1	Objectives of closed-loop wake redirection	46
4.2	General concept	47
4.3	Challenges and conclusions	49

This chapter presents the framework of lidar-based closed-loop wake redirection control and introduces the two tasks, the control task and the estimation task, which are the main parts of the concept. Parts of this chapter have been published in [72]. The chapter is structured as follows: First, the objectives and advantages of closed-loop wake redirection are presented in section 4.1. Second, in section 4.2 the general concept is introduced. Finally, the challenges and conclusions are discussed in section 4.3.

4.1 Objectives of closed-loop wake redirection

Lidar-based closed-loop wake redirection is a flow control concept. It introduces the advantages of closed-loop control to the concept of wake steering. Wake steering, in its current methodology, contains the following drawbacks:

- Optimized yaw angles are applied in an open-loop approach. Since the yaw angles are computed with assumptions, e.g. on atmospheric conditions, wind speed, or using a reduced-order model, the approach does not guarantee that the wake is taking the desired direction. Thus, the match/mismatch of the assumptions, like the quality of the model, which is used to compute the yaw angles, highly influences the control performance.
- An open-loop methodology is highly sensitive to disturbances. This means that any disturbance, e.g. cross wind or shear, will lead to an uncertain performance compared to the desired redirection computed by the model.

The concept of lidar-based closed-loop wake redirection, which was first introduced in [73] and [72] presents an alternative method to realize wake redirection control. The objectives of the concept are:

- an estimation of the wake position in a reliable and robust way using lidar wind speed measurements,
- a closed-loop control of the wake position to redirect the wake to a desired position,

and thus, an overall benefit for wake redirection control through the usage of feedback control. From an operational point of view, the concept introduces a new layer between the wind farm operation and the wind turbine operation which manages the wake steering. This means, the wind park operator or an automated optimization algorithm specifies the desired wake

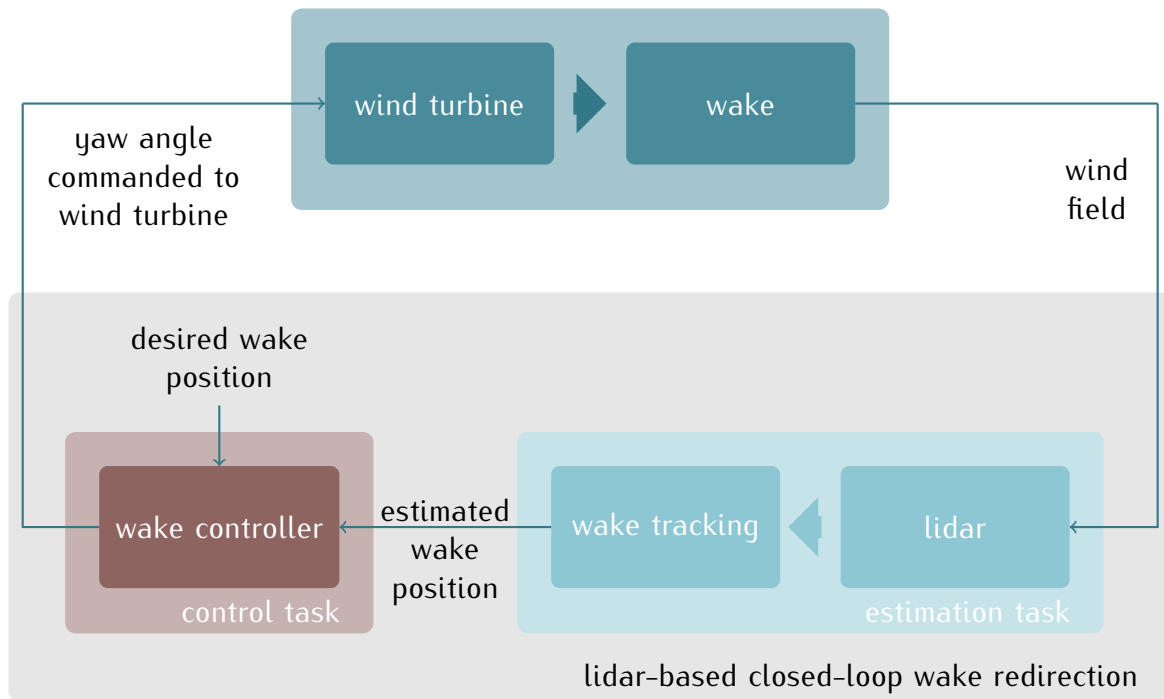


Figure 4.1: The general concept of lidar-based closed-loop wake redirection.

position of each turbine. Locally, on the wind turbine level, the controller tries to steer the wake to the desired position. However, this is only possible within the physical limitations of wake redirection.

The main objectives of the chapter are the introduction of the concept, the task separation which structures the methodology, and a discussion on challenges the concept raises.

4.2 General concept

The lidar-based closed-loop wake redirection concept consists of two main tasks: 1) the estimation task and 2) the control task. Figure 4.1 gives the closed-loop scheme of the concept. The control-loop is closed locally on the turbine level which has advantages in terms of scalability, implementation and communication. Nevertheless, the estimation task could also be realized on the farm level. It will be briefly discussed later in the specific section. Flow information will be provided by a lidar system and used in the estimation task to obtain a position information of the wake. In section 4.2.1 the main objectives of the estimation task are discussed. The position information of the wake is then provided to the wake controller, see figure 4.1. The control task deals with designing appropriate controllers which are able

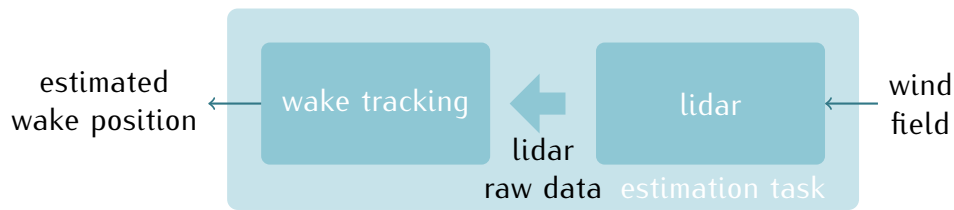


Figure 4.2: The wake position estimation task.

to steer the wake to a prescribed position. Section 4.2.2 will present the general idea and the objectives of the control task.

4.2.1 Estimation task

The estimation task deals with converting lidar measurement data into a position estimate of the wake. This task imposes some challenges since lidar can not provide full flow information, as already discussed in section 2.4. Moreover, estimation techniques have to be investigated to provide necessary quantities for the controller. This means first of all that the measurement data must be processed in such a way that it can be used to perform an estimation of the wake characteristics, like *e.g.* wake position, wake shape, decay, or recovery. Possible solutions to the estimation task are presented in chapter 6 where lidar-based wake tracking methods are discussed and a model-based wake tracking approach is presented. In figure 4.2, the general structure of the estimation task for lidar-based closed-loop wake redirection is diagrammed. The lidar obtains wind speed measurements in the wind field, and a wake tracking method estimates the wake position from the lidar measurement data.

4.2.2 Control task

In the control task, the wake controller is specified. The wake controller is designed to steer the wake position to a desired position. It uses the position information of the wake and the demanded wake position to provide a necessary yaw angle command which steers the wake to the desired position. The controller design needs to take into account the time constant which is imposed by the mean wind speed and the downwind location of the estimated wake center. Different control design approaches are presented and analyzed in chapter 7. Figure 4.3 presents the inputs and the output of the control task. It uses the estimated wake position and a desired wake position to set the yaw angle of the wind turbine.

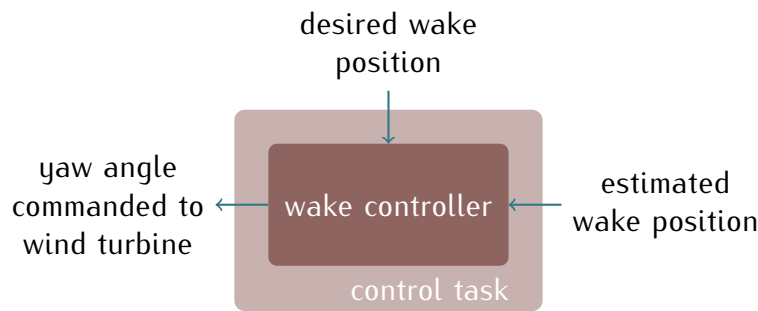


Figure 4.3: The wake redirection control task.

4.3 Challenges and conclusions

After having described the basic concept of lidar-based closed-loop wake redirection, the following section aims at outlining the main challenges which exist in the concept and gives some conclusions on it.

4.3.1 Challenges of the concept

Since the methodology relies on the availability of a wake position estimation, the availability of lidar measurements are crucial. From a practical point of view, this includes the system availability but also the reliability of the estimation method of the wake position. However, the practical implementation and related challenges are not considered in this work and need to be considered in future work.

Furthermore, the experience of the field-testing presented in chapter 3 has shown the difficulties and the trade-off in the choice of the measurement distance. Since the wake deficit is mitigated over distance, and furthermore the turbulent mixing is more predominant with increasing distance, the measurement location needs to be chosen well. When only interested in the wake deficit the choice would be as close as possible to the rotor, however, since the wake redirection is of interest and the wake is not steered instantaneously a certain distance is needed to get a measurable deflection. Furthermore, a measurement distance further downwind imposes performance limitations on the controller, since the time delay between actuation and reaction increases. Here, a trade-off needs to be found which depends on the site specific conditions.

4.3.2 Challenges of the estimation task

The aim of the estimation tasks is to determine indirectly the wake position. A challenge of great importance is the fact that the wake position is not well defined. The wake center is not a directly measurable quantity. Since the wake is the effect of the energy extraction of the wind turbine, the primal effect is the decrease in wind speed in the flow. Everything else, like a wake profile, an increase in turbulence intensity, or the wake position are observations of the physical behavior of the flow. They have been introduced to mathematically describe the wake in a systematic way. However, they are only partly measurable in reality due to limitations in the measurement techniques. This means, the estimation method indirectly determines the wake position definition. The wake position definition process is a difficult aspect since it is not measurable. Compared to other quantities, the wake center is a quantity that depends on its definition. This, however, hinders the comparability of different approaches since no unique definition exists. Moreover, there are several definitions, like a one dimensional or a two dimensional Gaussian fit of the wake deficit, threshold based methods, or the power-based method, see [74]. Altogether, they specify the wake position within the description of the wake characteristics or shape assumptions.

4.3.3 Challenges of the control task

The control task focuses on the controller design for closed-loop wake redirection. As mentioned, there is a trade-off between measurement location and time delay. This influences the controller design because the time delay limits the bandwidth of the controller. Furthermore, the controller needs to be synthesized to adapt to model uncertainties and disturbances. Disturbances of higher frequencies like wake meandering should not influence the control performance, although the amplitude of wake meandering may be noticeable.

4.3.4 Conclusion

This chapter has presented the general concept of lidar-based closed-loop wake redirection and it has given an introduction into the different aspects of the topic. First, the main objectives of the concept have been stated. The two main tasks, the estimation task and the control task, have been introduced as well. They enable the lidar-based closed loop wake redirection concept. The separation helps to design the methodologies independently and test the influence of uncertainties on both. In a next step, the challenges introduced by the concept

have been discussed. The importance of the estimation task has been highlighted and the challenge in the wake position definition has been described.

From a practical point of view, the future of nacelle-based lidar devices is not clear. Especially, downwind facing lidar devices have been used by researchers and are rare in commercial applications to date. However, this work wants to provide a first outlook on the concept and highlights the opportunities, while partly neglecting implementation questions. Nevertheless, at crucial points in this work, possible solutions are proposed that might overcome the main challenges.

After having introduced the structure and objectives of the concept, the following chapters derive and describe the different tasks. In the next chapter, the necessary models are derived which are needed in the two tasks mentioned above.

5

Wake modeling

*Not to us, Lord, not to us but to your name be the
glory, because of your love and faithfulness.*

— Psalm 115,1 *The Bible*

5.1	Objectives and assumptions	54
5.2	Wake deficit and wake evolution model	55
5.3	Wake deflection model	57
5.4	Wake modeling for controller design	58
5.5	Conclusions and recommendations	69

This chapter presents the necessary models for realizing the lidar-based closed-loop wake redirection concept. It further provides a methodology on how experiments can be conducted to estimate the model parameters.

In the following, the objectives and assumptions of the chapter are described in section 5.1. Then, in section 5.2 and 5.3 a reduced order wake model is presented which describes the main effects of the wake, the velocity deficit, the wake evolution, and the wake deflection. This model is later used in the model-based wake tracking approach. As a next step, in section 5.4 controller design models are derived considering only the dynamical behavior of the wake position with respect to the yaw angle. Different techniques are presented to estimate the parameters of the dynamic model using a model identification technique. Finally, in section 5.5 conclusions and recommendations are given.

5.1 Objectives and assumptions

Wake modeling is a broad research field and several applications exist in which the models are applied. Control-oriented wake models for optimizing the operation and deriving new controllers are rare because of the complexity of wakes. Here, wake models are presented which will be used in the lidar-based wake tracking and the wake redirection controller design.

The model requirements of the wake tracking application are the following:

- low computational effort,
- main wake effects, like deficit, evolution and redirection should be included,
- a minimal amount of model parameter and tuning variables.

The wake redirection controller design model has different requirements:

- dynamic model, since time constants are important for the controller design,
- separation and elimination of all unnecessary wake effects, like wake evolution.

Thus, the controller design models only include the wake redirection effect.

The consideration of the mentioned models seems to limit the validity of the approach, however, for the controller design process this is not the case. If the controller is designed with a robustness margin, undescribed dynamics or effects will be considered as disturbances and the controller will adapt to them. For the wake tracking, the limitation to deficit, evolution and redirection is a first assumption which has shown good results in prior work. The model can be easily adapted with modification.

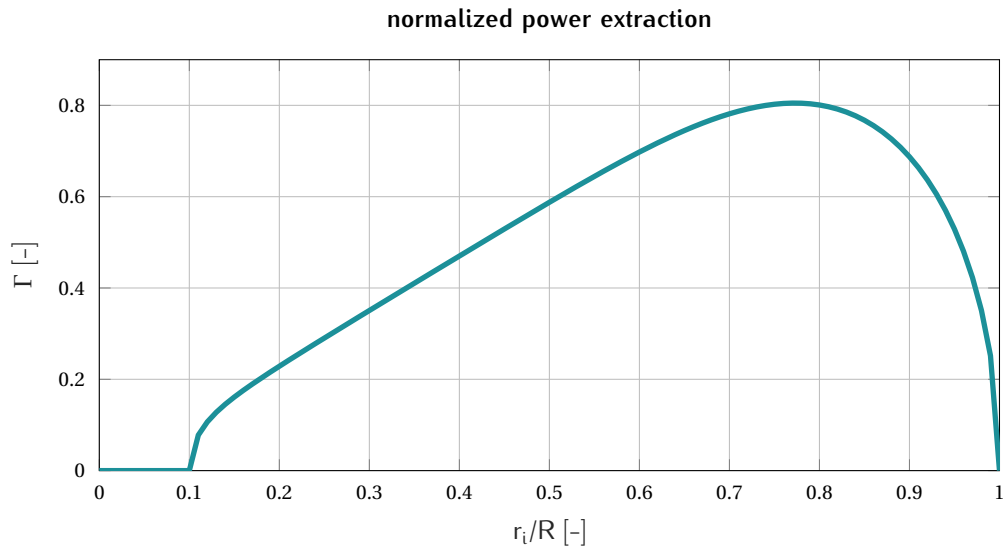


Figure 5.1: The normalized gradient of the power extraction along the blade radius.

5.2 Wake deficit and wake evolution model

The wake deficit is modeled with an initial wake deficit at the rotor disk with tip and root losses depending on the energy extraction. The initial deficit is calculated by mapping the energy extraction to the rotor as a function of the energy extraction along the blade (including root and tip losses). Therefore, the normalized wake deficit based on Prandtl's root and tip losses is used. We define Γ as the Prandtl's root and tip losses inside of the rotor radius R . At point $[y_i, z_i]$ at the rotor, the function is

$$\Gamma_i = \begin{cases} \left. \frac{dc_p}{dr} \right|_{r_i} & \text{if } \sqrt{y_i^2 + z_i^2} = r_i \leq R \\ 0 & \text{else} \end{cases} \quad (5.1)$$

with r_i the normalized radius at position $[x_i, y_i, z_i]$ along a specific blade. $\left(\frac{dc_p}{dr}\right)$ is the gradient of the power extraction over the blade which can be extracted with WTPerf, see [75]. An example of Γ is given in Figure 5.1 for the NREL 5 MW reference wind turbine. Having derived the normalized power extraction, the initial wake deficit results to

$$\Psi_{\text{initial}}(y_i, z_i) = \frac{-v_0}{\sum_j \Gamma_j^2} \left(\sum_j \Gamma_j - \sqrt{\left(\sum_j \Gamma_j \right)^2 - n_{\text{PI}} \sum_j \Gamma_j^2 c_P} \right) \Gamma(y_i, z_i), \quad (5.2)$$

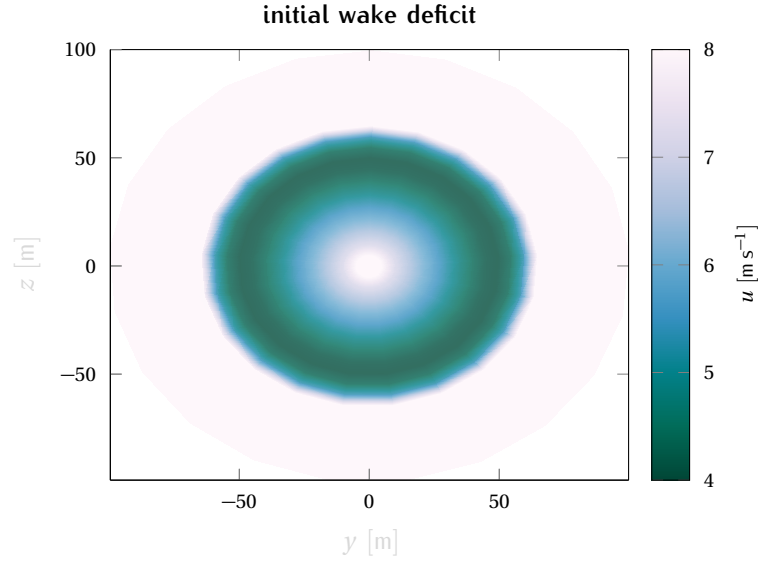


Figure 5.2: An example initial wake deficit at the rotor disk at a mean wind speed of 8 ms^{-1} .

with \sum_j the summation over the grid points, the rotor effective wind speed v_0 , the power coefficient c_p , and n_{PI} the number of grid points inside of the swept rotor area. Figure 5.2 shows an initial wake deficit at an inflow wind speed of 8 ms^{-1} and normal operation of the wind turbine.

The wake evolves moving downwind. Energy flows in from the free stream and mixes with the wake. This is modeled empirically by a two-dimensional Gaussian shape filter, Ξ . The filter describes the wake recovery behind the wind turbine and depends on the distance d behind the wind turbine. Furthermore, a dissipation parameter ϵ is specified which can be linked to the turbulence intensity or in other words, the amount of mixing. Thus, the filter at point $[y_i, z_i]$ at a distance d downstream is

$$\Xi(d, y_i, z_i) = \exp\left(-\frac{y_i^2 + z_i^2}{2\sigma_f^2(d)}\right) \quad (5.3)$$

with

$$\sigma_f(d) = \frac{\epsilon d}{2\sqrt{2\log(2)}}. \quad (5.4)$$

Having defined the initial wake deficit Ψ_{initial} in (5.2) and the wake evolution model in (5.3), the wake can be calculated. The wake deficit results from the convolution of the initial wake

deficit Ψ_{initial} with the filter $\Xi(d, y_i, z_i)$:

$$\Psi(d, y_i, z_i) = \Xi(d, y_i, z_i) * \Psi_{\text{initial}}. \quad (5.5)$$

5.3 Wake deflection model

The wake deflection caused by a yaw misalignment γ is additionally modeled. The relationship is derived in the study of [46], applied to the FLORIS wake model, and also used in this wake model. The angle of the wake with respect to the main wind direction is

$$\xi(d, c_T, \gamma) = \frac{\xi_{\text{init}}(c_T, \gamma)}{\left(1 + \beta \frac{d}{D}\right)^2}, \quad (5.6)$$

with the initial angle of the wake at the rotor

$$\xi_{\text{init}}(c_T, \gamma) = \frac{1}{2} \cos^2(\gamma) \sin(\gamma) c_T \quad (5.7)$$

and model parameter β , which defines the sensitivity of the wake deflection to yaw and is here assumed to be known in advance. Further, c_T is the thrust coefficient and D the rotor diameter. Further, the yaw induced deflection at the downwind position d is according to [18]

$$\delta_{\text{yaw}}(d, c_T, \gamma) = -\xi_{\text{init}}(c_T, \gamma) \frac{D}{30\beta} \left[15 \left(1 - \frac{1}{1 + \frac{2\beta d}{D}} \right) + \xi_{\text{init}}(c_T, \gamma)^2 \left(1 - \frac{1}{\left(1 + \frac{2\beta d}{D}\right)^5} \right) \right]. \quad (5.8)$$

The yaw induced deflection (5.8) shows the following behavior at the limits of the downwind distance d ,

$$d = 0 \Rightarrow \delta_{\text{yaw}}(d, c_T, \gamma) = 0 \quad (5.9)$$

$$d \rightarrow \infty \Rightarrow \delta_{\text{yaw}}(d, c_T, \gamma) \rightarrow -\xi_{\text{init}}(c_T, \gamma) \frac{D}{30\beta} (15 + \xi_{\text{init}}(c_T, \gamma)^2). \quad (5.10)$$

The rotation is applied to the wake deficit and yields a u - and v -component of the wake model,

$$\begin{bmatrix} \Psi_{u,i} \\ \Psi_{v,i} \\ 0 \end{bmatrix}_W = \begin{bmatrix} \cos \xi(d, c_T, \gamma) & -\sin \xi(d, c_T, \gamma) & 0 \\ \sin \xi(d, c_T, \gamma) & \cos \xi(d, c_T, \gamma) & 0 \\ 0 & 0 & 1 \end{bmatrix} \begin{bmatrix} \Psi_i \\ 0 \\ 0 \end{bmatrix}_W. \quad (5.11)$$

5.4 Wake modeling for controller design

In the previous sections, a reduced order wake model was presented which includes the main effects of the wake, the velocity deficit, the wake evolution, and the wake deflection. For controller design, however, a control-oriented model is needed. Therefore, in the following, first, time dependency is introduced to the model, and second, the model is reduced to its input-output behavior.

For closed-loop wake redirection control, as already introduced in section 4.2, the input is the demanded yaw angle and the output is the estimated wake center at a particular downwind distance of the wind turbine. Therefore, the wake deflection model presented in section 5.3 is used. Further, the wake deficit model and the evolution model is neglected since they specifically describe other effects of the wake.

In the following, first, the wake deflection model is used to derive a static gain for different conditions in section 5.4.1, then in section 5.4.2, the dynamics are derived and the time constants are derived from theoretical considerations.

5.4.1 Static wake deflection model

For deriving a model for controller design we want to start with the static wake deflection model of (5.8). In order to simplify (5.8), it is revisited, however, with partially neglected dependencies to clarify the main dependencies for wake redirection. As used in the reduced order wake model, depending on the yaw angle γ , the wake deflection can be described by

$$\delta_{\text{yaw}}(\gamma, d) = -\xi_{\text{init}}(\gamma) \frac{D}{30\beta} \left[15 \left(1 - \frac{1}{1 + \frac{2\beta d}{D}} \right) + \xi_{\text{init}}(\gamma)^2 \left(1 - \frac{1}{\left(1 + \frac{2\beta d}{D} \right)^5} \right) \right]. \quad ((5.8) \text{ revisited})$$

This model describes the lateral wake center displacement at a defined downstream position d at steady state conditions with an assumed thrust coefficient c_T , the rotor diameter D , and β describes the sensitivity of the wake deflection to yaw misalignment. From (5.8) a linear

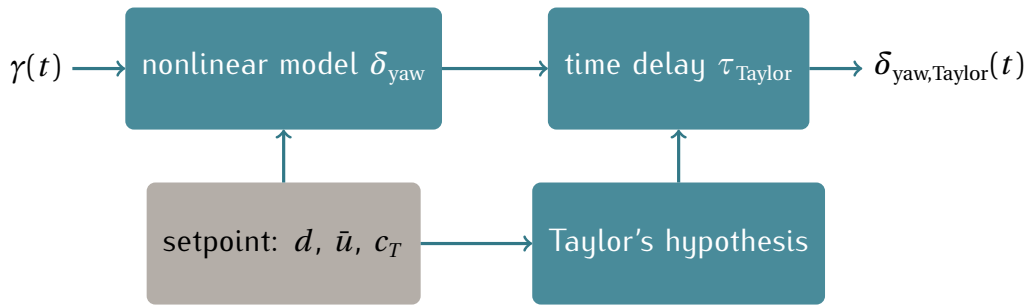


Figure 5.3: Flow chart of time delay based dynamic wake deflection model.

model can be derived by evaluating the gain at a defined setpoint. The static gain at distance d with respect to the yaw angle at a defined setpoint $p = [\gamma_0, c_{T,0}, d]$ is calculated as

$$K_p = \left. \frac{d\delta_{\text{yaw}}}{d\gamma} \right|_p. \quad (5.12)$$

Hence, for different setpoints the gain can be evaluated and the linear approximation around a setpoint is defined as

$$\tilde{\delta}_{\text{yaw}}(\gamma) = \delta_{\text{yaw}}|_p + K_p \gamma = \delta_{\text{yaw}}|_p + \left. \frac{d\delta_{\text{yaw}}}{d\gamma} \right|_p \gamma. \quad (5.13)$$

In a next step, the time dynamics are introduced because until now the wake deflection has been described in a static way.

5.4.2 Dynamic wake deflection model with time delay

In this section, the time dynamics are derived and discussed. There is not an instantaneous change in wake position because the estimation position is in a defined distance d downwind and the change needs to be propagated to the distance. In addition, there are flow dynamics involved. In the following, three approaches are presented with increasing complexity to approximate the wake dynamics.

Time delay based on Taylor's assumption

Following the assumptions of Taylor's hypothesis [76], the wind field is moving with a mean wind speed. Suppose that the wind direction is aligned with the x -axis, this implies that there

is a direct relationship between a distance Δx along the x -axis and a time period Δt that is

$$\Delta t = \frac{\Delta x}{\bar{u}}, \quad (5.14)$$

with the mean wind speed \bar{u} . Taking this assumption into account for the wake deflection model, it can be written as

$$\delta_{\text{yaw,Taylor}}(t) = \delta_{\text{yaw}}(d, \gamma(t - \tau_{\text{Taylor}})) \quad (5.15)$$

with $\gamma(t - \tau_{\text{Taylor}})$ the time signal of the yaw angle shifted by the time delay τ_{Taylor} based on (5.14) with $\Delta x = d$. Thus, the time delay is calculated to

$$\tau_{\text{Taylor}} = \frac{d}{\bar{u}}. \quad (5.16)$$

When evaluating the mean wind speed in the wake a reduction is visible. Therefore, Taylor's assumption may not be valid for wake propagation. Thus, in the following, the time delay is calculated based on the mean wind speed profile in the wake.

Time delay based on the wind speed profile

The wind speed in the wake is reduced because of the energy extraction of the wind turbine. According to [77] and [22], the velocity profile u can be approximated as an inverted hysteresis function. Together with the momentum conservation law (see [78]) this yields

$$u(x, w) = \left(1 - \frac{2}{\pi} w \left(\frac{\pi}{2} + \arctan \frac{2x}{D} \right) \right) u_{\infty} \quad (5.17)$$

the velocity u at distance x behind the wind turbine with the inflow wind speed u_{∞} , the induction dependent parameter w , and the rotor diameter D . Figure 5.5 gives an example velocity profile at 10 ms^{-1} inflow wind speed. Clearly the deceleration is visible, however, the wake mixing and the resulting wake decay is not considered in the equation. Therefore, the velocity profile converges to a constant value behind the wind turbine. Nevertheless, (5.17) enables calculating the time delay τ_{Profile} by solving the integral equation for τ_{Profile}

$$d = \int_0^{\tau_{\text{Profile}}} u(x(t), w) dt \quad (5.18)$$

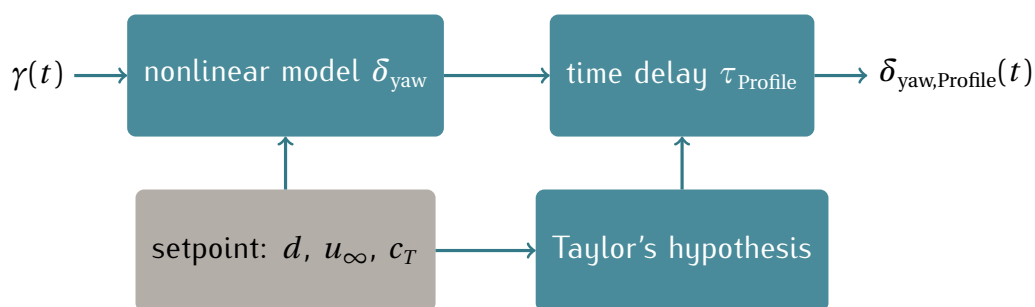


Figure 5.4: Flow chart of time delay based dynamic wake deflection model with the time delay calculated from the wake velocity profile.

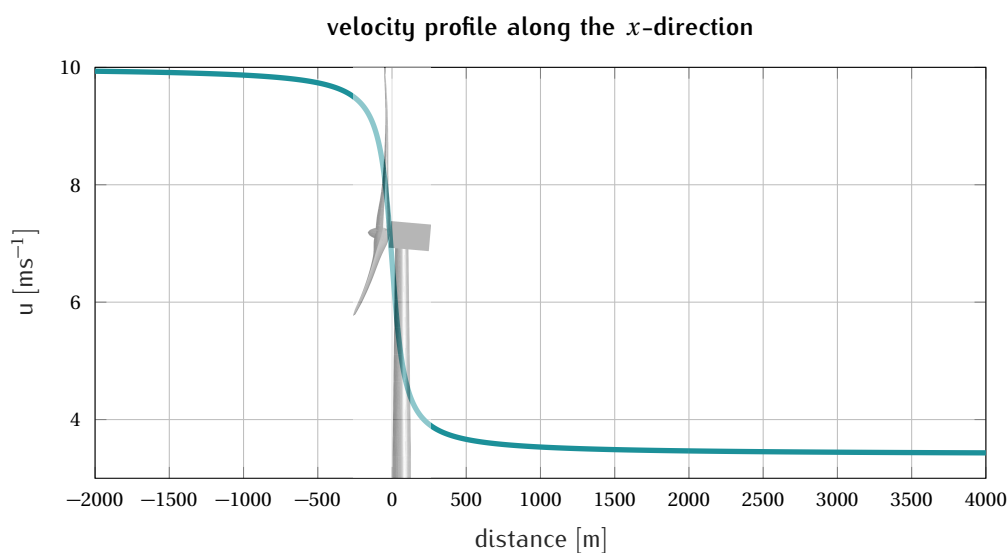


Figure 5.5: Example velocity profile along the x -direction of a wind turbine at 10 ms^{-1} inflow wind speed according to the approximation (5.17).

where d is the downwind position at which the wake center is estimated and $x(t)$ is the position at time t . This yields the model

$$\delta_{\text{yaw,Profile}}(t) = \delta_{\text{yaw}}(d, \gamma(t - \tau_{\text{Profile}})). \quad (5.19)$$

Having introduced time delay approximation for the wake redirection dynamics, in the next step, linear dynamic models are derived.

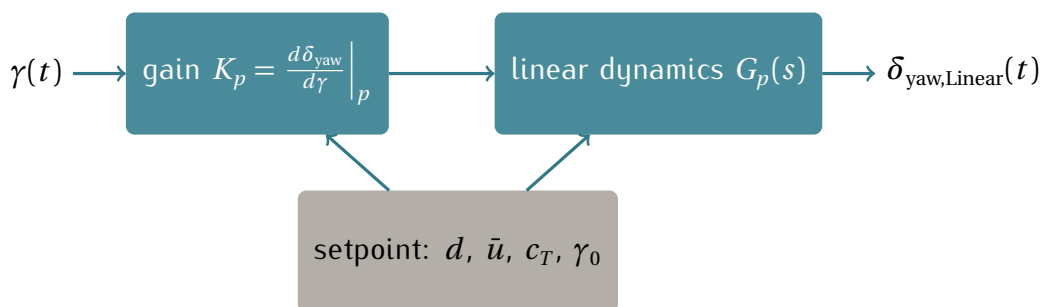


Figure 5.6: Flow chart of the dynamic wake deflection model with linear dynamics and setpoint dependent gain.

5.4.3 Linear dynamic wake deflection models

Since in reality the flow is not behaving like a time delay, an extension to dynamic models is proposed. The model is used for controller design and analysis and thus, a linear model is desirable. It consists of a dynamic system which is coupled to the gain of the linearization (5.13). Figure 5.6 presents the general overview on the linear parametric model. The advantage of this representation is the direct applicability in controller design. With a given setpoint $p = [d, \bar{u}, c_T, \gamma_0]$ the linear model can be expressed in the Laplacian space

$$G_{\text{yaw,Linear}}(s) = K_p G_p(s) \quad (5.20)$$

with K_p the linear wake deflection gain and $G_p(s)$ a linear transfer function. There are different ways of deriving the components of (5.20). One way is to use assumptions on the different parts, *e.g.* the wake deflection function of [46] and actuator and delay dynamics lumped in $G_p(s)$ as done in [73]. A second possibility is to parametrize the dynamics with wake redirection simulations or experiments. This methodology has been successfully applied in [79, 80] in simulation and is presented in the following.

5.4.4 Model parametrization

Model parametrization is a possibility for obtaining the parameters of derived model realizations. Open-loop experiments, either simulations or on the real wind turbine, need to be performed to estimate the model coefficients and parametrize the model. In the following, a model parametrization of (5.20) is performed. Wake redirection simulations are conducted to obtain output responses to input steps. They are used in a gray box identification procedure to parametrize the controller design model.

General setup of the model parametrization

The simulations are performed within the two-dimensional flow model WFSim. A single turbine is simulated with homogeneous inflow conditions. The simulated wind turbine is a NREL 5 MW reference wind turbine with a rotor diameter of $D = 126$ m. The alignment of the turbine is changed by yawing the turbine. A feasible way to determine the system dynamics is to analyze step responses of the system. A step on the input, the yaw actuator, is applied and the output, the estimation of the wake position at $2.5D$ downstream of the wind turbine, is recorded. Figure 5.7 shows an example of a step response of the wake, with a yaw step of 5 deg. The step responses can be used for the estimation of the wake deflection dynamics because a step input excites specifically those dynamics we want to control.

In this work, several step simulations are conducted to estimate the dynamics for different operational conditions. For the estimation, the steady state from the input and output is removed. First, different yaw setpoints are considered at the same wind speed. Then, the simulations are repeated for different wind speeds in order to estimate the dynamics at different wind speeds.

There are several methods to obtain a model from input-output time simulations. Here, a methodology with a predefined number of poles, zeros, and a time delay is used. The method is part of the Model Identification Toolbox of Matlab and yields a continuous transfer function. For more information on the methodology of the model identification see [81]. The Bode analysis in figure 5.8 shows the model obtained by the identification of the example step.

Model parametrization for different yaw setpoints

In the following, nine step responses are analyzed. They are obtained with five degree yaw actuation steps as inputs on different initial values of the yaw angle from -20 deg to 20 deg. Figure 5.9 shows the Δ position of the wake with respect to the initial value. The Δ in the wake position is used to visualize the differences in dynamic and steady-state at the different initial yaw angles. Further, all responses show non-minimum phase behavior (inverse response behavior) that limits the achievable closed-loop bandwidth. Sources of the inverse response behavior might be the change in pressure and velocities due to the change in flow and energy extraction of the wind turbine. However, to answer this question it needs to be addressed in detailed studies in a high fidelity model.

For each recorded step response, a model identification is conducted with a predefined model structure to parametrize the model of (5.20). The number of zeros and poles are chosen in a way such that the identification results in a normalized root mean square error less than

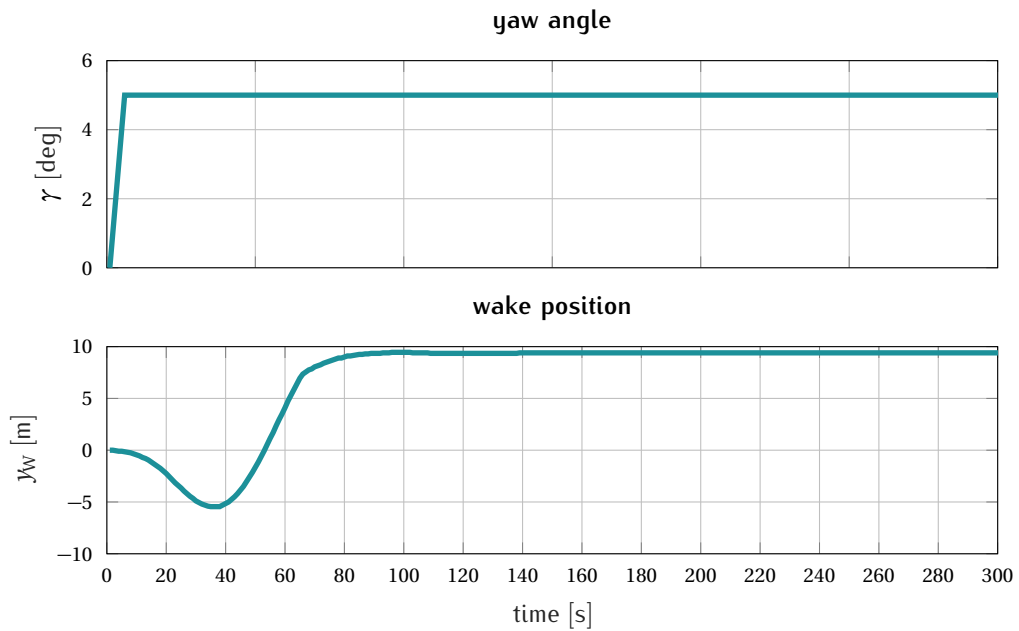


Figure 5.7: Step response of five degree step in the yaw actuator at an inflow wind speed of 8 ms^{-1} . The wake position is estimated at a distance 2.5 times the rotor diameter downwind of the wind turbine.

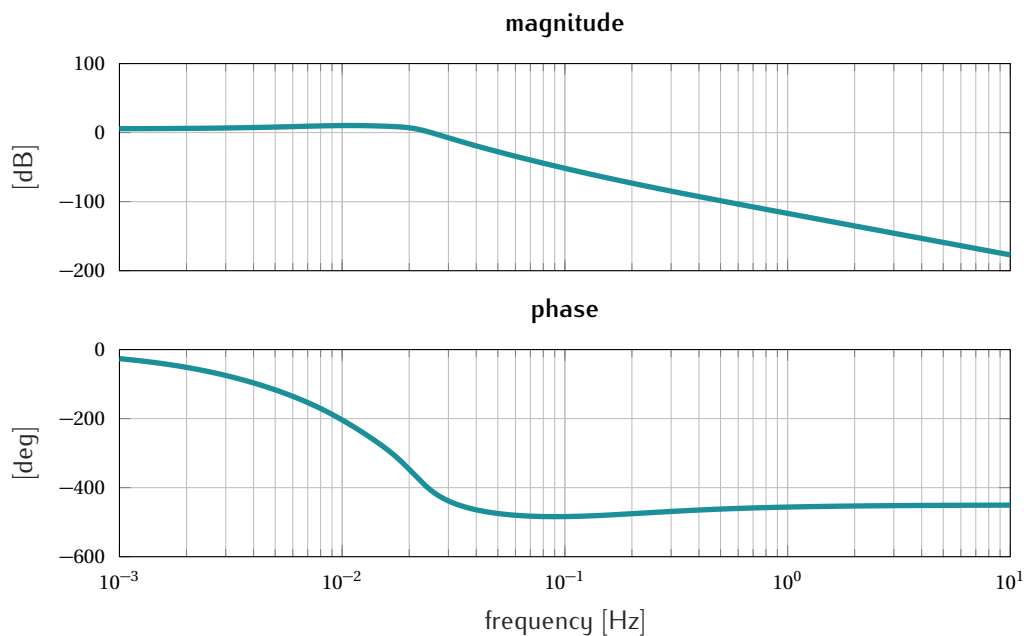


Figure 5.8: The Bode analysis of a model obtained from the example step of Figure 5.7. The settings for the parametrization are 5 poles, 2 zeros, and no delay.

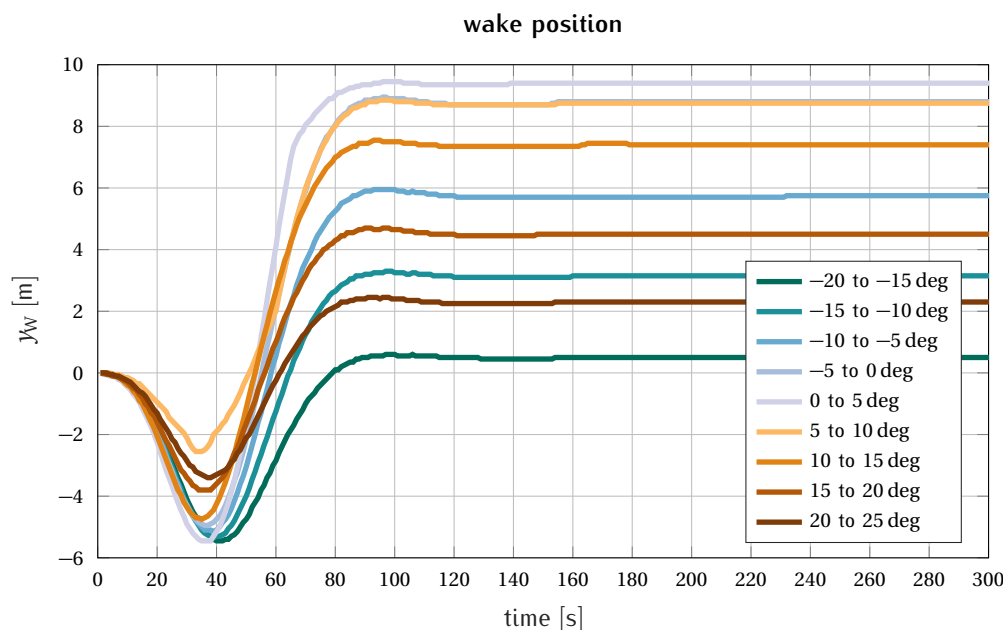


Figure 5.9: Step responses at different initial yaw angles (from -20 deg to 20 deg). The delta position is plotted to visualize the differences in dynamic and steady-state.

0.005 between model response and recorded output. The parameters of the identification are $n_z = 2$ (the numbers of zeros), $n_p = 5$ (the number of poles), with no additional time delay.

The identification yields a set of models of the form

$$G_{\text{yaw,Linear},i}(s) = K_{pi} \frac{(n_{i1}s + 1)(n_{i2}s + 1)}{(l_{i1}s + 1)(l_{i2}s + 1)(l_{i3}s + 1)(l_{i4}s + 1)(l_{i5}s + 1)} \quad (5.21)$$

with $-l_{ij}^{-1}$ the poles, $-n_{ij}^{-1}$ the zeros, and K_{pi} the static gain of the identified model $G_{\text{yaw,Linear},i}$. The Bode analysis in figure 5.10 shows the differences of the parametrization, the different static gains. An example for the location of the zeros and the poles of three models are given in figure 5.11.

Model parametrization for different wind speeds

As a next step, the dependency of the dynamic wake direction model on different wind speeds is analyzed. Therefore, the model parametrization is repeated for different wind speeds and analyzed. The different modeling approaches and analysis of section 5.4.2 clearly indicate the dependence of the dynamics on the wind speed. Thus, slower dynamics are expected for lower wind speeds and faster dynamics for higher wind speeds. Figure 5.12 compares the response

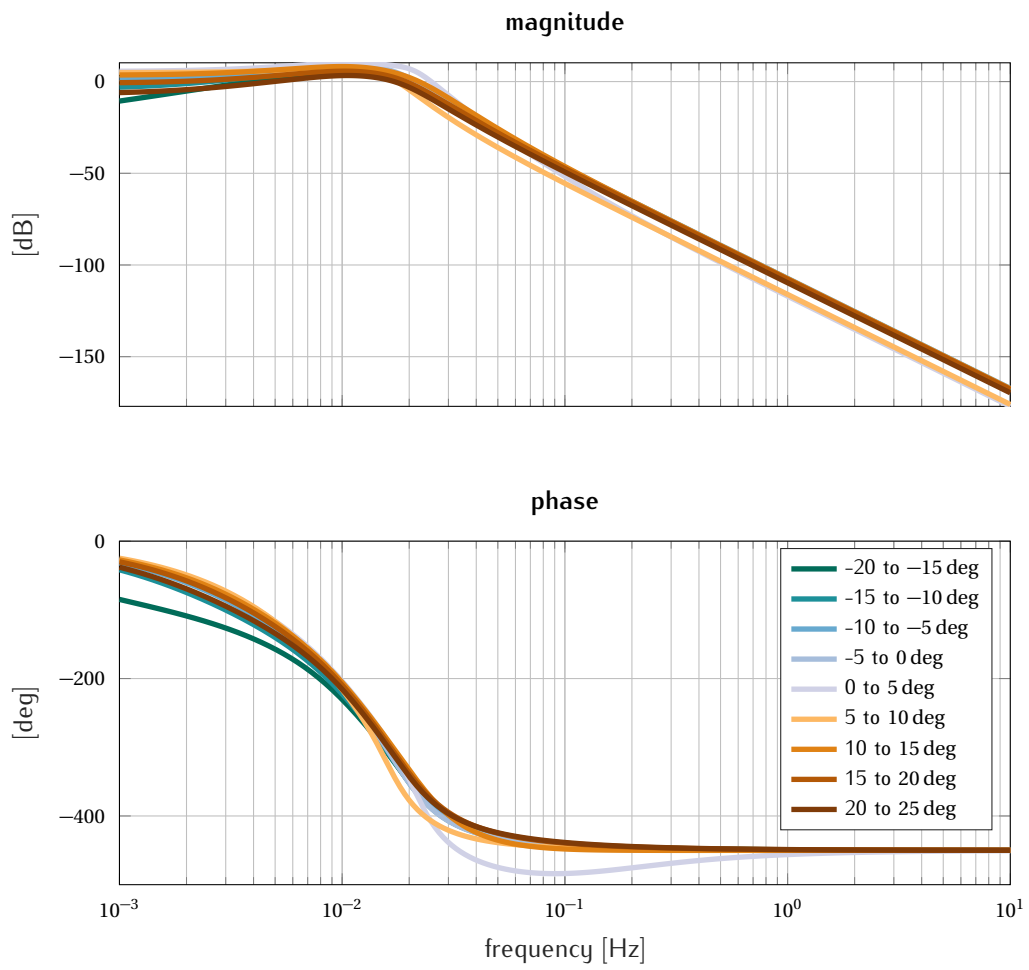


Figure 5.10: Bode plots of all identified models from the step responses of figure 5.9.

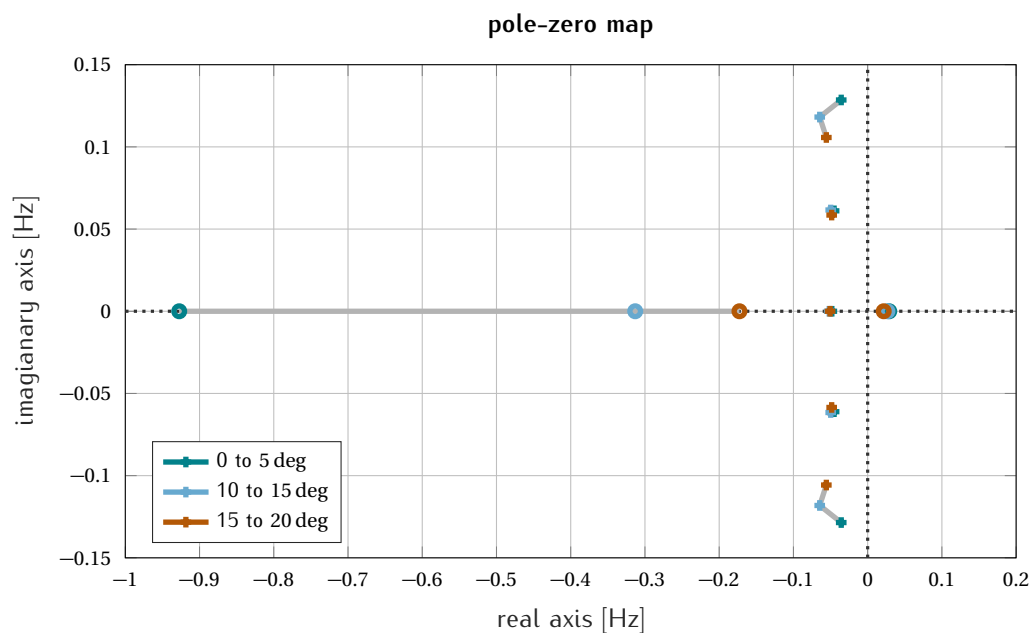


Figure 5.11: The pole-zero map of three identified models.

of the wake position to a step change in the yaw angle of five degrees. First, the difference in dynamic response is visible, however, differences in the steady states are also present. Figure 5.13 gives the Bode analysis of the parametrized models. The differences in the dynamics of the two models can also be seen there.

5.4.5 Linear parameter-varying wake deflection model

Analyzing the results of the previous section shows the differences in the dynamics and the gain of the model. Furthermore, the dependency on wind speed and yaw angle setpoint have been shown. For this reason, in the following the dependency is included in the linear dynamic model description by Linear parameter-varying (LPV) modeling.

LPV models form a special class of nonlinear models, see [82]. The basic idea is to approximate a nonlinear model with a linear model with varying parameter, $p(t)$. To obtain the actual model, the parameter is estimated or measured. This results in a set of linear models which are scheduled by the parameter. Thus, the LPV model can be used to design controllers using a classical linear controller design methodology for each model. Then, the total controller is scheduled by the parameter. Consider [82] for more information on LPV systems and control.

The analysis of the parametrization shows that the model gain depends on the yaw angle, see figure 5.9 and figure 5.10. Furthermore, the system dynamics, especially the dominant

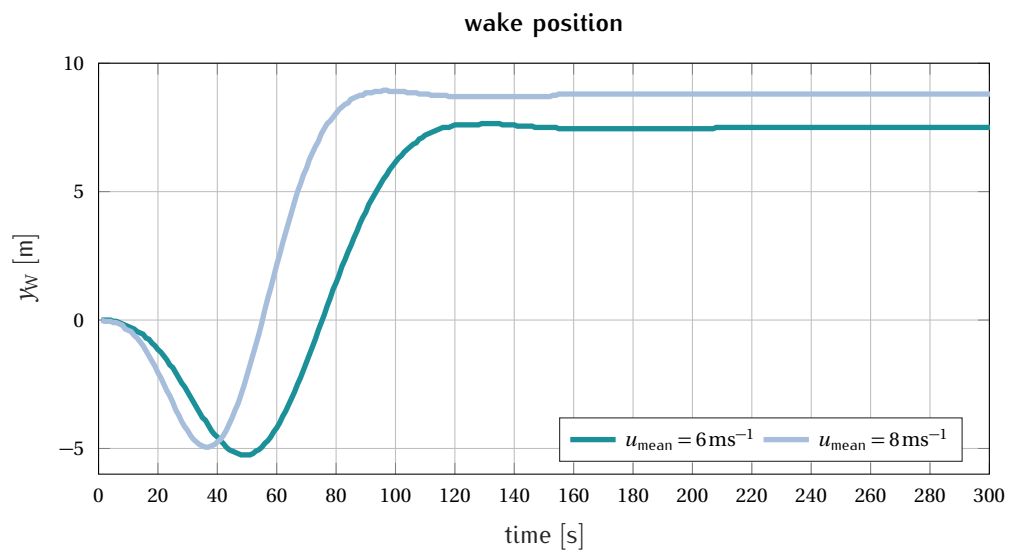


Figure 5.12: Comparison of the wake position response to the same yaw actuator step of five degree at 6 ms^{-1} and 8 ms^{-1} mean wind speed.

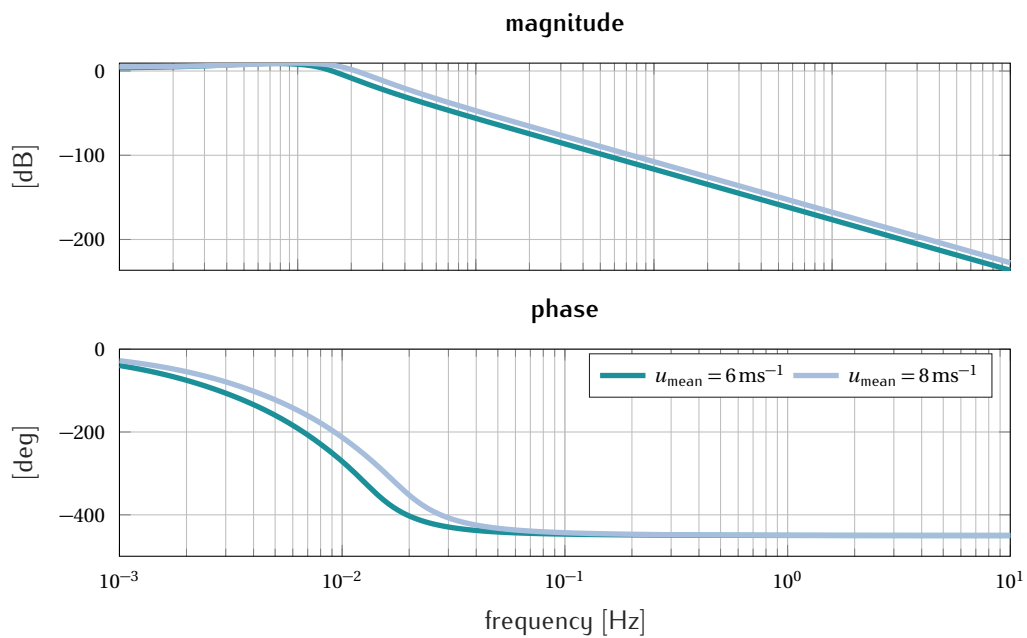


Figure 5.13: Bode analysis of the two step responses with mean wind speeds of 6 ms^{-1} and 8 ms^{-1} .

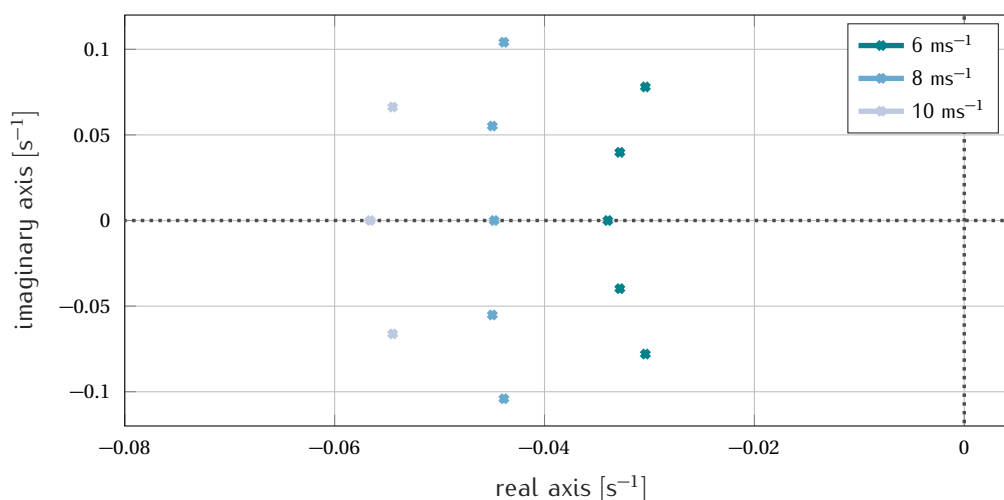


Figure 5.14: The poles of the linear wake redirection model for different wind speeds. The models are derived with a yaw angle of 5 deg.

time constant of the system, depend on the wind speed, see figure 5.12 and figure 5.13. Figure 5.14 gives the poles of the linear models at different wind speed setpoints. The models have the form of (5.21) and are obtained at a yaw angle of 5 deg. The analysis shows the shift of the poles for increasing wind speeds. The yaw and wind speed dependencies are included in a LPV model for wake redirection. A yaw dependent gain $K(\gamma)$ is introduced which covers the yaw dependency. For including the wind speed dependency of the dynamics, the zeros and the poles of the model are wind speed dependent. This modification yields

$$G_{\text{yaw,LPV}}(s) = K(\gamma) \frac{(n_{i1}s + 1)(n_{i2}s + 1)}{(l_{i1}(v)s + 1)(l_{i2}(v)s + 1)(l_{i3}(v)s + 1)(l_{i4}(v)s + 1)(l_{i5}(v)s + 1)} \quad (5.22)$$

with $(-l_{ij}(v))^{-1}$ the wind speed dependent poles, $-n_{ij}^{-1}$ the zeros, and $K(\gamma)$ the yaw dependent gain.

5.5 Conclusions and recommendations

This chapter has presented several main aspects on reduced order wake modeling for estimation and wake redirection control purposes. Models have been derived for the main effects of the wake: the wake deficit, the wake evolution, and the wake deflection. Static and dynamic models of wake deflection have been studied and different types of models have been ana-

lyzed. Finally, a linear model parametrization of dynamic wake deflection was performed for different setpoints and different wind speeds.

In order to use the time delay models for controller design, the Padé approximation can be used to obtain a dynamic approximation of the time delay, see [83]. A different possibility is to use the nominal model and consider the time delay indirectly in the controller design by adjusting the design performance.

The ideas of model parametrization, which was done for the linear model, can easily be translated to estimate the time delays and parametrize the time delay based wake redirection model.

An open question of this study is the inverse output response that was observed in the step simulations (see figures 5.7, 5.9, and 5.12). The source of this phenomenon or its existence in reality is not yet clear. A detailed analysis in a high-fidelity CFD simulation model like SOWFA needs to be performed to investigate this effect. Further, the source of this inverse response behavior needs to be clarified by analyzing velocity and pressure field in detail. An investigation should be performed to answer the relationship between the effect and the wind turbine model. Here, the question would be if the inverse response behavior results from the assumptions in modeling the wind turbine.

6

Lidar-based wake tracking

*Mach mich zum Wächter deiner Weiten, mach mich zum
Horchenden am Stein, gib mir die Augen auszubreiten
auf deiner Meere Einsamsein; lass mich der Flüsse
Gang begleiten aus dem abgetrennt, und hinter einem
blinden Alten des Weges gehn, den keiner kennt.*

— Rainer Maria Rilke

6.1	Objectives and assumptions	74
6.2	Classification of lidar-based wake tracking methods	75
6.3	Model-based wake tracking	76
6.4	Results	79
6.5	Conclusions and possible extensions	80

Lidar technology has opened new possibilities in assessing the wind flow. In some applications like resource assessment the technology has become mature, however, in others, like lidar-assisted control applications the step from being a research topic to an industrial application is currently still in progress.

This chapter presents a new application of using lidar measurements for wind energy control: the concept of lidar-based wake tracking for closed-loop wake redirection. A method is introduced that uses lidar measurements and a simplified wake model to estimate the wake position. This chapter is mainly based on [72] and gives a possible solution to the estimation task that was introduced in chapter 4.

It is structured as follows: First, the background, the objectives and assumptions are described and discussed in section 6.1. Then, different wake tracking techniques are classified in section 6.2. Section 6.3 presents the concept of lidar-based wake tracking and describes the methodology in detail. In section 6.4 wake-tracking results are presented and finally, in section 6.5, a summary is given and possible extensions of the methodology are discussed.

6.1 Objectives and assumptions

As briefly discussed in chapter 4, the concept of closed-loop wake redirection needs wake position information that is used in the controller, see figure 4.1. A lidar system can provide wind speed measurements at different positions in space. Although a lidar device has limitations (see section 2.4), it offers the possibility of measuring wind speed information in the wake of a turbine. For the purpose of lidar-based wake tracking for wake redirection, a downwind looking scanning lidar system is assumed in this work like the one installed in the field testing campaign presented in chapter 3 and shown in figure 3.2. Nevertheless, there are other feasible approaches and setups to estimate the wake position, such as a long range lidar scanning the whole wind farm as depicted in figure 6.1. Moreover, other remote sensing technologies like radio detection and ranging (radar) can be used to estimate the wake position, see [84] and [85].

The main objectives of this chapter are a classification of lidar-based wake tracking methods and a model-based wake tracking method which uses a reduced-order wake model to estimate the wake characteristics.

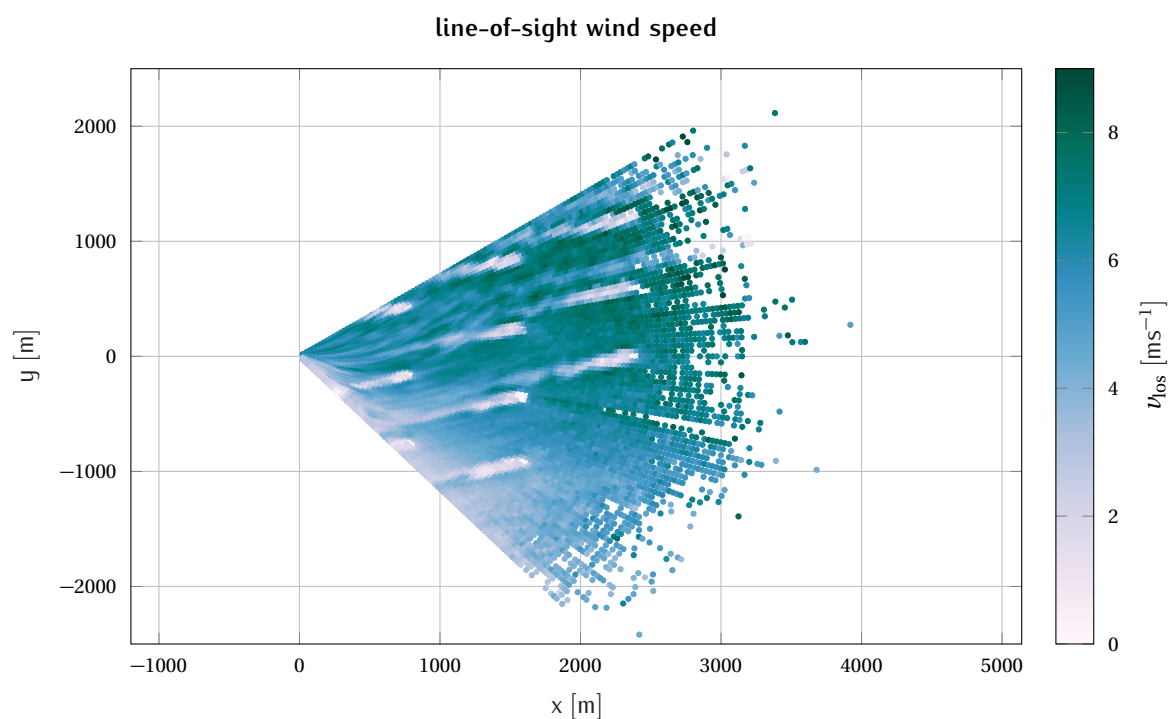


Figure 6.1: A long-range lidar measurement in a wind farm.

6.2 Classification of lidar-based wake tracking methods

As already pointed out, the objective of lidar-based wake tracking is to estimate the position of a wake using lidar measurements. There are different methodologies which approach the task. Generally, they can be grouped in two categories: template fitting methods and wake model based methods. They have their origin mainly in the CFD field since many wake studies and analyses have been performed with CFD. In the following, a short overview on both concepts is given together with examples from both categories.

The general idea of the template fitting methods is that assumptions on the shape of the wake deficit are made, like a Gaussian shape of the wake deficit. The assumption is expressed with a basic function or a basic criteria (the template). In the estimation step, the template is fit to the measurement data by adjusting parameters of the basis function. Examples for the pattern fitting method are the Gaussian method, the double-Gaussian method, and the minimum power method, see [74] for the definitions of the methods. In [86] lidar-based wake tracking with Gaussian and double-Gaussian methodology have shown promising results in tracking the wake. The assumption of a Gaussian shape also agrees with theoretical and experimental findings, see [11]. But there are also other approaches like the contour methodology

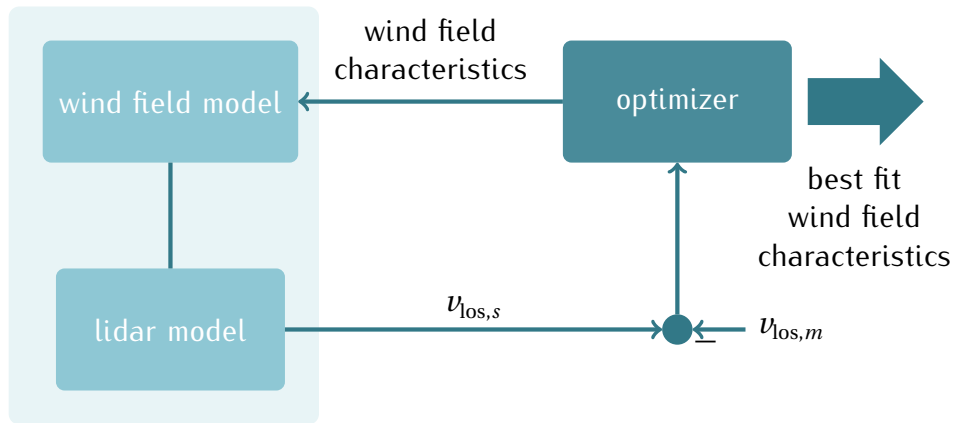


Figure 6.2: The general idea of model-based wind field reconstruction. An optimizer obtains the best fit of wind field characteristic of the wind field model $v_{los,s}$, for the given lidar measurement data $v_{los,m}$.

used in [62] in which all measured velocities within a threshold are grouped and the center of the area of this region is computed to determine the wake position. Later in this work, the Gaussian shape method is used in the LES implementation where the feasibility of the closed-loop concept is shown in a demonstration case.

In contrast, the wake model based wake tracking method uses a wake model and the techniques of wind field reconstruction to estimate the wake center. This method was first presented in [72]. In the next section, the methodology of the wake model-based wake tracking is presented and described in detail.

6.3 Model-based wake tracking

As classified before, the model-based wake tracking method uses a wake model in the estimation of the wake position. In the following, the general concept is presented in section 6.3.1. Then, the model-based wake tracking approach is presented in sections 6.3.2 and 6.3.3, and results are shown in section 6.4. Finally, conclusions and recommendations are given in section 6.5.

6.3.1 Methodology

The methodology of model-based wake tracking was mainly presented in [72]. It applies the general concept of model-based wind field reconstruction as introduced in section 2.5. The general approach of wind field reconstruction from lidar data is to estimate wind field char-

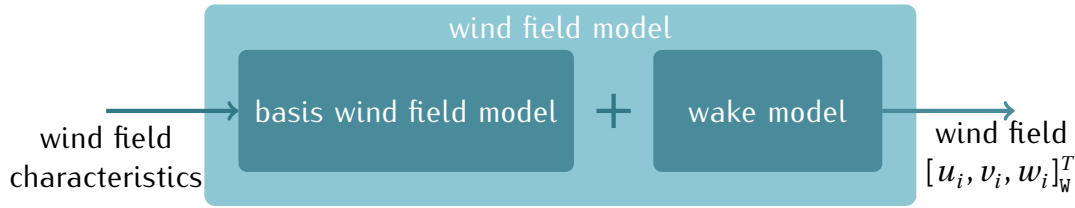


Figure 6.3: Composition of the wind field model for model-based wake tracking.

acteristics from an internal wind field model by fitting modeled (simulated) lidar data to the measured ones. An optimizer is used to obtain the best fit of wind field characteristics for the given measurement data. Figure 6.2 presents the basic idea of model-based wind field reconstruction. For lidar-based wake tracking, the wind field model is expanded with a wake model. In the next section the total model is described.

6.3.2 Model formulation

The concept of wind field reconstruction is used for model-based wake tracking by expanding the wind field model with a wake model. Figure 6.3 shows the composition of the wind field model. The wind field model is described in the wind coordinate system W as introduced in section 2.1.2. The general wind field model can be written as

$$\begin{bmatrix} u_i \\ v_i \\ w_i \end{bmatrix}_W = A_i \Upsilon_{\text{wind}} + F(\Upsilon_{\text{wake}}, x_i, y_i, z_i), \quad (6.1)$$

where in Υ_{wind} and Υ_{wake} the wind field characteristics and the wake characteristics are summarized at the position $[x_i, y_i, z_i]_W$. In the following, the particular wind field and wake models that were used for the approach are described.

Wind model

The basic wind model $A_i \Upsilon_{\text{wind}}$ is a linear wind field model as introduced in (2.14). The simplest wind model considers a homogeneous rotor effective wind speed as defined in (2.15). A necessary addition to that is the consideration of the linear vertical shear since this wind field

characteristic is present in real measurement data. Thus, (2.15) is extended to

$$\begin{bmatrix} u_i \\ v_i \\ w_i \end{bmatrix}_w = \begin{bmatrix} 1 & z_i \\ 0 & 0 \\ 0 & 0 \end{bmatrix} \begin{bmatrix} v_0 \\ \delta_v \end{bmatrix}, \quad (6.2)$$

with v_0 the rotor-effective wind speed, δ_v the linear vertical shear and z_i the z -position in the wind field coordinate system.

Wake model

Following the approach presented in Figure 6.3, a wake model is used to capture the wake effects for the wind field model. The models presented in chapter 5 are used. They cover the main wake effects, the velocity deficit and the wake evolution (see section 5.2), and the wake redirection (see section 5.3). An additional degree of freedom for the optimizer is added by applying a lateral offset to the wake position.

Lidar model

To complete the model description for the model-based wake tracking framework, a lidar model is needed. With the lidar model, the wind field and the wake model are evaluated to obtain a line-of-sight velocity description, similar to what the lidar device is providing. Therefore, the point lidar model described in section 2.4.3 in (2.33) is used.

The total description of lidar measurements in the wake at a defined measurement point $[x_i, y_i, z_z]_I$ is

$$v_{losi} = \frac{1}{f_i} \left(x_{i,I} u_{i,I} + y_{i,I} v_{i,I} + z_{i,I} w_{i,I} \right). \quad (6.3)$$

6.3.3 Model-based wake tracking algorithm

As depicted in figure 6.2 the model based wind field reconstruction method estimates the model parameters by minimizing the error between the measured line-of-sight wind speed $v_{los,m}$ and simulated line-of-sight wind speed $v_{los,s}$. A nonlinear optimization problem results from the n measurement points:

$$\min_p f(x) = \min_p \begin{bmatrix} (v_{los,m,1} - v_{los,s,1})^2 \\ \vdots \\ (v_{los,m,n} - v_{los,s,n})^2 \end{bmatrix}, \quad (6.4)$$

Table 6.1: The free model parameters for the wind field model which are estimated in the optimizer.

underlying wind field		wake model	
v_0	rotor effective wind speed	a	axial induction
δ_v	vertical linear shear	γ	turbine yaw angle
		ϵ	wake dissipation coefficient
		l_y	wake lateral offset

where all free model parameters are included in p . The free model parameters are listed in table 6.1.

6.4 Results

In the following, the feasibility of model-based wake tracking is shown by analyzing a time period of the previously introduced lidar wake measurement campaign at NREL.

6.4.1 Setup and considered measurement data

The measurement setup has already been described in chapter 3. High resolution lidar data is used here to track the wake position. Data from the period from March 28th, 11:30 pm to March 29th, 2017, 12:00 pm are used (12.5 h). A running median of 10 trajectories is applied. This is due to the fact that the wind conditions are more turbulent and the measurement conditions at the NREL site are difficult because of the altitude and a low aerosols concentration in the air. Furthermore, the availability of further downwind measurement positions are generally lower. Because of the bad signal-to-noise ratio, they are often rejected by the processing of the raw lidar data.

As previously described in the general testing procedure in chapter 3, different yaw offsets were applied to the wind turbine to misalign it with respect to the wind direction. In the considered time period, the sequence of yaw offsets is [18, 12.5, -12.5] deg. Each offset is applied for 1 h repetitively. The mean wind speed during the considered time period is 8.1 ms^{-1} and a mean power output of 398 kW is obtained. The availability of the measurements decrease with the measurement distance and is 89% for the first distance, 90% for the second, 88% for the third distance, and 65% and 50% for the fourth and fifth distances. For the estimation of the wake position, only the measurement data of the first three distances are used.

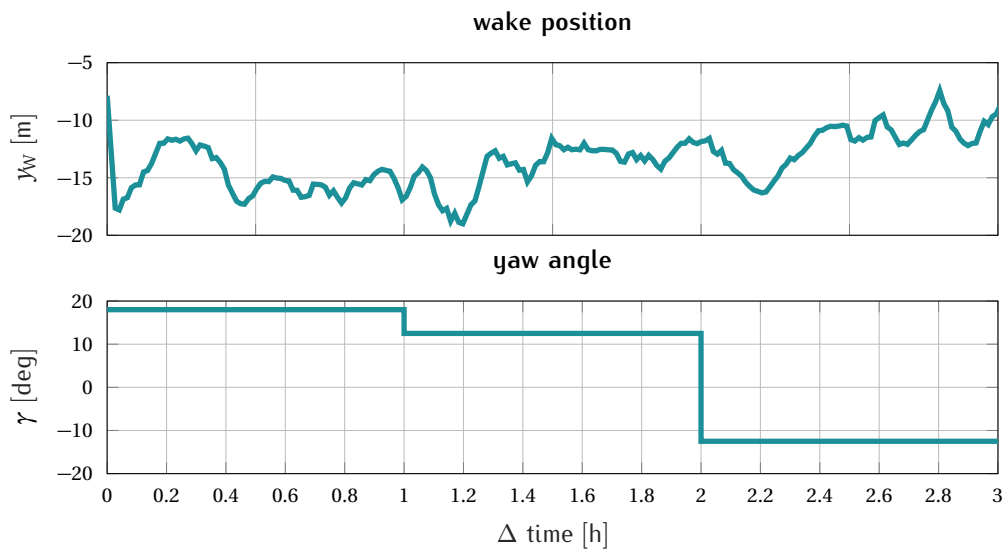


Figure 6.4: The estimated wake position of the considered time period and the applied yaw offsets are shown.

6.4.2 Results of model-based wake tracking

Figure 6.4 shows estimation results of the wake position from the previously described measurement period. A change in mean wake position is visible from the estimation, however, the magnitude and the offset are different to what has been seen in simplified simulation studies. This might be caused by the influence of wind direction changes (the standard deviation of the 10 min averages of the wind direction measurements at the met mast is 8.4 deg) and the change in wind speed over the period (the standard deviation of the 10 min averages of the power output is 106 kW). Especially the wake deflection is less than expected for the last offset (−12.5 deg). This might be caused by a misalignment of the wind turbine to the mean wind direction in this period. Other aspects may have influenced the wake behavior as well. Figure 6.5 is presenting an example of the estimation step of the wake tracking algorithm. In the second row the measurement data is plotted which is used in the estimation. The first row shows the velocity predicted by the fitted wake model. The black dot indicates the estimated wake center position of the estimation step.

6.5 Conclusions and possible extensions

This chapter has presented different aspects of using lidar measurement data to estimate the wake position. A classification of different techniques on lidar-based wake tracking has been

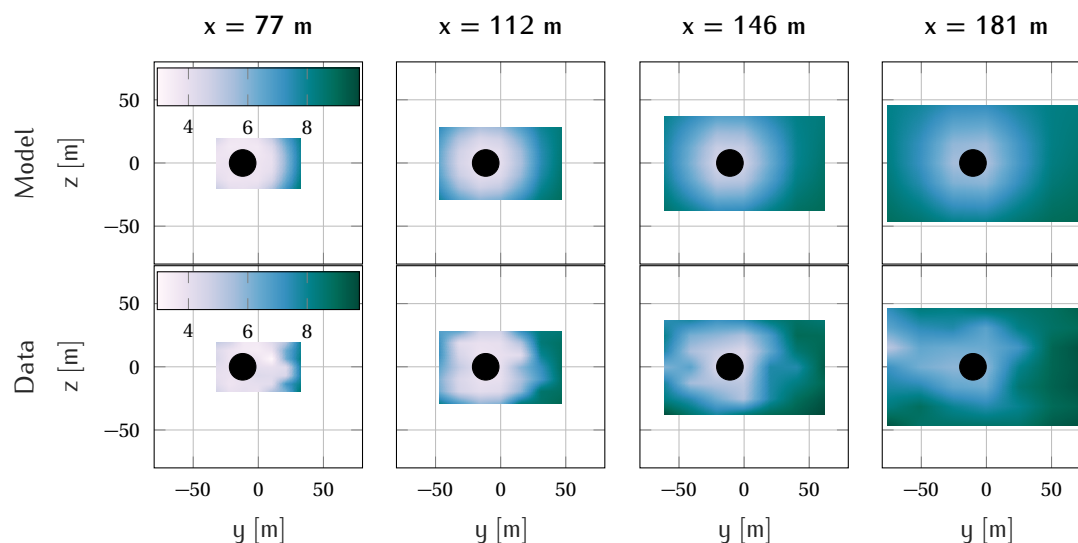


Figure 6.5: An example of an estimation step is shown. In the first row the u -component of the fitted wake model is given. The last row shows the measured lidar data that is used in the estimation step. The black dot indicates the estimated wake center position.

performed. A model-based wake tracking technique has been introduced and described in detail. The approach is to use a reduced order wake model and to estimate the wake by fitting the model to the lidar measurements. The different wake tracking methodologies enable the next steps in realizing a closed-loop wake redirection controller. Moreover, the methodology gives the possibility to analyze the wake behavior based on the chosen wake model.

Extensions in this methodology could be the adaptation of the wake model with more details depending on the meteorological conditions, like turbulence intensity or atmospheric stability. The balance between the convergence to a reasonable solution of the problem and the level of accuracy and therefore the number of parameters is a very important criteria for this methodology. A further development step would be to move to a dynamic model and to design an observer, such as those in [87, 88, 13]. These concepts lead to a more complex reconstruction of the flow field that can be used together with a different estimation method to obtain the wake position.

7

Wake redirection controller design

*Man sieht nur mit dem Herzen gut. Das Wesentliche
ist für die Augen unsichtbar.*

— Antoine de Saint-Exupéry

7.1	Objectives and assumptions	84
7.2	Internal model wake redirection control	85
7.3	\mathcal{H}_∞ wake redirection control	94
7.4	Robust wake redirection control	106
7.5	Conclusions and possible extensions	119

This chapter deals with the development of different controllers for closed-loop wake redirection control. The interest in wake redirection control has grown in recent years since new strategies to increase the power output of wind farms are gaining more and more interest. Several simulation studies have shown the ability to increase the power output of a wind farm by redirecting the wake of wind turbines intelligently, see [37, 57, 19, 10, 18, 58, 22]. As already pointed out in the background chapter in section 2.7.3, the general idea is to misalign the wind turbine with respect to the wind direction to redirect the wake.

This chapter is structured as follows: First, the objectives of the controller development and the general assumptions for the controller design are described in section 7.1. Then, in the following sections, different controllers are developed, an internal model controller in section 7.2, a \mathcal{H}_∞ controller in section 7.3, and a robust controller in section 7.4. Finally, a summary and possible extensions for wake redirection controller design are given in section 7.5.

7.1 Objectives and assumptions

The main objective of this chapter is the development of controllers that enable a closed-loop wake redirection. Figure 7.1 shows the control task and the closed-loop wake redirection framework. The main goal of the control task is to convert the wake center information and the demanded position to a demanded yaw signal. The feedback controller needs to steer the wake to its desired position and compensates for the uncertainties in the models. Since the reaction of a change in the yaw can be measured with a delay, which is due to the wake propagation time, the controller has to be designed in such way that it takes this time delay into account properly.

Important performance criteria to evaluate different controllers and their overall performance are the output sensitivity \mathcal{S} , the complementary sensitivity \mathcal{T} and the controller sensitivity \mathcal{U} . They quantify the influence of the disturbances or references to the output or the controller. With a given plant model G and the controller K , the performance criteria can be evaluated. More precisely, according to [83], the sensitivity \mathcal{S} gives the closed-loop transfer function from an output disturbance to the system output, the complementary sensitivity \mathcal{T} is the closed-loop transfer function from the reference to the output and is further the com-

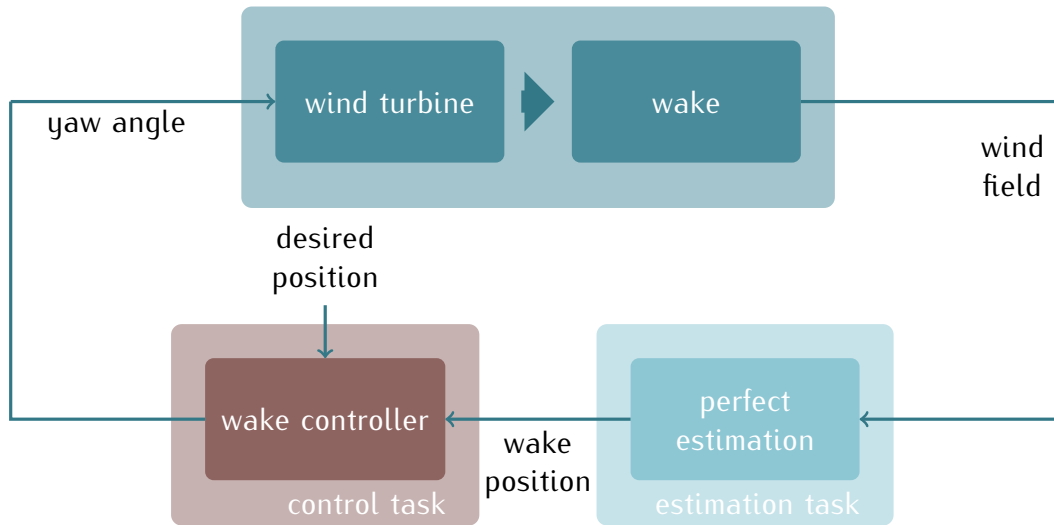


Figure 7.1: The control task in the framework of closed-loop wake redirection control and the assumption of measurability of the wake center.

plement of S , and $-\mathcal{U}$ is the transfer function from the disturbance to the control signal. Thus,

$$S = \frac{1}{1 + GK}, \quad (7.1)$$

$$\mathcal{T} = \frac{GK}{1 + GK}, \text{ and} \quad (7.2)$$

$$\mathcal{U} = \frac{K}{1 + GK}. \quad (7.3)$$

For closed-loop, a good disturbance rejection is desired and therefore S should be small for low frequencies. Further, the control effort should be limited by having a roll-off in \mathcal{T} after the bandwidth.

For the controller design, it is assumed that the wake center is measurable and available to the controller. This helps to separate the control task from the estimation task and to assess the performance of the different controllers.

7.2 Internal model wake redirection control

This section deals with the development of an Internal Model Controller (IMC) for lidar-based wake redirection. The IMC is a predictive controller; for more information on the general concept of IMC see [89]. IMC uses a model of the system in the controller to predict the reaction

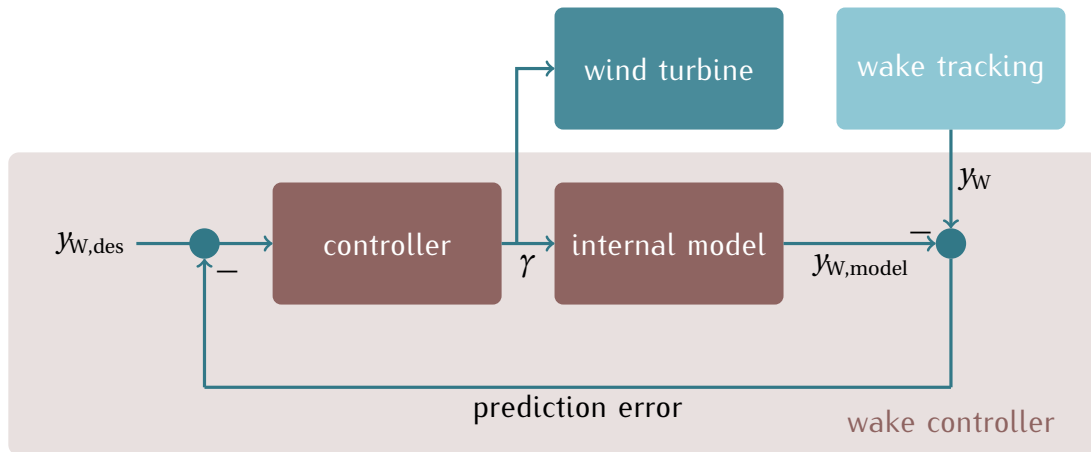


Figure 7.2: The internal model wake redirection controller: the general layout with the controller, an internal model and the reality. The predicted wake center $y_{W,model}$ is compared to the actual wake position y_W and the desired value $y_{W,des}$ and fed back to the controller.

of the system to the input. The IMC therefore consists of a controller and an internal system model. See figure 7.2 for the general layout of the IMC for wake redirection control.

In the following, this controller concept is adapted to the lidar-based wake redirection control task. A controller is designed, analyzed, and tested in the medium-fidelity CFD model WFSim. Part of this work has been presented in [73].

7.2.1 Controller design

In the following, the IMC concept is adapted to wake redirection control. The primary goal of a wake redirection controller is to redirect the wake to a desired position. The IMC uses the reduced order model of the wake position dynamics, described in section 5.4.2 in the controller concept. Because of the dominant time delay, a modification is made to adapt to the time lag. The error feedback is split into an immediate feedback and a delayed feedback of the error. Figure 7.3 shows the modification because of the time delay and describes the proposed controller concept. A filter is needed in the feedback loop to remove uncontrollable frequencies since the wake center dynamics are modeled with a time delay which limits the controller bandwidth. Figure 7.4 shows the internal model that is used in the wake controller with its two outputs, the wake position before the time delay $\tilde{y}_{W,model}$ and the delayed wake position $y_{W,model}$ and its input the yaw angle γ .

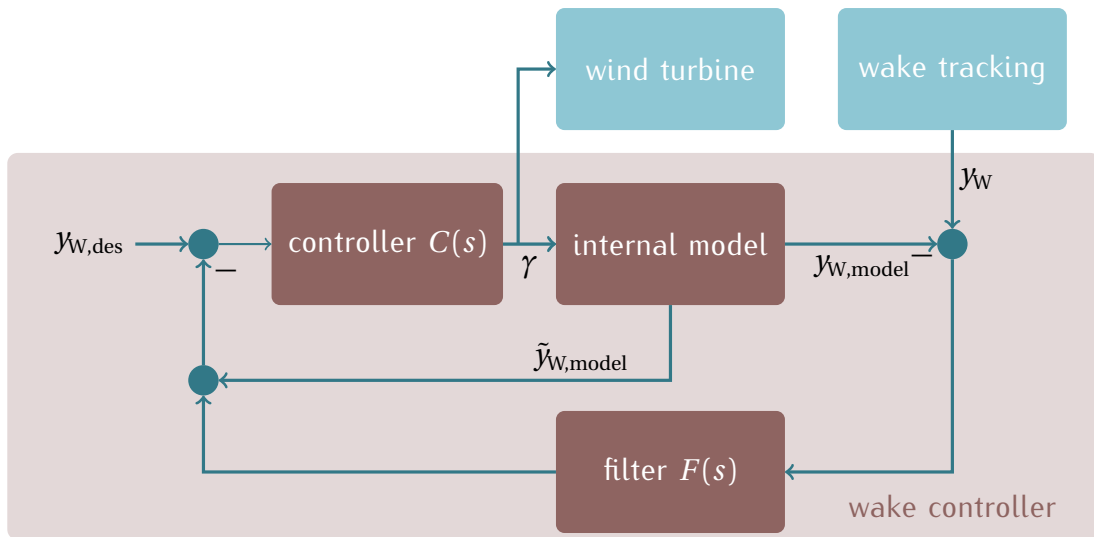


Figure 7.3: The general concept of the internal model controller for lidar-based wake redirection. Two feedback loops are used to compensate the dominant time delay in the system.

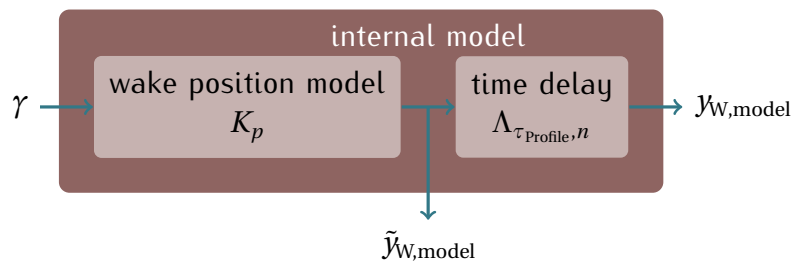


Figure 7.4: The internal model of the wake controller.

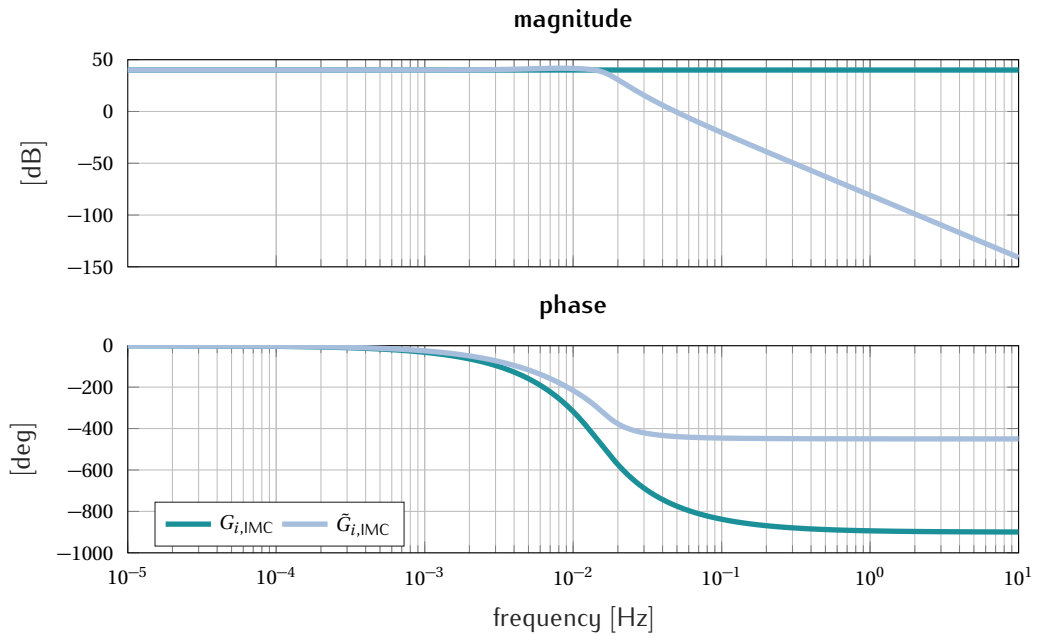


Figure 7.5: Bode plots of the internal controller design model $G_{i,IMC}$ of the IMC and the parametrized linear model $\tilde{G}_{i,IMC}$. For the internal model, the gain was extracted from the model parameterization and a Padé approximation order $n = 5$ was set.

Wake position model

As previously mentioned, the model of section 5.4.2 is used as the internal controller model. The results of the model parametrization of section 5.4.4 are used to estimate the static gain of the model since WFSim is used later to realize the closed-loop wake tracking. The time delay is calculated using the velocity profile behind the wind turbine in (5.18). The time delay is approximated with the Padé approximation for time delays, see [83]. This yields the controller design model

$$G_{p,IMC}(s) = K_p \Lambda_{\tau_{\text{Profile}},n}(s) \quad (7.4)$$

with $\Lambda_{\tau_{\text{Profile}},n}(s)$ the Padé approximation of the time delay τ_{Profile} with system order n and K_p the wake deflection gain. Figure 7.5 shows the Bode plots of an approximated system $G_{i,IMC}$ and in comparison to a parametrized linear system $\tilde{G}_{i,IMC}$, like the one introduced in section 5.4.4. The step responses of both models are shown in figure 7.6.

Controller

Besides an internal model, a feedback controller needs to be designed for IMC. A Proportional-Integral (PI) controller is chosen and designed such that the phase margin is

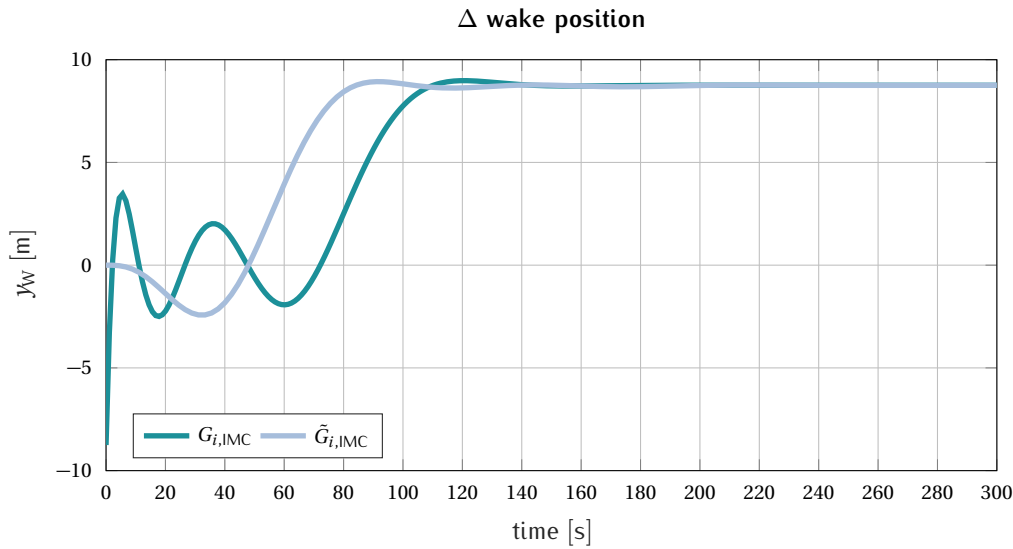


Figure 7.6: Step responses of the controller design model $G_{i,IMC}$ which is used in the IMC and the parametrized model $\tilde{G}_{i,IMC}$ derived in the model identification.

60 deg and a closed-loop bandwidth of $\omega_{CL} = \frac{1}{2\tau}$ is achieved. With the proportional constant H_p and the integral time constant H_i , the transfer function of the PI controller $C(s)$ is

$$C(s) = H_p \left(1 + \frac{1}{H_i s} \right). \quad (7.5)$$

The wake controller stabilizes dynamics up to ω_{CL} , however, wake meandering effects at higher frequencies are not well damped. To avoid high frequency actuation, the filter is used to suppress those control actions. Since the time delay depends on the mean wind speed, see section 5.4.2, the filter is designed to be adaptive with respect to the time delay τ .

Adaptive Filter

The filter depends on the time delay τ which is a function of the mean wind speed \bar{u} and the distance behind the wind turbine in which the wake position is measured (see time delay τ_{Taylor} in (5.16) or $\tau_{Profile}$ in (5.18)). Therefore, the filter is designed to damp all uncontrollable frequencies by setting the cutoff frequency to $\omega_c = \frac{\pi}{2\tau}$. A second order Butterworth low-pass filter is designed which yields

$$F(s) = \frac{1}{(s\omega_c^{-1})^2 + \sqrt{2}(s\omega_c^{-1}) + 1}. \quad (7.6)$$

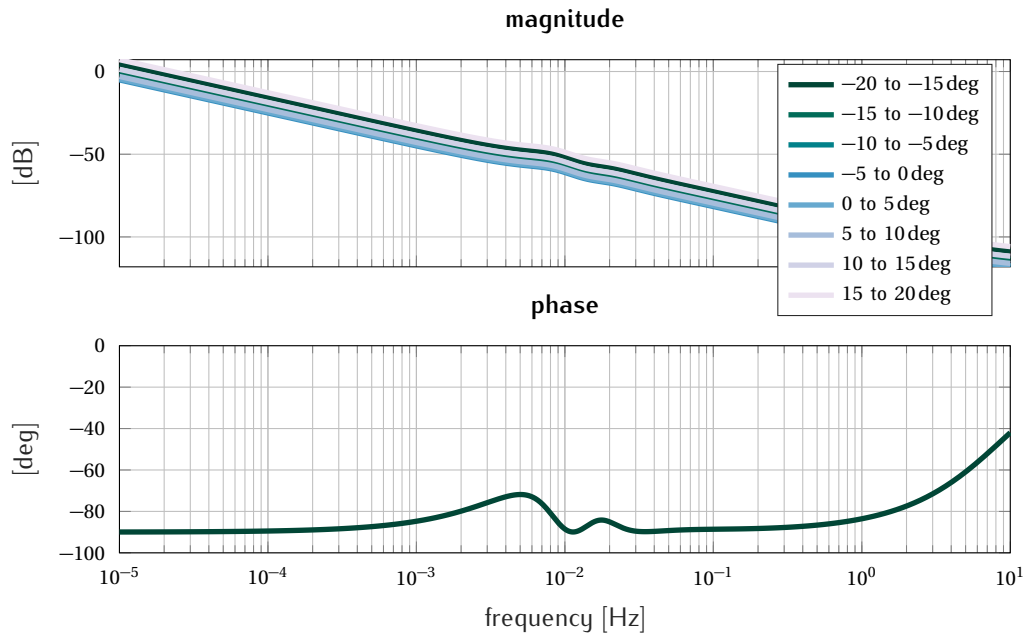


Figure 7.7: Bode plots of the IMC at different yaw angle setpoints at 8 ms^{-1} wind speed. All phase plots are identical.

7.2.2 Controller analysis

In the following, the IMC is analyzed and nominal simulations are performed. For the performance analysis of the IMC, the total controller transfer function needs to be derived. It includes all elements of the IMC as indicated in figure 7.3. Merging them the controller $K(s)$ becomes

$$K(s) = \frac{C(s)}{1 + C(s)K_p(1 - F(s)\Lambda_{\tau_{\text{profile},n}}(s))}. \quad (7.7)$$

Since the dynamics of the internal model (7.4) only depend on the wind speed, controllers for particular wind speeds only differ in the gain K_p . This can be seen in the Bode plots of $K(s)$ in figure 7.7. The sensitivity \mathcal{S} and controller sensitivity \mathcal{U} are shown in figure 7.8. Since the plant dynamics do not change for different setpoints, the sensitivities for all controllers at 8 ms^{-1} wind speed are equal. The controller sensitivities differ because of the different gains in the controllers. The sensitivity shows a good damping behavior for the low frequencies and no overshoots because no peaks exist in the sensitivity. The controller sensitivities show activity for low frequencies and enough roll-off at higher frequencies.

In order to verify the performance in time simulations, first a nominal step simulation is performed, which means the controller is applied to the controller design model and a step on the desired wake position is applied at 100 s. In a second simulation, an output disturbance is

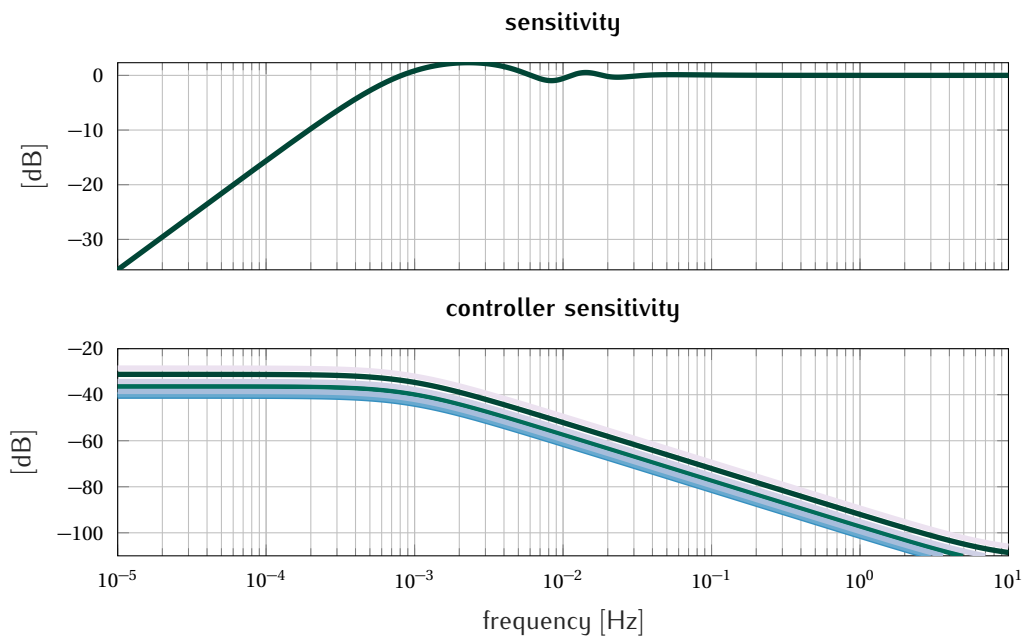


Figure 7.8: Sensitivity \mathcal{S} and controller sensitivity \mathcal{U} analysis of the closed-loop with the IMC controllers at 8 ms^{-1} wind speed. The models and color order are according to the previous figure's setpoints (see figure 7.7).

applied with a random noise signal with zero mean offset. The simulation results are shown in figure 7.9. Finally, an additional output disturbance with a mean offset of 5 m is added which approximates a static model offset between the controller design model and the reality. Figure 7.10 compares the simulation results with the nominal closed-loop behavior. Because of the integral behavior of the controller, the offset is compensated.

7.2.3 Simulation results with a medium-fidelity CFD model

After having derived the IMC and having analyzed it for different setpoints, the controller is applied to a closed-loop wake redirection scenario in WFSim. Two different cases are analyzed to highlight the capabilities and challenges of the controller.

Wake redirection at controller design setpoint

As previously described, the controller is designed at a specific wind speed setpoint $\bar{u} = 8 \text{ ms}^{-1}$, and yaw angle setpoint of 5 deg. Then, the controller is applied to a one-turbine simulation scenario. The wake center is estimated at 3 D behind the wind turbine and different desired wake positions are applied. Figure 7.11 shows the simulation results. As expected,

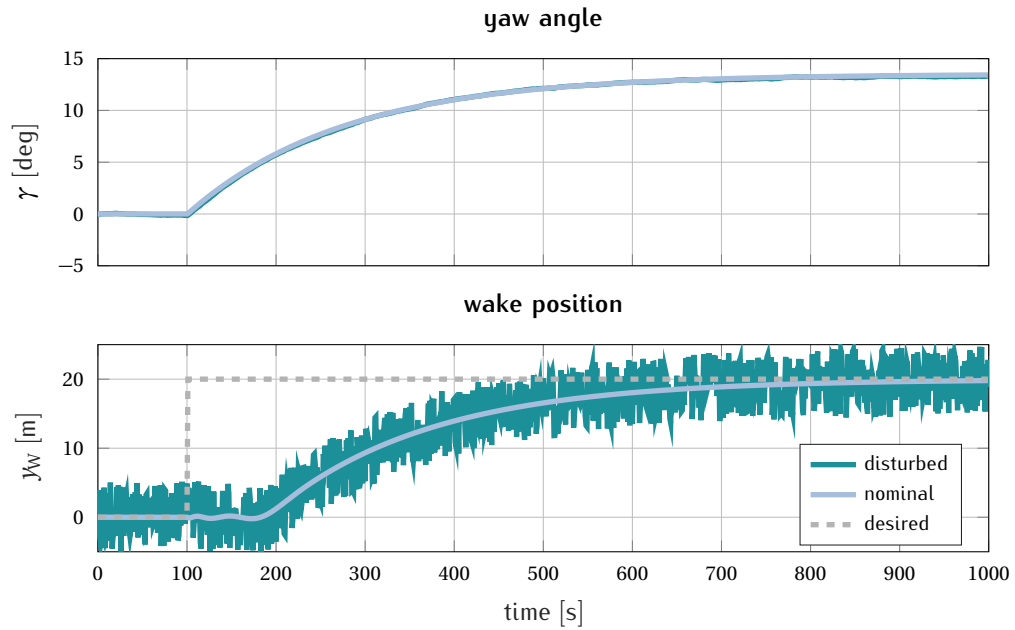


Figure 7.9: Closed-loop time simulation results with the IMC. Comparison of two step response simulations of the nominally controlled system without and with output disturbance.

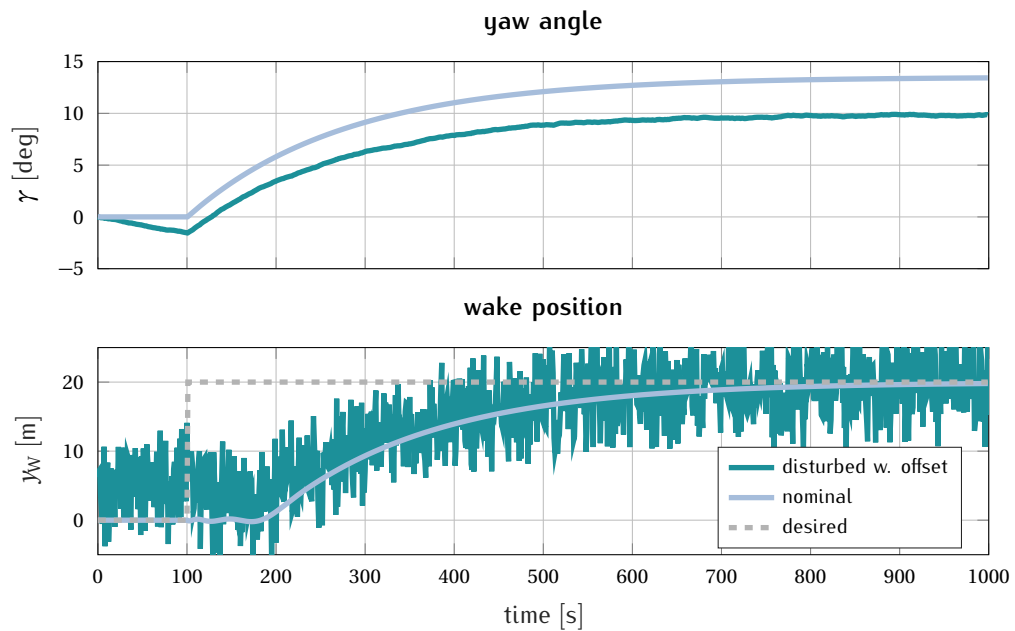


Figure 7.10: Closed-loop time simulation results with the IMC. Comparison of two step response simulations of the nominally controlled system without and with output disturbance.

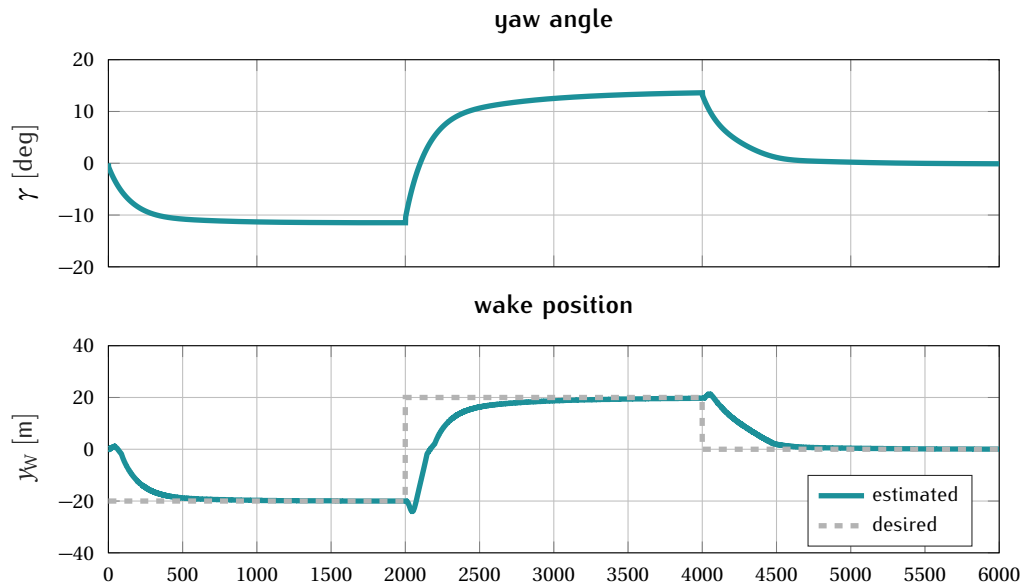


Figure 7.11: Closed-loop wake redirection simulation results obtained with WFSim. The simulation is conducted at a mean wind speed of $\bar{u} = 8 \text{ ms}^{-1}$.

the controller steers correctly the wake to the desired positions, however, because of the different gain at higher yaw angles, the integral behavior of the controller adapt to the nonlinearity. This issue can be solved by designing a gain scheduling over the entire yaw angle region. Figure 7.12 shows two snapshots of the simulation conducted with WFSim with the IMC controller.

7.2.4 Summary and possible extensions

In the last section an IMC for wake redirection was introduced. The general structure of the controller has been described. The internal model and the other parts of the IMC have been presented and discussed in detail. Then, nominal simulations have been performed in an undisturbed and a disturbed scenario. Finally a closed-loop simulation has been performed in WFSim to show its applicability for a control task in a flow simulation environment.

Possible extensions of the IMC wake redirection controller are improvements in the internal model, since the behavior of the IMC strongly depends on the used model. Furthermore, different tuning methodologies for the IMC could be used to obtain a more robust controller tuning, especially when directly considering the delay time in the tuning.

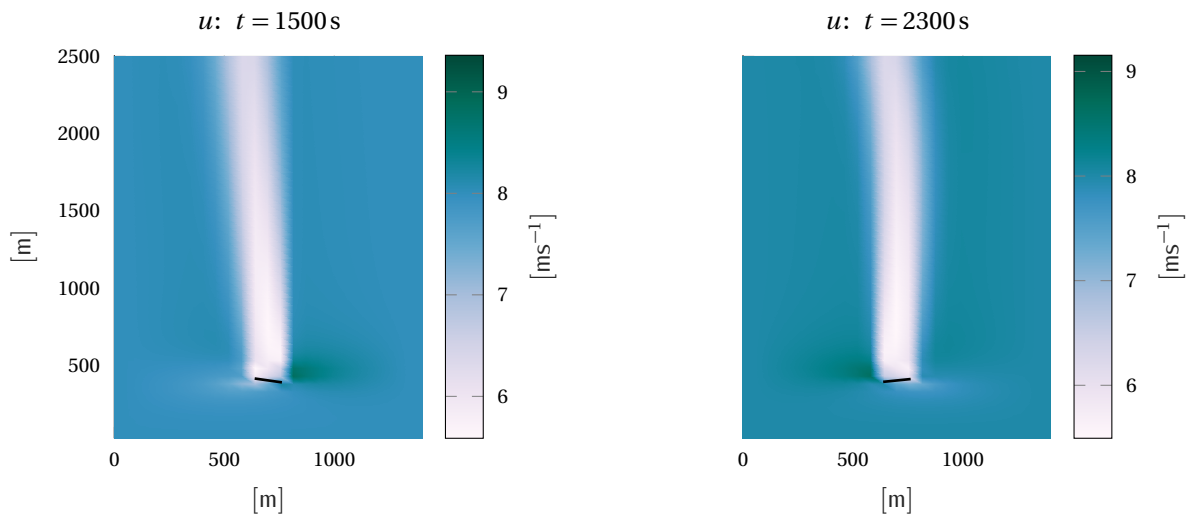


Figure 7.12: Two flow snapshots of the closed-loop simulation using the IMC at mean wind speed of $\bar{u} = 8 \text{ ms}^{-1}$.

7.3 \mathcal{H}_∞ wake redirection control

Having presented a first control approach, an IMC, now in the following, a more systematic controller design approach for wake redirection is presented. An \mathcal{H}_∞ controller design synthesis is used to obtain a wake redirection controller. The advantage of this approach is the possibility to define directly the controller performance in frequency domain. This section presents the procedure and the strategy in developing a \mathcal{H}_∞ wake redirection controller and is an extension to [79].

The section is structured as follows: First, the controller design model is formulated in a structured way in the generalized plant in section 7.3.1. Then the \mathcal{H}_∞ controller is designed in section 7.3.2 and analyzed in section 7.3.3. Simulation results with the medium-fidelity CFD simulation model WFSim are presented and discussed in section 7.3.4. Additionally, in section 7.3.5, the lidar-based wake redirection concept is transferred to an LES simulation tool and the \mathcal{H}_∞ controller is used in a case study. Finally, in section 7.3.6 the approach is summarized and possible extensions are discussed.

7.3.1 Generalized plant

\mathcal{H}_∞ controller synthesis makes use of the general control configuration, shown in figure 7.13, where P is the generalized plant and K the generalized controller. The idea of formulating a general control problem is to minimize a specific norm of the transfer function from input w

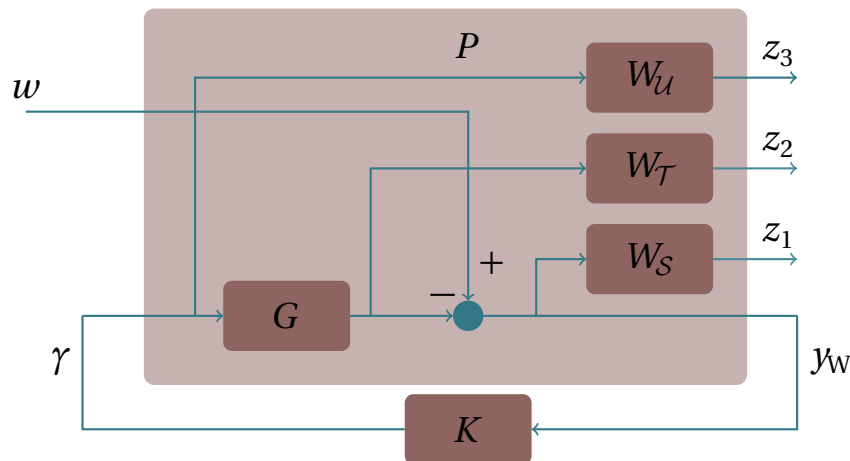


Figure 7.13: Generalized plant P with the performance signals z_1 , z_2 , and z_3 , which give the output of the sensitivity \mathcal{S} , the complementary sensitivity \mathcal{T} , and the controller sensitivity \mathcal{U} , respectively. The input w can represent a desired value or a disturbance, γ is the yaw angle, and y_w the wake position.

to performance output z , see [83], as performance measure. Here, the controller design problem is to find a controller K which minimizes the norm. The input w represents a theoretical disturbance d disturbing the output with $w = -d$, or a reference command r with $w = r$, see [83]. The general plant further provides different weighted performance measures as outputs z_1 to z_3 : of the sensitivity \mathcal{S} , the complementary sensitivity \mathcal{T} , and the controller sensitivity \mathcal{U} , respectively. The generalized plant is typically used to design \mathcal{H}_2 or \mathcal{H}_∞ controllers. The advantages of \mathcal{H}_∞ controller design is mainly the ability of shaping closed-loop transfer functions and setting stability and robustness margins. Furthermore, compared to the IMC approach of section 7.2, the \mathcal{H}_∞ controller design synthesis is a more straight forward approach. In addition to the following description and analyses, it is extended to a robust version considering an uncertain plant model in section 7.4.

For the controller design, an adequate model G is needed that represents well the wake deflection dynamics. In the following, the controller will be designed using the parametric linear model of section 5.4.4. The parametrization of the transfer function is performed as described in section 5.4.4 using step response simulations and a parameter identification.

7.3.2 Controller design

The general plant is used in the \mathcal{H}_∞ controller synthesis to design the controller. The three performance measures for the sensitivity \mathcal{S} , the complementary sensitivity \mathcal{T} and the controller sensitivity \mathcal{U} , see (7.1) - (7.3), are used as system outputs of the generalized plant to

design the controller, see figure 7.13. In the design of the \mathcal{H}_∞ controller, the \mathcal{H}_∞ norm of the generalized plant is minimized. The concept allows directly shaping the closed-loop behavior by applying performance weights on the performance outputs. This yields a controller which fulfills the performance goals when the controller synthesis is feasible.

A controller bandwidth of $\omega_{\text{CL}} = \frac{1}{2\tau}$ is used with the delay time τ_{Profile} , as used successfully in the previous work, like [73] and [79]. The maximum applicable controller bandwidth is also given by the zero in the model when dealing with non-minimal phase models. Having a real positive zero, the maximum controller bandwidth is limited to $\omega_{\text{CL}} = \frac{z}{2}$ which is the frequency at which the frequency asymptote of the magnitude of the inverse plant transfer function crosses 1, (for more information, see [83]).

The performance weights are W_S , W_T , and W_U . They are specified in the following and their usage in the design process is described. $W_S(s)$ is chosen to yield a slope of 20 dB/dec in $|S|$ for the low frequency region as follows

$$W_S(s) = \frac{s/M + \omega_{\text{CL}}}{s + A\omega_{\text{CL}}} \quad (7.8)$$

with the desired closed-loop bandwidth ω_{CL} , A the desired disturbance attenuation inside the bandwidth, and M the desired bound on $\|S\|_\infty$. As indicated, W_S shapes the sensitivity S and is therefore used to minimize the influence of disturbances on the closed-loop output performance.

The complementary sensitivity is neglected by setting $W_T(s) = 0$ since it is indirectly defined by S because of the relation

$$S + T = I. \quad (7.9)$$

The controller sensitivity is penalized at high frequencies by

$$W_U(s) = 75 \frac{1000^2 (s^2 + \sqrt{2}\omega_1 s + \omega_1^2) (s^2 + \sqrt{2}\omega_2 s + \omega_2^2)}{(s^2 + 1000\sqrt{2}\omega_1 s + (1000\omega_1)^2) (s^2 + 1000\sqrt{2}\omega_2 s + (1000\omega_2)^2)} \quad (7.10)$$

with $\omega_1 = 0.05$ and $\omega_2 = 0.1$.

The controller is designed in a way that the weighted \mathcal{H}_∞ norm of transfer functions from w to z_1 , z_2 , and z_3 is minimized. The controller is obtained by minimizing the following mixed

sensitivity problem with respect to the controller K

$$\begin{aligned} \min_K \kappa \\ \text{s.t. } \left\| \begin{array}{l} W_S \mathcal{S} \\ W_T \mathcal{T} \\ W_U \mathcal{U} \end{array} \right\|_{\infty} \leq \kappa, \end{aligned} \quad (7.11)$$

where

$$\left\| \begin{array}{l} W_S \mathcal{S} \\ W_T \mathcal{T} \\ W_U \mathcal{U} \end{array} \right\|_{\infty} = \left\| \begin{array}{l} W_S(1 + GK)^{-1} \\ W_T GK(1 + GK)^{-1} \\ W_U K(1 + GK)^{-1} \end{array} \right\|_{\infty}, \quad (7.12)$$

with κ the bound on the \mathcal{H}_{∞} norm and the weights $W_S(s)$, $W_T(s)$, and $W_U(s)$, respectively.

Since the parametrization of the controller design models has shown different gains for different yaw setpoint values and a changing dynamic behavior for different wind speeds, different controllers would be necessary to achieve the desired performances at each condition. This yields either a scheduled controller or a relaxation of the performance criteria and the usage of a single controller for all conditions. A different approach is presented later where the model differences are described as uncertainty in an uncertainty set and considered in the controller design process. In the following, a single controller is chosen for all conditions, analyzed and applied in nominal medium-fidelity CFD and LES closed-loop wake redirection simulations.

7.3.3 Controller analysis

In the following, an \mathcal{H}_{∞} controller is analyzed in the frequency domain and simulations with the controller design model are conducted. The controller is designed with the bounds described in 7.11. Figure 7.14 shows the Bode plots of the controller. Further, the closed-loop performances, the disturbance sensitivity and the controller sensitivity are evaluated in figure 7.15.

In order to verify the performance in time simulation, first a nominal step simulation is performed, which means, the controller is applied to the controller design model and a step on the desired wake position is applied at 100 s. In a second simulation, an output disturbance is applied with a random noise signal with zero mean offset. The time results are shown in figure 7.16. Finally, an additional output disturbance with a mean offset of 5 m is added which

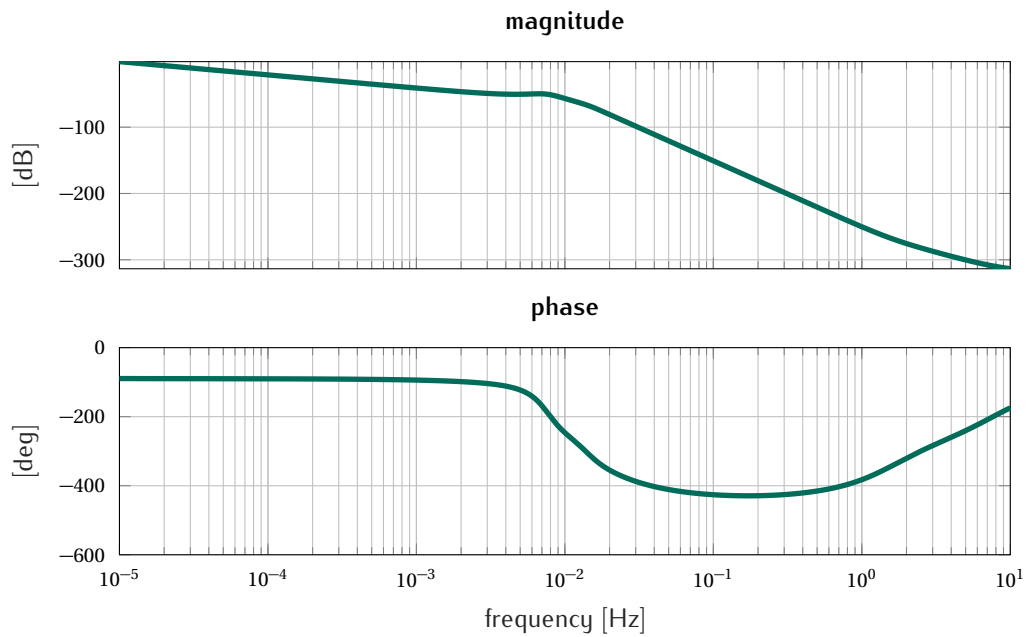


Figure 7.14: \mathcal{H}_∞ wake redirection controller designed at a mean wind speed of $\bar{u} = 8 \text{ ms}^{-1}$ and yaw setpoint of 0 deg.

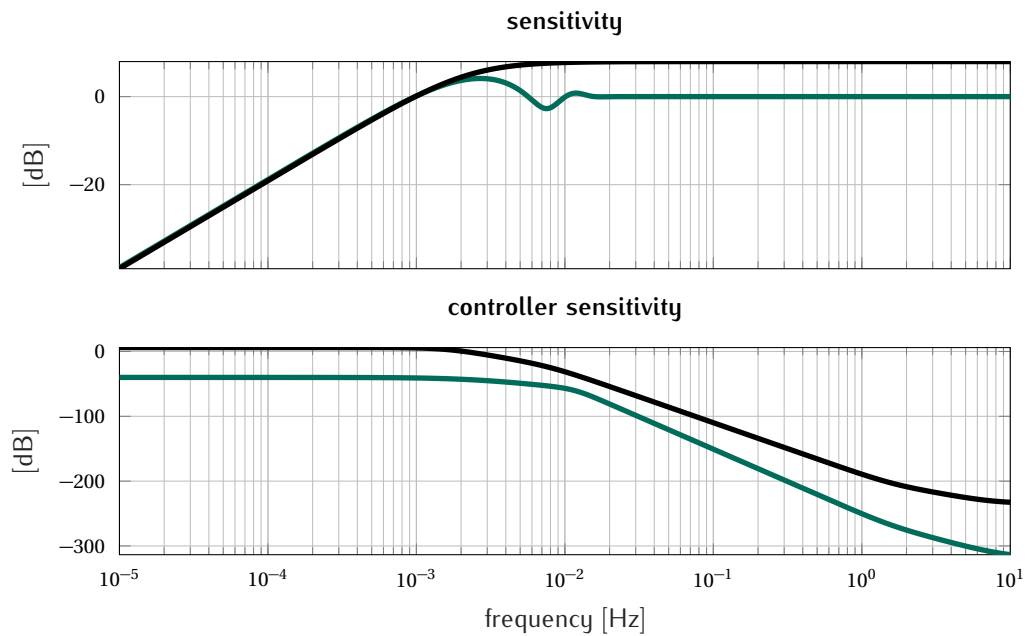


Figure 7.15: Performance evaluation of the controller design: disturbance sensitivity and controller sensitivity. The desired performance boundaries are shown in black.

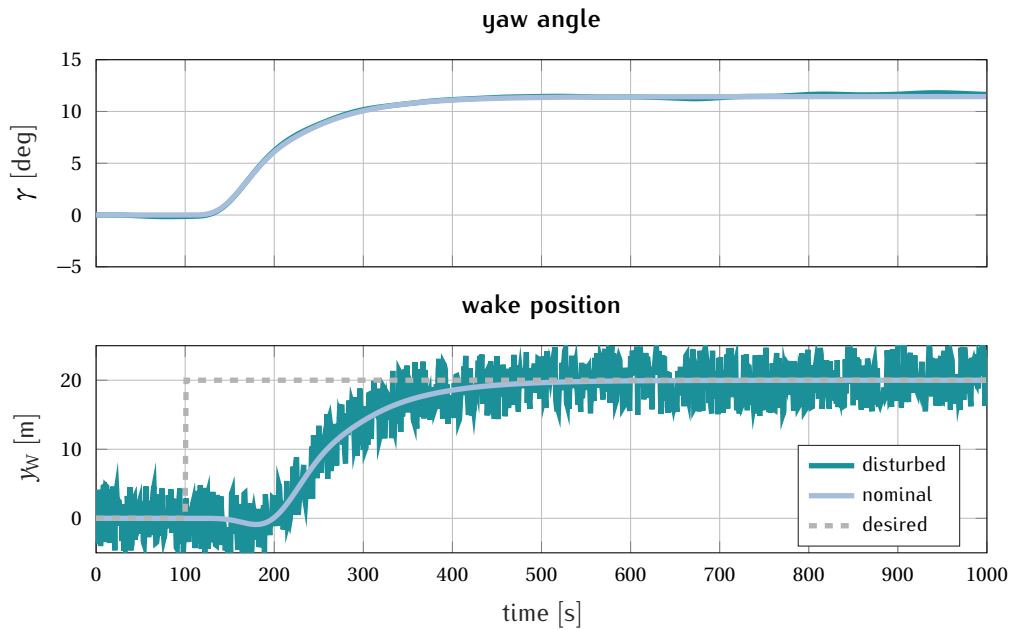


Figure 7.16: Closed-loop time simulation results with the \mathcal{H}_∞ controller. Comparison of two step response simulations of the nominally controlled system without and with output disturbance.

approximates a static model offset between controller design model and reality. Figure 7.17 compares the simulation results with the nominal closed-loop behavior. Because of the integral behavior of the controller, see figure 7.14, the offset is compensated.

7.3.4 Simulation results using a medium-fidelity CFD model

In the following, the \mathcal{H}_∞ controller is applied to closed-loop wake redirection cases in the medium-fidelity CFD simulation model WFSim. Two scenarios are considered: First, a scenario where the controller is used at its design conditions. Second, the controller is used in conditions where a different gain and wake redirection dynamics are present.

Wake redirection at controller design setpoint

The previously designed and analyzed controller is used in WFSim. It was designed at a mean wind speed of $\bar{u} = 8 \text{ ms}^{-1}$ and a yaw setpoint of 5 deg. In the simulation model a homogeneous inflow velocity of 8 ms^{-1} is set. The wake center is estimated at 3 D behind the wind turbine and different desired wake positions are set. Figure 7.18 shows time results of the yaw angle and the estimated wake position. Clearly, the controller steers the wake to its desired position.

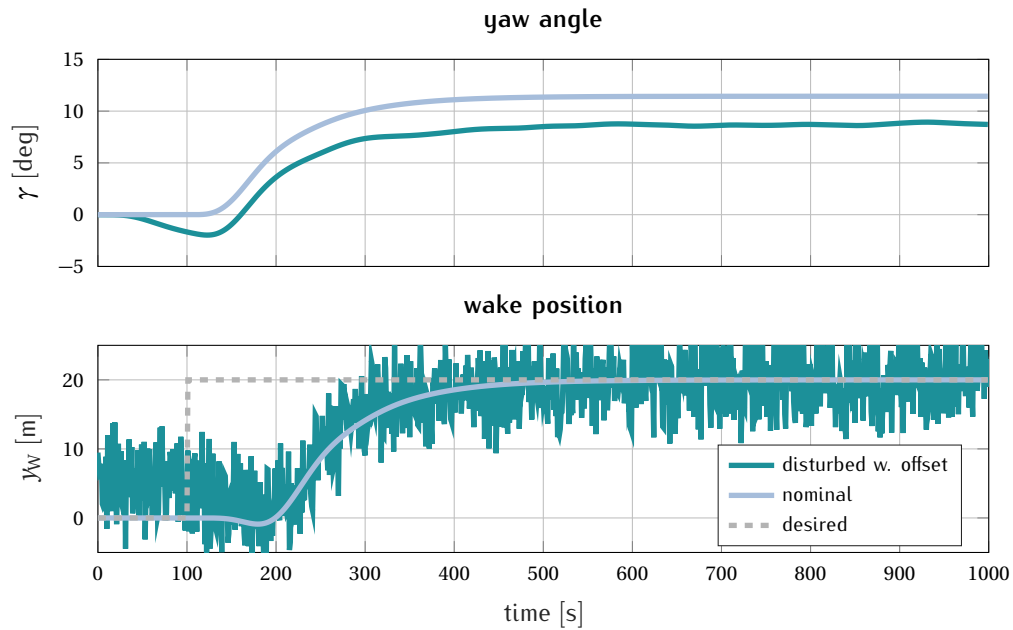


Figure 7.17: Closed-loop time simulation results with the \mathcal{H}_∞ controller. Comparison of two step response simulations of the nominally controlled system without and with output disturbance. An additional offset is added which simulates a model offset.

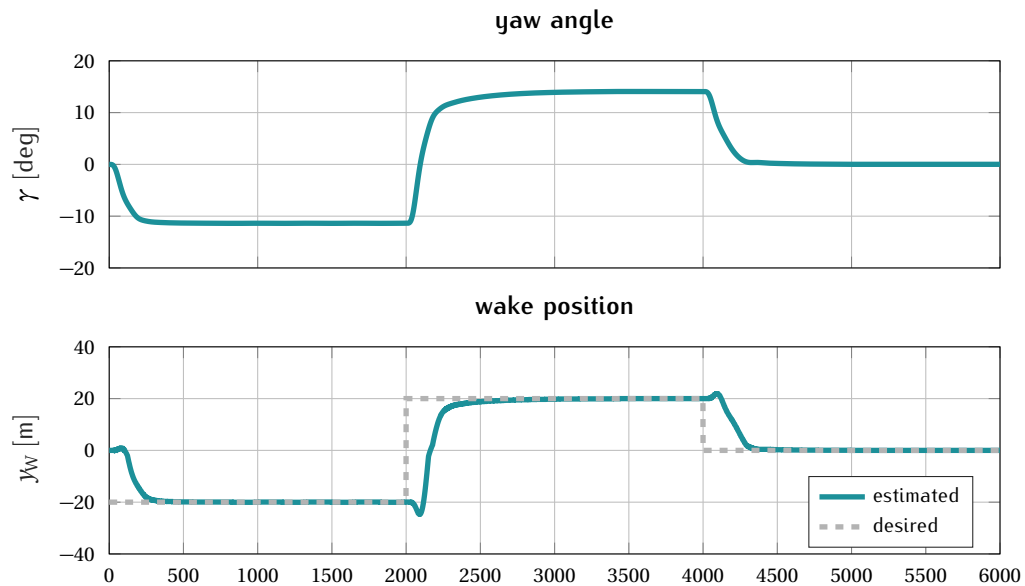


Figure 7.18: Closed-loop time simulation results with the reduced-order CFD simulation model WFSim using the derived \mathcal{H}_∞ controller. The mean wind speed is 8 ms^{-1} and a homogeneous inflow condition is set.

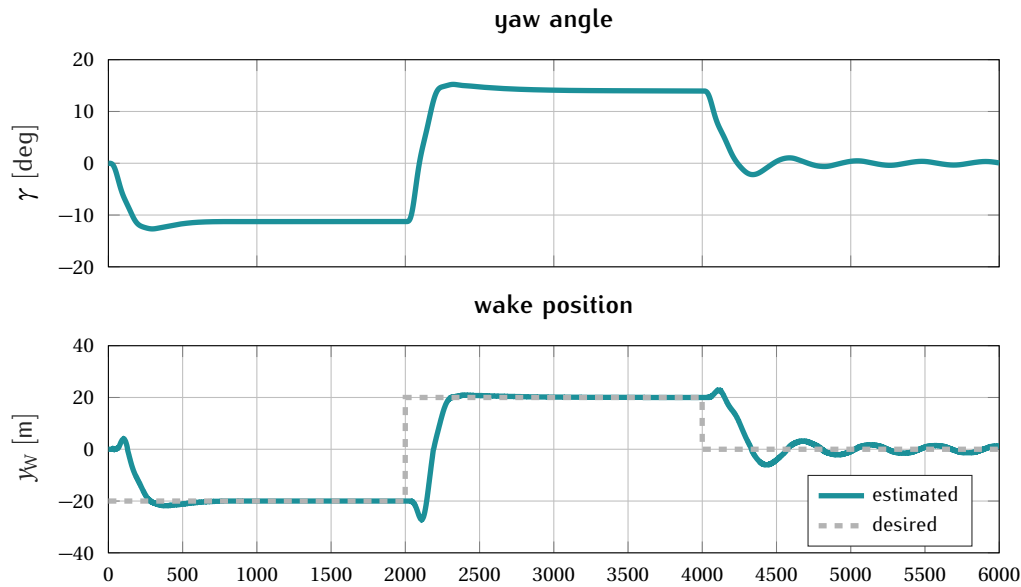


Figure 7.19: Closed-loop time simulation results with the reduced-order CFD simulation model WFSim using the derived \mathcal{H}_∞ controller. The homogeneous inflow wind speed is 6 ms^{-1} .

Wake redirection at different setpoint

As a next step, the controller is used at a different inflow wind speed. Thus, the controller design model that was used to design the controller does not fit to the actual wake redirection dynamics of the simulation case. The controller was designed at a mean wind speed of $\bar{u} = 8 \text{ ms}^{-1}$ and a yaw setpoint of 5 deg. However, in the simulation model a homogeneous inflow velocity of 6 ms^{-1} is set. The wake center is estimated at 3 D behind the wind turbine and different desired wake positions are set. Figure 7.19 shows time results of the yaw angle and the estimated wake position. For the first two desired wake positions the control performance is good, however, for the last desired value at a wake position of 0 m the controller overshoots and oscillates due to the different dynamics between the controller design model and the simulation model. This issue is considered later by using several models in the controller design and introducing a constant offset as model uncertainty.

7.3.5 Simulation results with the LES model PALM

After having used the controller in the medium-fidelity simulation model WFSim, now the lidar-based wake redirection concept is transferred to a three-dimensional LES simulation model. In the following, first, the simulation setup is described. Then, the simulation results are presented and discussed.

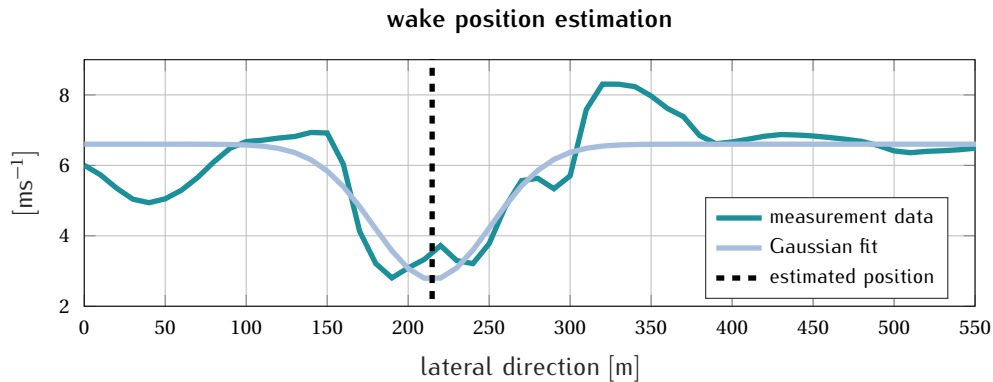


Figure 7.20: An example of how a Gaussian shape function is fit to simulated lidar measurement data, from which the wake position can be derived. The wake center is estimated to be at 214.8 m (dashed black line).

Simulation setup

To demonstrate the concept of lidar-based wake redirection, the methodology is transferred into the LES simulation model PALM [31]. The model is based on the filtered, incompressible Navier-Stokes equations and can represent turbines using the rotating actuator disk model (ADM-R), see [34]. A baseline controller is implemented which operates the wind turbine in normal operation. The yaw angle is commanded by the \mathcal{H}_∞ controller to redirect the wake to a desired position.

In the simulation case, two NREL 5 MW turbines (see section 2.2.4 or [35] for a general description of the turbine) are staggered behind each other. A temporal crosswind $v(t)$ is added to disturb the wakes and redirect the wake of the first turbine towards the second turbine. The task of the closed-loop wake redirection controller is then to maintain the wake position at its desired value. A fully developed flow field is generated in the precursor with the desired free-stream wind velocities $u_\infty = 8 \text{ ms}^{-1}$, $v_\infty = \tilde{v}(t)$, and $w_\infty = 0$, and a turbulence intensity of approximately 5% at hub-height in front of the wind farm. The function $\tilde{v}(t)$ is a time varying function that describes the crosswind perturbation. Then, for the specific topology considered in this work, the flow is propagated 900 s in advance with constant control settings so that the wakes are fully developed. Here, non-cyclic boundary conditions and time-dependent turbulent inflow data by using a turbulence recycling method [31] are imposed. The flow field obtained after these 900 s is utilized as the initial flow field for the simulation.

A lidar system is simulated. It measures the wind speeds 3 D downstream of the wind turbine at hub-height. A lidar measurement is obtained at each grid point at the particular distance and height. The wake tracking is done by a pattern fit methodology because of the sim-

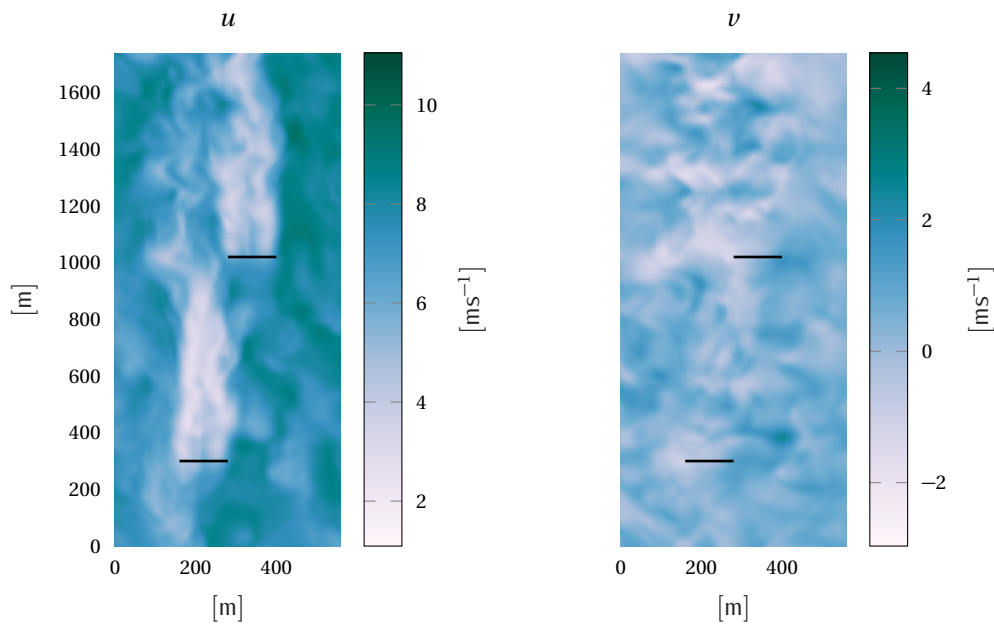


Figure 7.21: The u - and v - component of a flow field at $t = 200$ s in the open-loop case.

plicity of the method and the intention to focus on the adaptivity of the controller to the high-fidelity simulation environment and the crosswind disturbance. A Gaussian shape function is fit to the simulated lidar measurement data to estimate the wake position. Figure 7.20 shows an example of how the fit looks like at $t = 200$ s. In the following, the simulation results are presented and discussed.

Simulation results

The simulation is conducted on a high-performance cluster and ran for 9.7 hours (simulation time/real time is 35:1 s). First, two horizontal snapshots at hub-height are shown in figure 7.21 that give a first impression on the layout and the flow situation, showing the u - and the v -components of the flow field at $t = 200$ s. The flow field has a turbulence intensity around $T_i = 5\%$ and a mean wind speed of $\bar{u} = 8 \text{ ms}^{-1}$. Because of the crosswind, in an open-loop scenario, the wake of the first turbine moves toward the second turbine which is located downwind. Figure 7.22 shows such a flow situation at time $t = 800$ s. The crosswind has moved the wake and it is impinging the second turbine.

Figure 7.23 shows the flow snapshot at time $t = 800$ s of the closed-loop case in which redirection of the wake is visible. The controller counteracts the disturbance and adapts to it. To compare the results of the two cases, several variables are extracted from the simulation

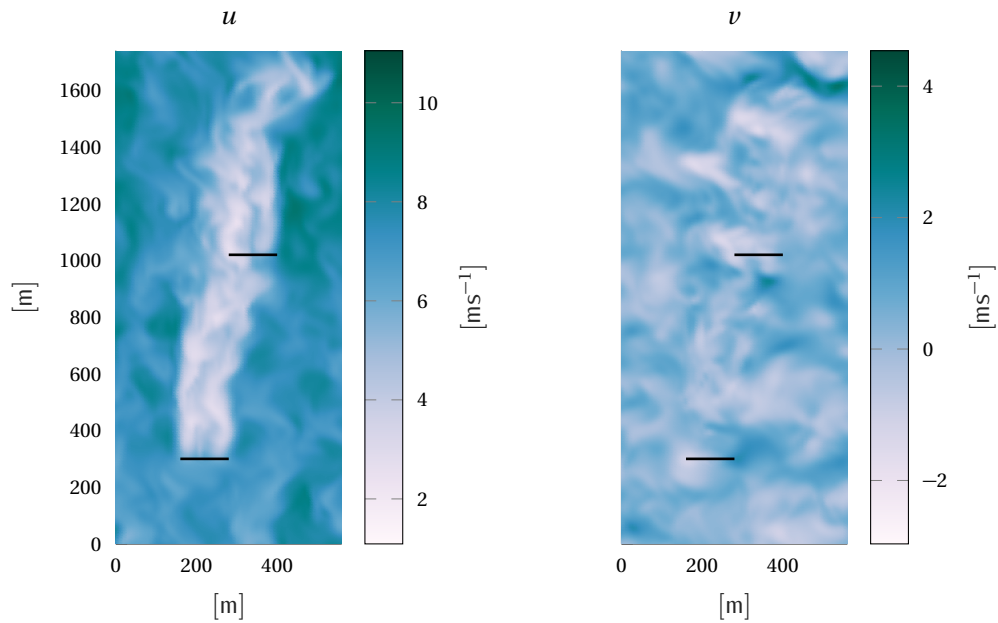


Figure 7.22: The u - and v -components of the flow field at time $t = 800$ s in the open-loop scenario. The crosswind moves the wake of the first turbine towards the second turbine.

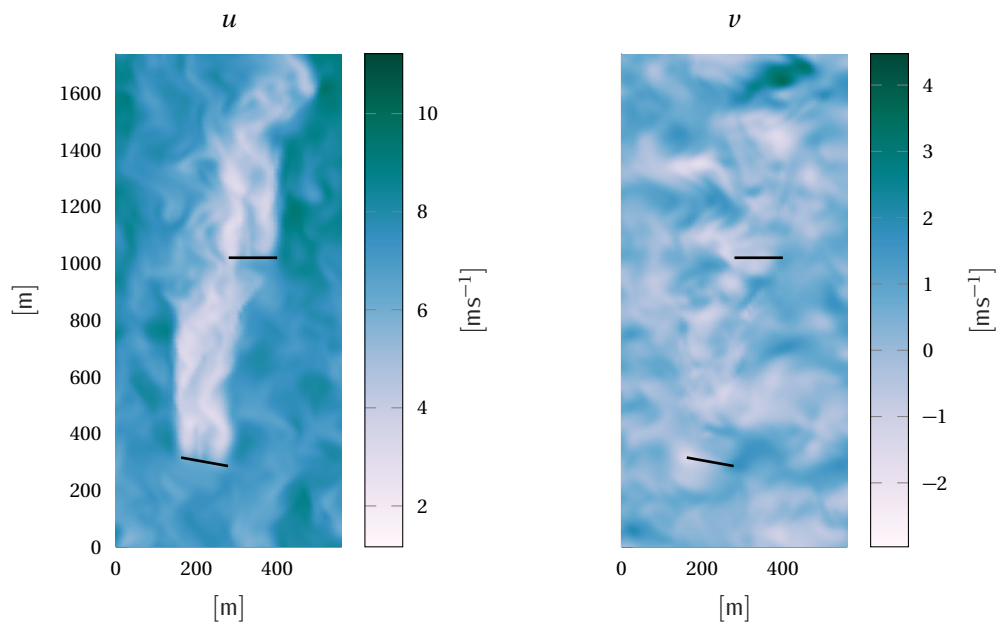


Figure 7.23: The u - and v -components of the flow field at time $t = 800$ s in the closed-loop scenario. The \mathcal{H}_∞ controller has redirected the wake of the first turbine.

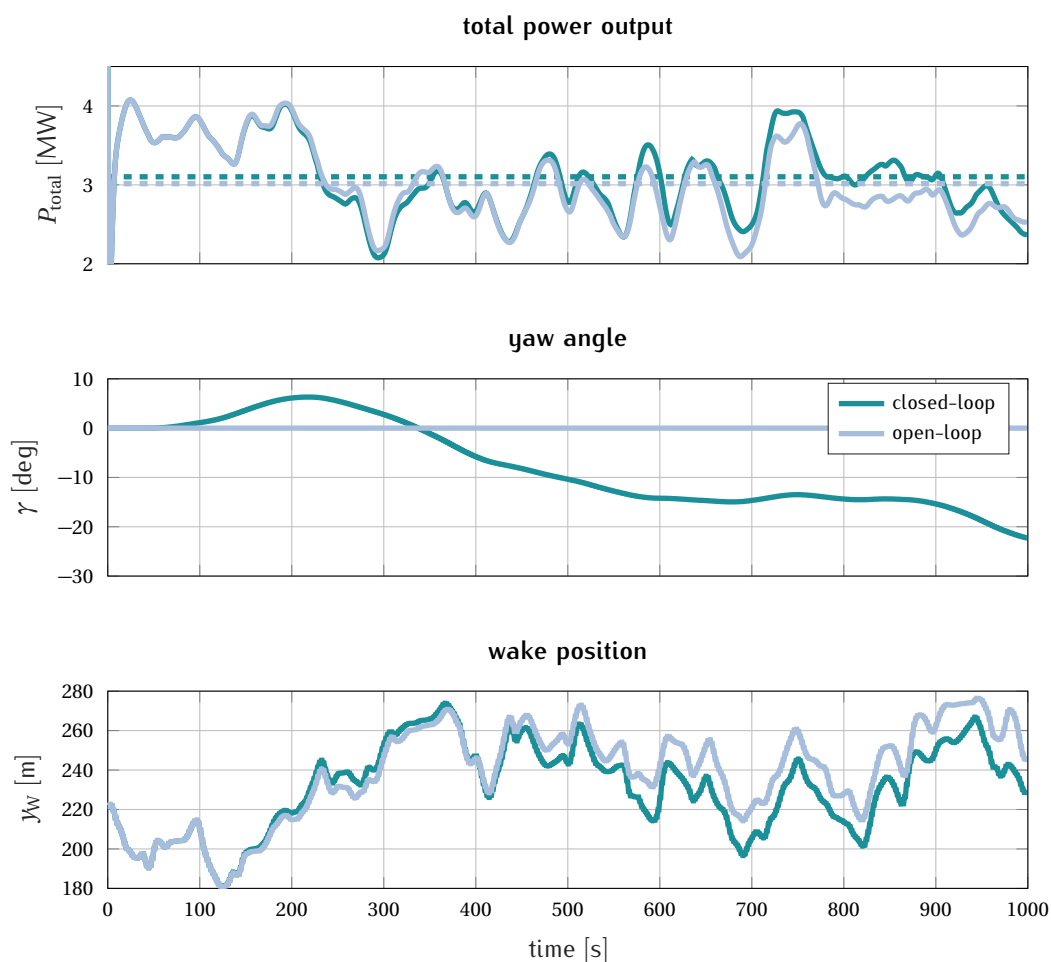


Figure 7.24: Comparison between open-loop and closed-loop simulation results of the previously described simulation scenario with crosswind. The cumulative power of the two turbines is compared in the first plot. Further, the mean power output of each scenario is shown with dashed lines. The second plot compares the commanded yaw angles of the first turbine. The last plot gives the result of the wake position estimation for the two cases.

results and considered in figure 7.24. The figure presents the comparison between the open-loop and closed-loop simulation results and gives first the total power of the two turbines. Furthermore, the mean power of each simulation is shown with a dashed line style. The closed-loop case yields an increased total power output of 2.9 % over the time horizon compared to the open-loop case. This is due to the fact that the second turbine is influenced less by the wake of the first turbine. The second plot of figure 7.24 shows the yaw angle of the first turbine and the last plot the estimated wake position of the first turbine. In the closed-loop case the wake position is steered closer to the reference signal, but stays oscillating because of other effects like wake meandering.

7.3.6 Summary and possible extensions

The \mathcal{H}_∞ controller design synthesis was applied to wake redirection control and a \mathcal{H}_∞ controller was derived. A linear controller design model that was parametrized as previously described was used in the controller design process. The advantage of the \mathcal{H}_∞ design is the direct specification of performance measures like the sensitivity \mathcal{S} . The derived controller was analyzed and tested in the medium-fidelity CFD simulation model WFSim. Furthermore, the applicability of the controller in an LES simulation model was shown by using it in a demonstration case where a temporary crosswind is disturbing the wake and steering it toward a downwind turbine. The concept adapts well to the more complex flow conditions and also to the crosswind disturbance.

Nevertheless, the approach also shows the weaknesses of the proposed controller in terms of control performance. Oscillations have been observed in a simulation scenario where a controller was used that was designed for a different mean wind speed. The change of wake redirection dynamics that was previously described in section 5.4.4 impacts the control performance. This issue is considered in the following section where a robust \mathcal{H}_∞ controller design is carried out and different models are considered within an uncertainty set.

7.4 Robust wake redirection control

As pointed out before, the design margins of sensitivity and controller sensitivity are not guaranteed since the models of the different setpoints (*e.g.* different wind speed or yaw setpoints) are not included in the controller design process. Instead, a \mathcal{H}_∞ controller is designed only for a single setpoint (model) and its applicability to different setpoints has to be assessed after-

wards. The main points of this adaptation are presented in [80] and they are extended here. In the following, the different models of ranges of wind speeds and yaw setpoints are included as model uncertainty in the \mathcal{H}_∞ controller design process by a robust controller synthesis. The procedure is the following: 1) identify several models, 2) calculate a nominal model representative of the identified models, and 3) define the uncertainty set.

In the following, first, the uncertain plant is introduced. Then, the robust controller is designed and analyzed. Finally, simulations with the nominal and the medium-fidelity CFD simulation model WFSim are performed to show its benefits. Finally, conclusions and possible extensions are given.

7.4.1 Uncertain plant

The robust control synthesis allows to directly consider uncertainties in the model for controller design. Therefore, the nominal controller design model is augmented with an uncertainty model. For wake redirection the different model dynamics result from different setpoints in wind speed and yaw as well as other dynamics that are not included in the design model. The uncertain linear model has the form

$$G_*(s) = G(s) \left(1 + W(s)\Delta(s) \right) \quad \text{with } \Delta(s) \in \underline{\Delta} \quad (7.13)$$

with the nominal plant $G(s)$, a weighting filter $W(s)$, and the uncertainty $\Delta(s)$. $G_*(s)$ will be referred to as the uncertain plant that is needed for the robust \mathcal{H}_∞ controller synthesis. The model parametrization of section 5.4.4 is used to derive a set of controller design models. Several step simulations are performed on the nonlinear medium-fidelity CFD model WFSim described in section 2.3.2 for different wind speed and yaw setpoints. Figure 7.25 shows all step responses which are available from the model parametrization. They result from step simulations at three different wind speeds of 6, 8, and 10 ms^{-1} . Yaw steps have been applied with a step magnitude of $\Delta 5$ deg from 0 to 20 deg. For a better comparability, the offset of the wake position is removed. To build up the uncertain plant, 10 most relevant models are used in the following for the derivation of the uncertain plant. Figure 7.26 shows the steps and the color order of the models which are used in the following. The Bode plot of the parametrized models are shown in figure 7.27.

It is assumed that the SISO system has complex uncertainty hence $\Delta \in \mathbb{C}$ with property $\|\Delta(s)\|_\infty \leq 1$. In order to define the nominal model $G(s)$ we, for each frequency ω_j , first com-

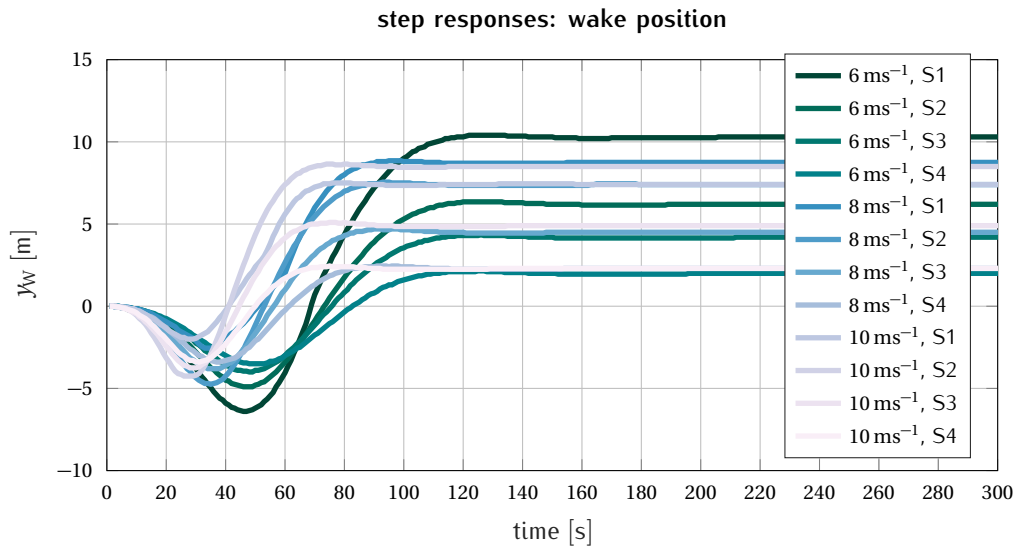


Figure 7.25: The step simulation results which were used in the model parametrization. For comparability, the initial values of the wake position are removed. The step responses result from $\Delta 5$ deg steps of the yaw actuator at wind speeds of 6, 8, and 10 ms^{-1} .

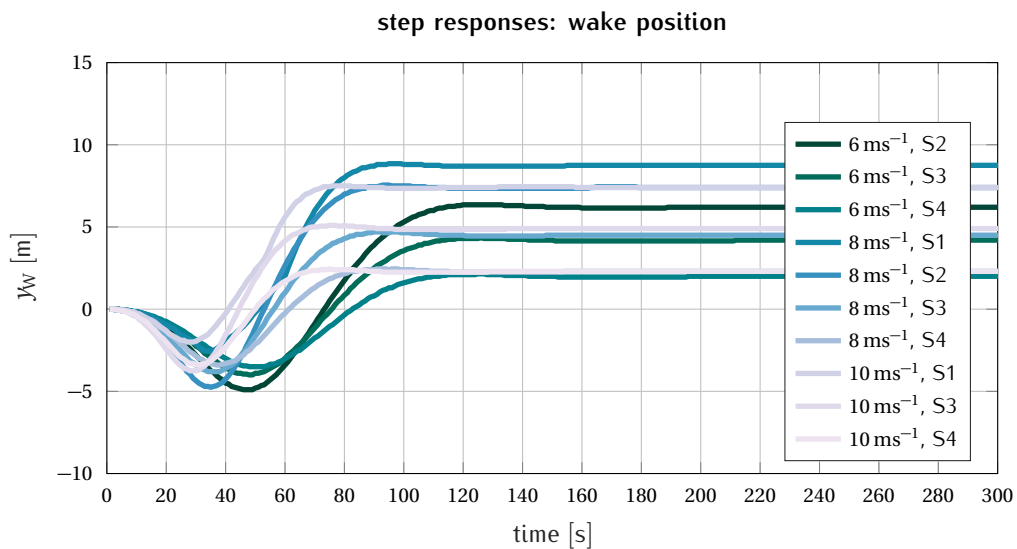


Figure 7.26: The used steps in the design of the uncertain plant. For comparability the initial values of the wake position are removed. The step responses result from $\Delta 5$ deg steps of the yaw actuator at wind speeds of 6, 8, and 10 ms^{-1} .

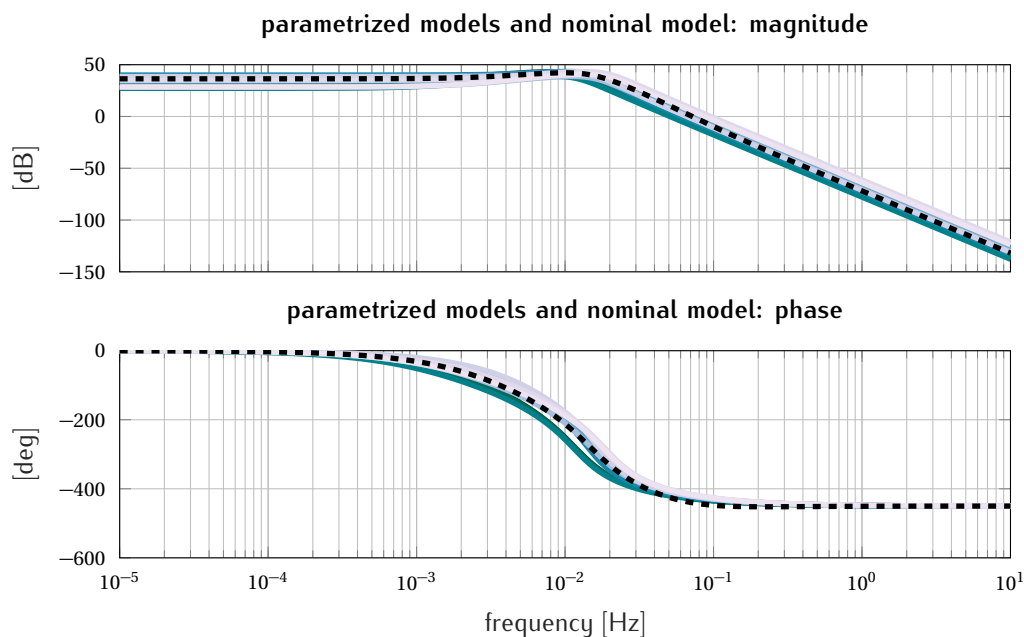


Figure 7.27: The resulting models for the controller design synthesis that have been parametrized from the step responses of figure 7.26. The nominal model G (dashed) results from all considered models.

pute:

$$\begin{aligned}
 |g(i\omega_j)| &= \frac{1}{m} \sum_{\ell=1}^m |G_{\ell}(i\omega_j)|, \\
 \angle g(i\omega_j) &= \frac{1}{m} \sum_{\ell=1}^m \angle G_{\ell}(i\omega_j),
 \end{aligned} \tag{7.14}$$

with $\angle g(i\omega_j)$ defined as the average phase of $G(s)$ for the frequency ω_j and $|g(i\omega)|$ the average amplitude. m is the number of considered models ($m = 10$). The average model for the frequency ω_j is then defined as:

$$g(i\omega_j) = |g(i\omega_j)|^{i\angle g(i\omega_j)} \tag{7.15}$$

In order to obtain an equivalent model structure for the parametrized models, an identification is performed on $g(i\omega_j)$ resulting in the nominal plant $G(s)$. Having obtained the nominal plant $G(i\omega)$, the uncertainty set can be calculated by evaluating

$$L_{\ell}(i\omega_j) = \left| \frac{G_{\ell}(i\omega_j) - G(i\omega_j)}{G(i\omega_j)} \right|, \tag{7.16}$$

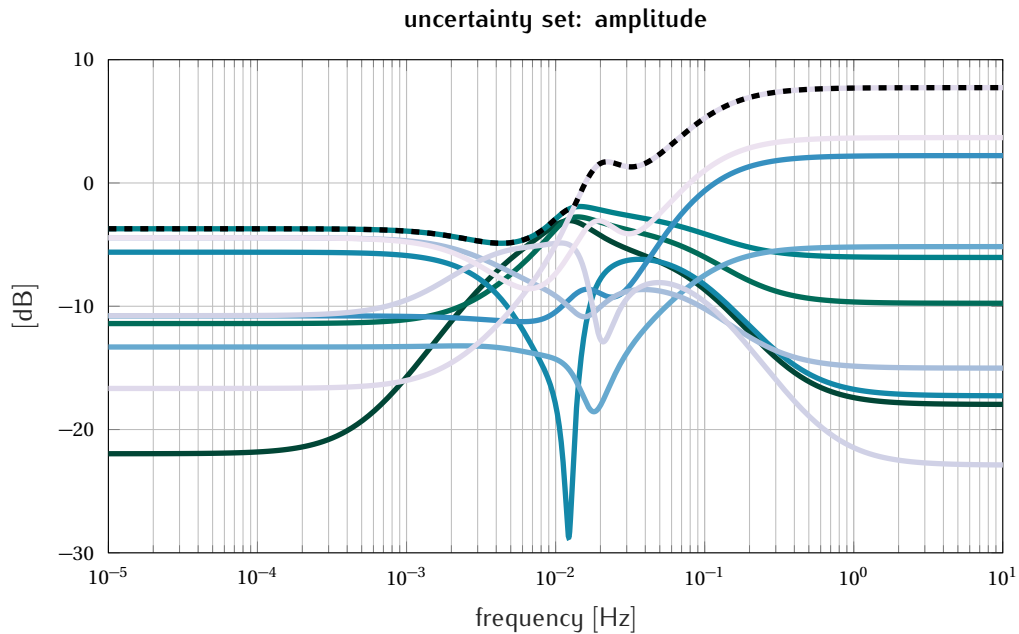


Figure 7.28: The uncertainty set calculated by (7.16) and the resulting weighting filter $W(i\omega)$ (dashed).

for all ℓ models. The amplitude of the set is plotted in figure 7.28. The weighting filter $W(s)$ determines the uncertainty size and should have the property

$$W(i\omega_j) \geq L_\ell(i\omega_j). \quad (7.17)$$

In order to ensure this property, the following expression can be used to define the amplitude of $W(s)$ for the frequency ω_j :

$$|W(i\omega_j)| = \max_l \left| \frac{G_l(i\omega_j) - G(i\omega_j)}{G(i\omega_j)} \right|, \quad (7.18)$$

Since we assume $W(s)$ to be without right-half-plane zeros, the uncertainty weight is uniquely defined by its amplitude response given in (7.18). It is of interest to have a low order weighting filter because this order will generally determine the controller order. Hence, the choice of this order is important, we fit a fixed order transfer function on $W(s)$. In the following section a controller will be designed for the uncertain plant.

The robust \mathcal{H}_∞ controller design approach is applied, similar to the approach for the \mathcal{H}_∞ controller synthesis. By placing and choosing performance weights, closed-loop transfer functions can be shaped, and in addition, performance can be ensured for all closed-loop plants in the set assuming nominal stability. It is illustrated in figure 7.29 how the perfor-

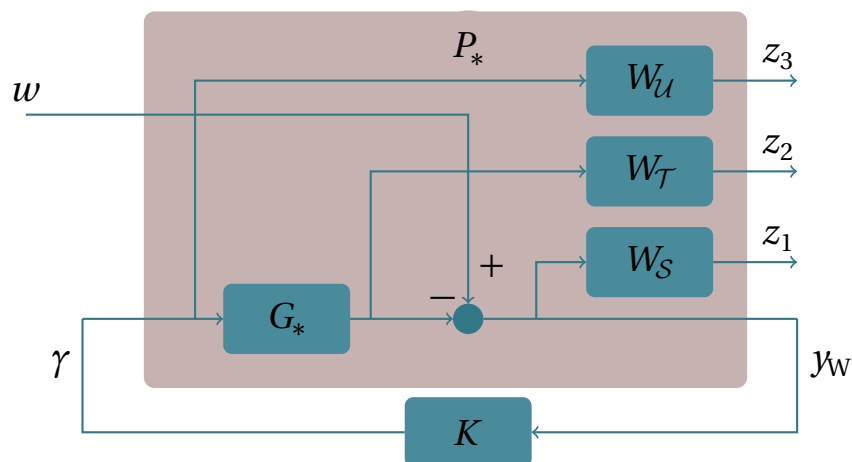


Figure 7.29: Generalized plant P_* with performance signals $z_1, z_2,$ and z_3 and wake center position reference w . Furthermore, we have the identified uncertain model G_* , the performance weights W_S, W_U and W_T and controller K with yaw control signal γ and the wake position y_w .

mance weights are placed. The performance measures are defined with the uncertain plant similar to (7.1)-(7.3) but with the uncertain plant G_* as

$$S_p = \frac{1}{1 + G_* K}, \quad (7.19)$$

$$\mathcal{T}_p = \frac{G_* K}{1 + G_* K}, \text{ and} \quad (7.20)$$

$$\mathcal{U}_p = \frac{K}{1 + G_* K}. \quad (7.21)$$

Then the map of the reference position w to the performance signal $z = [z_1 \ z_2 \ z_3]^T$ can be written as

$$z = N_p w \quad (7.22)$$

with

$$N_p = \begin{bmatrix} W_S S_p \\ W_T \mathcal{T}_p \\ W_U \mathcal{U}_p \end{bmatrix}. \quad (7.23)$$

N_p can be also be written using the linear fractional transformation lft as (see [83])

$$N_p = \text{lft}(\Delta, \text{lft}(P, K)). \quad (7.24)$$

7.4.2 Controller design

The robust \mathcal{H}_∞ controller is synthesized by solving the following problem:

$$\begin{aligned} \min_K \kappa \\ \text{s.t. } \|N_p\|_\infty \leq \kappa. \end{aligned} \quad (7.25)$$

Robust performance is achieved when $\|N\|_\infty < 1$ assuming nominal stability for all $\|\Delta(s)\| \leq 1$ with $N = \text{lft}(P, K)$. This definition and the definition of the linear fractional transformation lft are according to [83].

We would like to ensure robust stability and robust performance. However, by the main loop theorem, it is sufficient to ensure robust performance since this implies robust stability. When we look at the robust performance, it is convenient to use D-K-iterations for the problem given in (7.25). The performance weights are defined as

$$\begin{aligned} W_S &= \frac{s/M + \omega_{\text{CL}}}{s + \omega_{\text{CL}}A} \\ W_U &= 0.4B^2 \frac{s^2 + \sqrt{2}\omega_2 + \omega_2^2}{s^2 + B\sqrt{2}\omega_2s + (B\omega_2)^2} \\ W_T &= 0 \end{aligned} \quad (7.26)$$

with ω_{CL} the desired closed-loop bandwidth, A the desired disturbance attenuation inside the bandwidth, and M the desired bound on $\|S_p\|_\infty$ and $\|T_p\|_\infty$. In this work the desired closed-loop bandwidth is set to $\omega_{\text{CL}} = 0.001$, the design bandwidth $\omega_2 = 0.05$ and the parameters $M = 4$, $B = 20$ and $A = 10^{-6}$ are used to shape the desired performances.

7.4.3 Controller analysis

In the following, the robust \mathcal{H}_∞ controller is analyzed in both the time and frequency domains. First, its Bode plots are compared to those of the nominal \mathcal{H}_∞ controller that is designed using the nominal plant. Figure 7.30 shows the comparison between the two controllers which are designed with the similar design weights W_S , W_U , and W_T .

Furthermore, the closed-loop performances, the disturbance sensitivity and the controller sensitivity, are evaluated in figure 7.31. Compared to the \mathcal{H}_∞ design that is presented in the previous chapter, the robust \mathcal{H}_∞ controller has a lower bandwidth. This is due to the positive zeros at lower frequency numbers. In the previous \mathcal{H}_∞ controller design in section 7.3, the

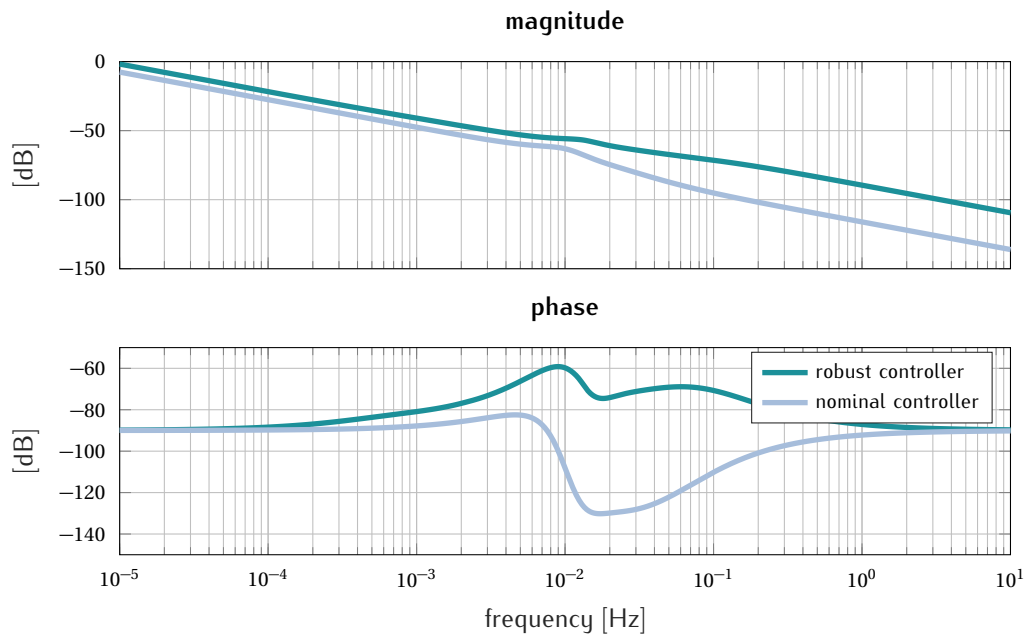


Figure 7.30: Bode plots of the robust \mathcal{H}_∞ controller as well as the \mathcal{H}_∞ controller that is designed with the nominal plant.

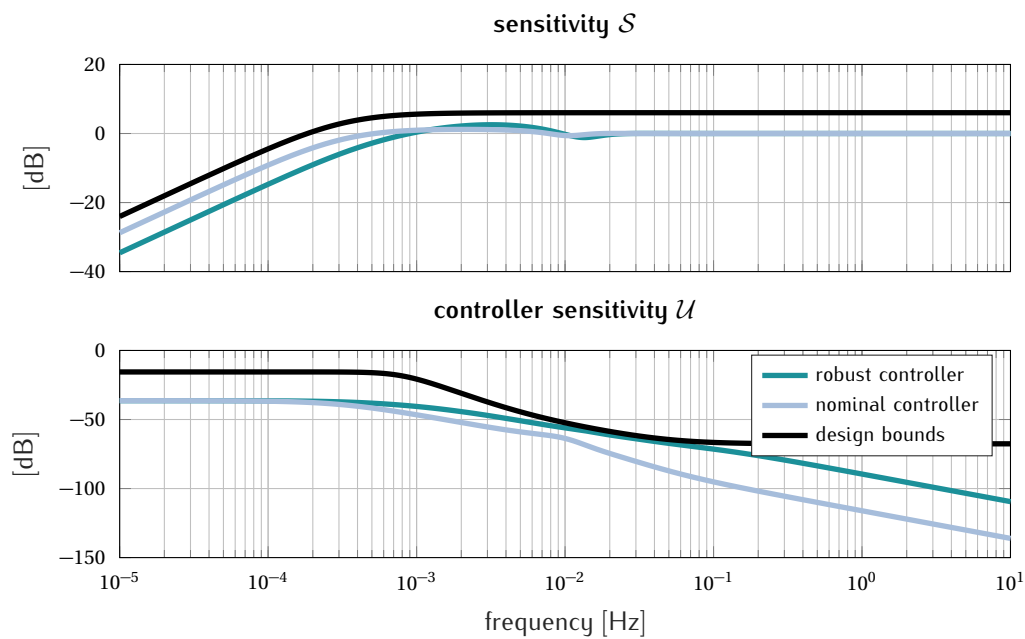


Figure 7.31: Comparison of the performance evaluation of the robust \mathcal{H}_∞ controller and a nominal \mathcal{H}_∞ controller with the nominal plant model. The nominal \mathcal{H}_∞ controller is designed with the nominal plant model (averaged model).

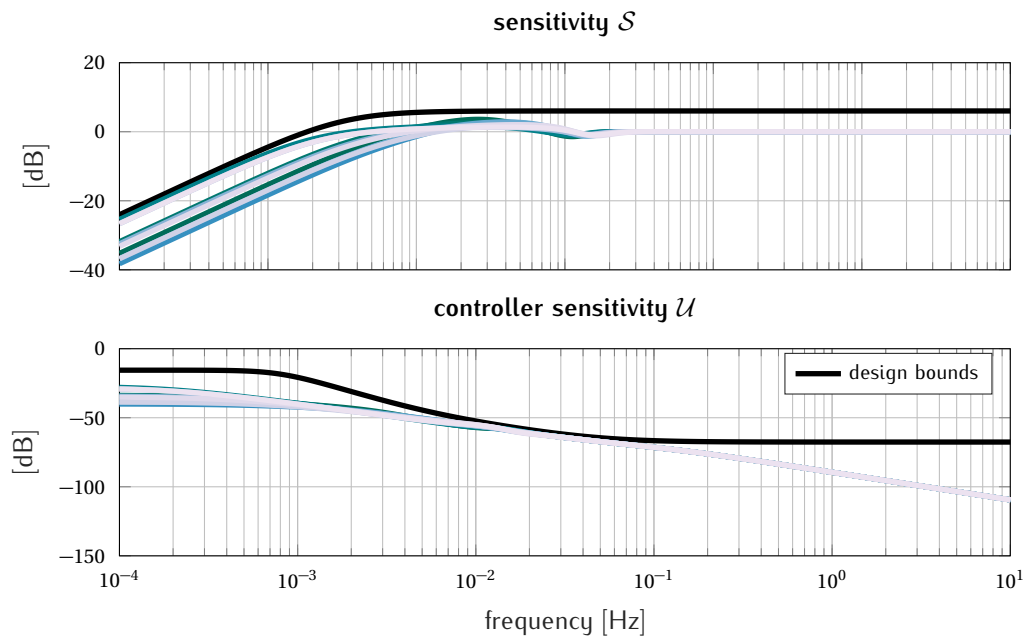


Figure 7.32: The performance assessment of the robust \mathcal{H}_∞ controller with all considered models that are used in the robust controller synthesis.

controller was directly designed for a specific setpoint of wind speed and yaw offset. Thus, the control bandwidth is only limited by the zeros of this model. Since in the robust controller synthesis several models are considered in the design, the zeros at lower frequencies are limiting the closed-loop bandwidth. Therefore, the robust controller is slower and more conservative than a nominal controller. However, it has the benefit of achieving the desired performances for all considered models. Figure 7.32 assesses the performance of the robust \mathcal{H}_∞ controller with all considered models. The controller achieves satisfying performance with all models. In contrast, a \mathcal{H}_∞ controller is designed with the same design margins as the robust \mathcal{H}_∞ controller to analyze the impact of the uncertainty set on the controller design. Figure 7.33 shows the performance of the nominal controller. Clearly, the violations of the design bounds are observable at low frequencies.

Finally, nominal step simulations (with the nominal model as simulation model) are performed with the robust \mathcal{H}_∞ controller. First a nominal step simulation is performed, which means the controller is applied to the averaged controller design model and a step on the desired wake position is applied at 100 s. In a second simulation, an output disturbance is applied with a random noise signal with zero mean offset. The simulation results are shown in figure 7.34. Finally, an additional output disturbance with a mean offset of 5 m is added which approximates a static model offset between the controller design model and the reality. Figure

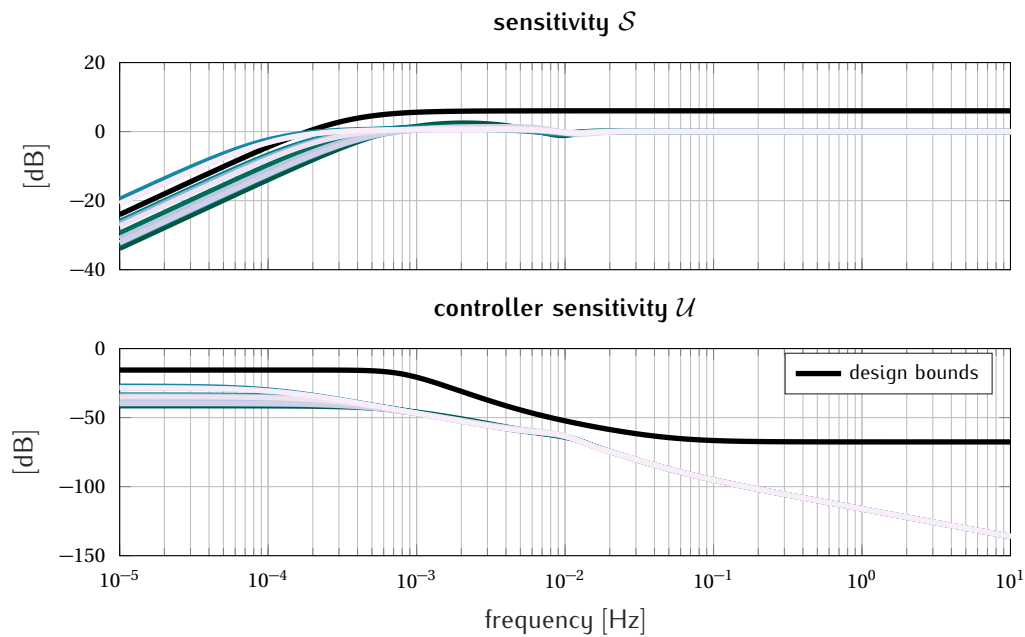


Figure 7.33: The performance assessment of a nominal \mathcal{H}_∞ controller designed with the same design bounds as the robust \mathcal{H}_∞ controller. For the nominal \mathcal{H}_∞ controller design, the uncertainty is not considered in the controller synthesis.

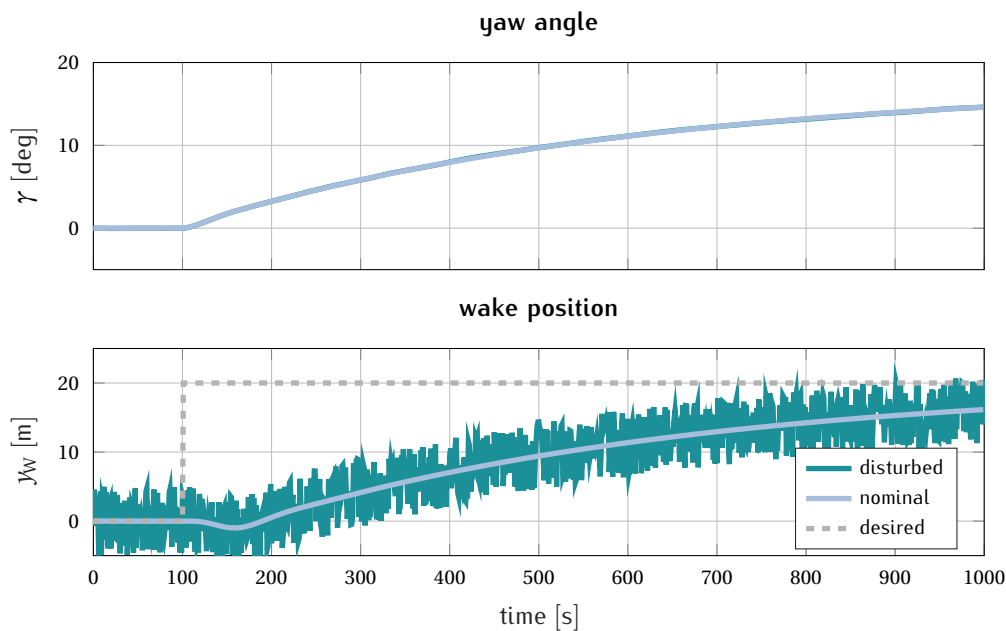


Figure 7.34: Closed-loop time simulation results with the robust \mathcal{H}_∞ controller applied to the averaged model. Comparison of two step response simulations of the nominally controlled system without and with output disturbance.

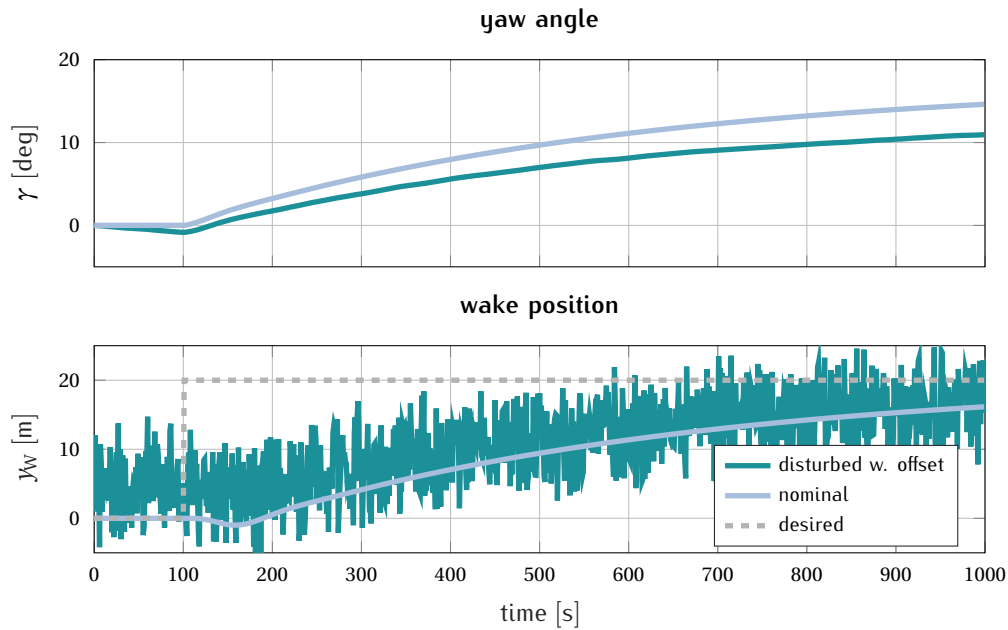


Figure 7.35: Closed-loop time simulation results with the robust \mathcal{H}_∞ controller. Comparison of two step response simulations of the nominally controlled system without and with output disturbance.

7.35 compares the simulation results with the nominal closed-loop behavior. Because of the integral behavior of the controller, see figure 7.30, it adapts to the offset.

7.4.4 Simulation results using a medium-fidelity CFD model

In the following, the \mathcal{H}_∞ controller is applied to closed-loop wake redirection cases in the medium-fidelity CFD simulation model WFSim. Two scenarios are considered. First, a scenario where the controller is used at its design conditions. Second, the controller is used in conditions where a different gain and wake redirection dynamics are present.

Wake redirection at nominal design setpoint

The previously designed and analyzed controller is used in WFSim. It was designed at a mean wind speed of $\bar{u} = 8 \text{ ms}^{-1}$ and a yaw setpoint of 5 deg. In the simulation model, a homogeneous inflow velocity of 8 ms^{-1} is set. The wake position is estimated at 3 D behind the wind turbine and different desired wake positions are set. Figure 7.36 shows time results of the yaw angle and the estimated wake position. Clearly, the controller steers the wake to its desired position, however, compared to previous nominal simulations, the time to converge is longer than before. Table 7.1 gives an approximation of the convergence times of the controllers.

Table 7.1: Approximated convergence time of the different controllers.

controller	convergence time
IMC	800 s
\mathcal{H}_∞	500 s
robust \mathcal{H}_∞	1200 s

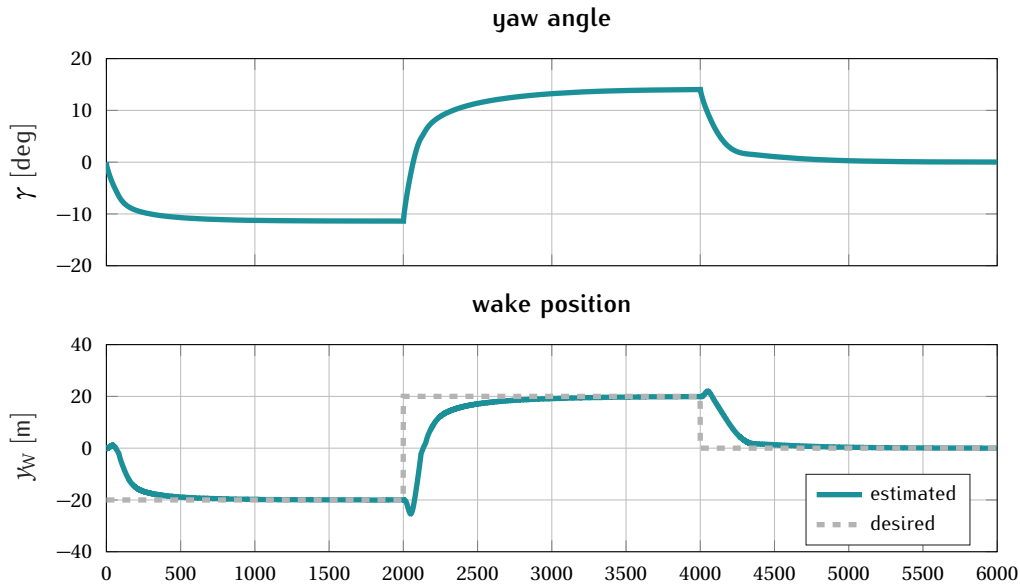


Figure 7.36: Closed-loop time simulation results with the reduced-order CFD simulation model WFSim using the derived robust \mathcal{H}_∞ controller. The mean wind speed is 8 ms^{-1} and a homogeneous inflow condition is set.

The longer time to converge is due to ensuring robustness in considering a range of different models with their specific dynamics. Figure 7.37 shows two snapshots of the flow field during the closed-loop simulation.

Wake redirection at different setpoint

To evaluate the robustness, the controller is used at a different inflow wind speed. Thus, the controller design model that was used to design the controller does not match the actual wake redirection dynamics of the simulation case. The controller was designed at a mean wind speed of $\bar{u} = 8 \text{ ms}^{-1}$ and a yaw setpoint of 5 deg. In the simulation model, a homogeneous inflow velocity of 6 ms^{-1} is set. The wake center is estimated at 3 D behind the wind turbine and different desired wake positions are set. Figure 7.38 shows time results of the yaw angle and the estimated wake position. For the first two desired wake positions, the control per-

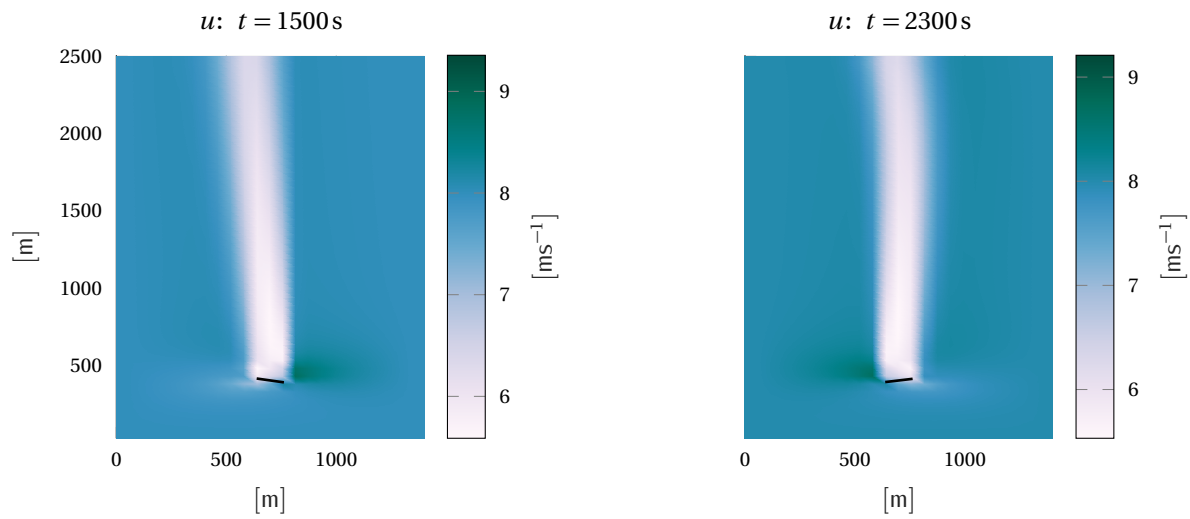


Figure 7.37: Two flow snapshots of the closed-loop simulation using the robust \mathcal{H}_∞ controller at a mean wind speed of $\bar{u} = 8 \text{ ms}^{-1}$.

formance is good. Comparing the result of the robust \mathcal{H}_∞ controller to the \mathcal{H}_∞ controller in figure 7.19) when the setpoint changes to the desired wake position of 0 m, the controller overshoots less and the steering is well damped.

7.4.5 Summary and possible extensions

A robust \mathcal{H}_∞ control synthesis for closed-loop wake redirection was presented. The uncertainty of different wake redirection dynamics due to different wind speeds and the differences in the gain have been considered as structural model uncertainty in the controller design approach. This guarantees that the robust controller satisfies the desired design margins of sensitivity \mathcal{S} and controller sensitivity \mathcal{U} for all models within the uncertain plant (the nominal model together with the uncertainty set). However, the limitation of the control bandwidth is due to the slowest positive zeros in all considered models. Nevertheless, the robust controller performed well in the test cases and has also performed well with increasing wind speed and random noise as simulated turbulence in [80].

Further work should assess the presence of the positive zeros because they limit the performance significantly. Furthermore, the robust controller should be tested in high-fidelity simulation studies to assess if the applicability over the same wind speed range is feasible.

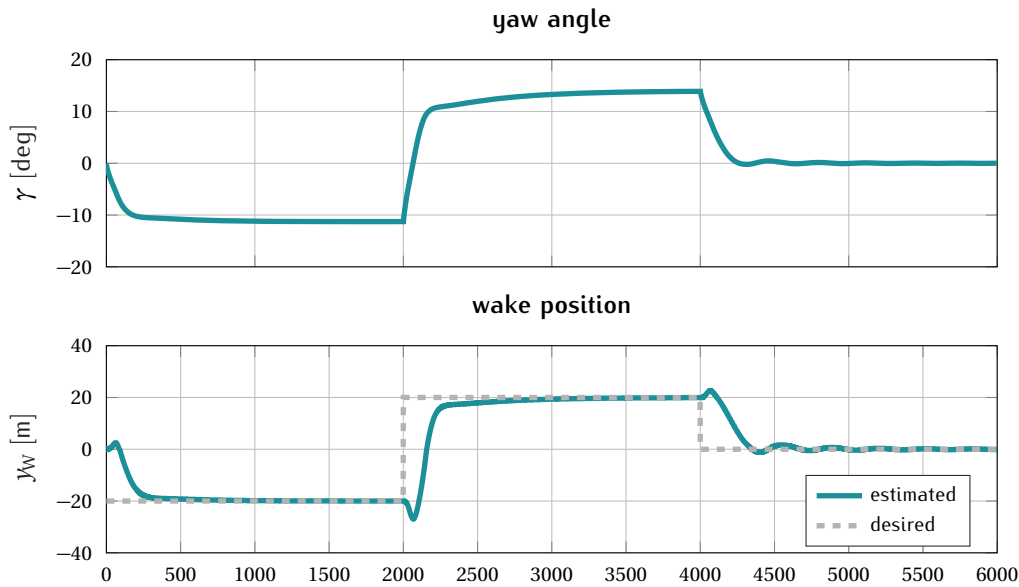


Figure 7.38: Closed-loop time simulation results with the reduced-order CFD simulation model WFSim using the derived robust \mathcal{H}_∞ controller. The homogeneous inflow wind speed is 6 ms^{-1} .

7.5 Conclusions and possible extensions

This chapter has presented different controller approaches to realize lidar-based closed-loop wake redirection. In the following, first a summary of the three controller approaches is given and then the main conclusions are discussed.

First, an IMC control approach was used together with parametrized models. The controller works well and good performance has been achieved. However, the controller tuning is difficult since the controller transfer function consists of the internal feedback controller, the internal model, and a filter. The performance of the controller depends on the choice of filter parameter and local feedback gains, which is why an iterative procedure is helpful to achieve good control performance.

Second, a \mathcal{H}_∞ wake redirection controller was introduced. A parametrized controller design model was used to obtain an \mathcal{H}_∞ controller that meets desired performance margins. The bandwidth is set according to the approximated delay time, considering the positive zero of the plant. The controller performs well although there are oscillations when applying the controller in a simulation case at a different setpoint than the design setpoint. Additionally, this controller was implemented in a case study in a LES simulation model to mitigate a crosswind disturbance in a two turbine layout. The total power output was increased due to the con-

troller and a first demonstration of closed-loop wake redirection was done in a high-fidelity simulation model.

Third, the \mathcal{H}_∞ controller was extended to a robust version by introducing an uncertain plant description, in which different models of different setpoints are included. The uncertainty set is directly used in the design process, hence the designed robust \mathcal{H}_∞ controller meets the performance criteria for all models covered by the uncertainty set.

General conclusions on the controller design are the following: The controller synthesis depends on the used model and the assumptions that were made to obtain the model. In particular, the already mentioned trade-off between measurement distance and the time delay influences the controller design. Altogether, it makes sense to lower the control bandwidth and increase the robustness of the controller to synthesize a controller which is applicable to several setpoint conditions.

Furthermore, possible extensions are the introduction of gain scheduling to cover a wider range of models. This would also lead to higher performances at higher wind speeds since the dynamics depend on the wind speed, as described before. In addition, since the robust \mathcal{H}_∞ controller is obtained by D-K iterations, a structured \mathcal{H}_∞ controller may be a nice future work, since the controller structure can be set directly before designing the controller. A really important extension, in terms of performance, could be the augmentation with an open-loop wake redirection controller. This would improve the performance and moreover the controller could cope with disturbance rejection and model uncertainties. In this combined feedforward-feedback control approach, the responsibilities of tracking and disturbance rejection are shared between the open-loop and the closed-loop. Thus, the feedback controller doesn't need to be tuned very aggressive and e.g. the robust \mathcal{H}_∞ controller, presented before, can be used. Based on estimations of atmospheric conditions, the open-loop controller is then commanding the main yaw action and the feedback is concentration on adjusting to uncertainties and disturbances.

8

Conclusions

Das Leben eines Menschen spielt eine Melodie, die einzigartig und unverkennbar ist. [...] Mal laut intensiv und kräftig, mal sanft und leise erklingt diese Melodie; und vereint sich im Rhythmus der Zeit zur unendlichen Symphonie des Lebens.

— Steffen Raach, *Symphonie des Lebens*

8.1	Summary	124
8.2	Future research	127
8.3	Outlook	128

The objective of this study was to introduce lidar-based closed-loop wake redirection. This chapter summarizes the thesis. The main conclusions of the different objectives are drawn and future research is addressed. Finally, an outlook is given on how the concept can contribute to the goals of wind farm control.

8.1 Summary

This work has introduced the concept of lidar-based closed-loop wake redirection and has elaborated on different fields within the concept. The general task of the concept is separated in two subtasks: the estimation task and the control task (figure 8.1). Within the two subtasks different aspects have been considered to realize lidar-based closed-loop wake redirection. In the estimation task the question is addressed of how a lidar device can provide wake position information for wind farm control. The control task deals with the use of the wake position information in a closed-loop controller. It uses a desired position and the estimation to command the yaw angle of the wind turbine.

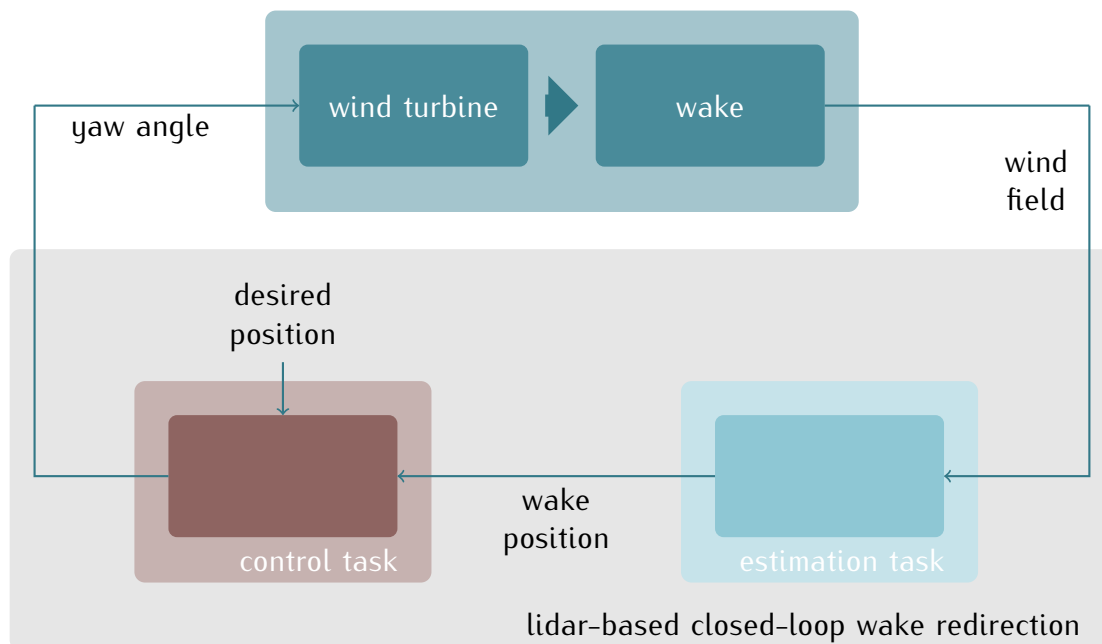


Figure 8.1: The general concept of lidar-based closed-loop wake redirection control. The general task is separated in two subtasks: the estimation task and the control task.

In detail, the concept has been motivated by analyzing the open-loop wake redirection concept and the presentation of field testing results of open-loop wake redirection. The setup of

the field testing has been described and recommendations for future wake redirection field testings have been given. With the help of the field testing the advantages and disadvantages of open-loop wake redirection have been pointed out.

Afterwards, the lidar-based closed-loop wake redirection concept has been introduced and described in detail. This concept tries to present a framework that can adapt to the main disadvantages of the open-loop concept. To assess the different fields of the concept, it has been separated in two main parts: the estimation task and the control task. The conclusions on the general concept of lidar-based closed-loop wake redirection are the following:

- The concept is an alternative to the open-loop methodology to obtain the yaw angles for wake steering.
- It is based on lidar measurements and a closed-loop approach.
- The concept is implemented as a local controller at the turbine level and the desired wake positions are commanded at the wind farm level by *e.g.* an operator, a higher level optimization or automation.
- The separation of the general task in this study into the estimation task and the control task helps to address the specific questions separately.

The objective of the estimation task is to process lidar measurement data in such a way that the wake position can be estimated. The main results and conclusions from the estimation task are the following:

- A lidar system gives insight into the flow situation in the wind farm. Moreover, its data can provide useful information to wind farm control.
- To realize wake tracking, the lidar measurement data needs to be processed to obtain the wake position information that is used in the controller.
- A nacelle-based downwind looking scanning lidar system can be used to scan in different distances the wake flow and provide measurements for the estimation.
- Wake position estimation techniques can be categorized as pattern fitting and wake model-based approaches.
- Pattern fitting approaches benefit from their simplicity and are based on assumptions on wake shapes.

- The presented model-based wake tracking approach fits a wake model to lidar measurements. It offers a good possibility to perform the wake position estimation, however, a convergence of the fitting is not guaranteed.

In the second major task of this thesis, questions of the control task are addressed. The control task deals with the use of the wake position information and the desired wake position to determine the commanded yaw angle. Three controller synthesis solutions have been given: an Internal Model Controller (IMC), an \mathcal{H}_∞ controller and a robust \mathcal{H}_∞ controller. All synthesized controllers are tested in different simulation environments. Mainly, the closed-loop simulations are performed in the medium-order Computational Fluid Dynamics (CFD) simulation tool known as the dynamic Wind Farm SIMulator (WFSim). Furthermore, a closed-loop wake redirection is implemented in the Large Eddy Simulation (LES) tool Parallelized Large-Eddy Simulation Model (PALM). In a demonstration case, the adaptivity of the concept to disturbances as well as model uncertainties is shown. The main conclusions of the control task are:

- Closed-loop wake redirection offers the possibility to adapt to changing situations, model uncertainties and local disturbances.
- The controller uses the wake position estimation and a desired position to calculate the commanded yaw angle.
- A controller design model is needed to design and analyze the controller. There are different methodologies for how a model can be obtained, either by good assumptions, by linearization, or by parametrization of a desired model structure with the use of experimental data.
- The results of this study indicate that controller robustness is of higher importance than control speed.
- With the current design of the closed-loop wake redirection, wake meandering is not an issue for wake steering because of the different time scales.

Altogether, the feasibility of lidar-based closed-loop wake redirection has been shown.

8.2 Future research

This study has introduced the concept of lidar-based closed-loop wake redirection. In the following, open research questions are raised and aspects are mentioned that need to be answered to realize lidar-based closed-loop wake redirection in an industrial application.

8.2.1 General concept of lidar-based closed-loop wake redirection

The thesis has shown the feasibility of lidar-based closed-loop wake redirection control. Further work is needed to apply the concept and analyze the impact and limitations of the concept. As a next step the overall benefits need to be clarified. A main question is whether the advantages of open-loop wake redirection control on power production can be kept or even be improved. The overall benefit of the closed-loop approach as well as its limitations compared to the open-loop approach should be addressed in detail. Furthermore, the impact of operating the wind turbine misaligned to the wind direction on the structural loads needs to be clarified in high-order simulation models. From an economic point of view, there is a trade-off between harvesting more electrical power and adding additional loads.

8.2.2 Estimation task

Concerning the estimation task, the reliability of different estimation methodologies needs to be clarified and compared. The model-based wake approach seems to be promising since the model can be easily adapted with additional wake effects. However, other methods like the Gaussian shape pattern fitting method has also resulted in suitable position estimation. The sensitivity against different atmospheric conditions should be further investigated by high-order LES simulations. Furthermore, the scalability of the estimation task to the wind farm level needs to be investigated. Here, using several long range scanning lidar systems with a feasible estimation technique might be a good solution, however, their ability to provide wake position estimation should be investigated in simulation as well as in field experiments. For the realization of wake tracking aspects like measurement position accuracy, the orientation of the lidar system and the yawing of the wind turbine as well as changing inflow conditions need to be considered in the design of the measurement setup and the choice of the devices. Furthermore, the influence of the spatial and temporal resolution on the quality of the estimation results should be considered in the decision. Moreover, atmospheric conditions like

turbulence intensity or the density of aerosols impact the results. Here, a site-specific analysis is really needed to decide well on the main measurement setup properties.

8.2.3 Control task

The investigations in the control task have shown the need for control-oriented wake models for the controller synthesis. It is recommended to further investigate the input-output dynamics of wake steering. A nonlinear reduced-order model could help to analyze the designed controller at different operation points before performing simulations and furthermore can be used in more advanced control approaches. Additionally, the inverse response behavior needs clarification. The simulated experimental data from step responses has shown such behavior. However, the origin of this behavior should be clarified in a detailed CFD study. For the design, the main recommendation on the controller design is to synthesize the controller with robustness margins. This seems more important than designing a fast controller.

8.2.4 Field experiments

As already pointed out in the field-testing chapter, there are few experiences in lidar measurements of wake steering. The first open-loop field experiment indicated that the power output can be maximized, however, more tests are needed to assess the benefit of wake redirection in reality [] [62]. Furthermore, the realization of closed-loop wake redirection involves major changes in the control system and needs to be planned well to assess the effects. Moreover, the flow situation should be monitored to learn from the field-tests.

8.3 Outlook

Wind farm control can address three control goals: power maximization, minimization of structural loads of the wind turbines, and grid services.

Lidar-based closed-loop wake redirection can contribute to realize a higher power output by avoiding flow interactions between wind turbines. Therefore, wind turbines that were initially hit by a wake can operate at a higher power level and achieve a higher total power output. The concept can be triggered by specific wind directions and atmospheric conditions to maximize the total power output of the wind farm and to benefit the most from the concept.

Furthermore, the concept can be used as an input layer for the wind farm operator to avoid wake impingements on specific wind turbines, *e.g.* if a wind turbine is damaged and needs

maintenance, further damage can be prevented. An additional use of the new flexibility in steering the wakes that the concept introduces is the ability to avoid partial wake situations. Here wake detection algorithms from structural loads might trigger the change of the desired wake position as well as considerations of the layout and static wake models. In both aspects, the concept contributes to minimize the structural loads of wind turbines in the wind farm.

In the future, grid services of wind farms offer new opportunities in operating them. Moreover, wind farms need to contribute to grid stability and provide active grid services. This will open the market for new business cases. New possibilities like providing a power reserve by the wind farm or actively participating in grid control can help to reduce the levelized cost of energy (LCOE). Wind farm control techniques will then play a more and more important role because the decision on the optimal wind farm operation will become more complex. Lidar-based closed-loop wake redirection control can serve as one methodology of how the wind farm operation is modified to operate in a more optimal way.

From a control point of view, the combination of open-loop and closed-loop approaches offers the possibility to benefit from both concepts. This could lead to faster control actions because of the feedforward aspect and would maintain the benefits of the closed-loop approach. This combination might be the most promising approach in terms of reliability and adaptivity for the wake redirection concept. Furthermore, the lidar measurement data can be used to adapt the open-loop model to the site-conditions. Parameter tuning methods or observer approaches can be used to adapt the model and to gain higher model accuracy for the feedforward part.

Appendix

Bibliography

- [1] The General Assembly of the United Nations, “Transforming our world: the 2030 agenda for sustainable development,” *Resolution adopted by the General Assembly*, 2015.
- [2] Delphi234, “Wind turbine size increase 1980-2015.png,” 2015. [Online]. Available: https://commons.wikimedia.org/wiki/File:Wind_turbine_size_increase_1980-2015.png
- [3] G. van Kuik and J. Peinke, *Long-term research challenges in wind energy - A research agenda by the European Academy of Wind Energy (EAWE)*. Springer, 2016, vol. 6.
- [4] T. Knudsen, T. Bak, and M. Svenstrup, “Survey of wind farm control-power and fatigue optimization,” *Wind Energy*, 2015.
- [5] S. Boersma, B. M. Doekemeijer, P. M. O. Gebraad, P. A. Fleming, J. Annoni, A. K. Scholbrock, J. A. Frederik, and J.-W. van Wingerden, “A tutorial on control-oriented modelling and control of wind farms,” in *Proceedings of the American Control Conference (ACC)*, 2017.
- [6] CL-Windcon, “Website of the CL-Windcon project which has received funding from the European Union’s Horizon 2020 research and innovation programme under grant agreement No 727477,” 2017. [Online]. Available: www.clwindcon.eu
- [7] M. I. Blanco, “The economics of wind energy,” *Renewable and Sustainable Energy Reviews*, vol. 13, no. 6, pp. 1372 – 1382, 2009.
- [8] N. O. Jensen, *A note on wind generator interaction*. Risø National Laboratory, No. 2411, 1983.
- [9] I. Katic, J. Højstrup, and N. O. Jensen, “A simple model for cluster efficiency,” in *Proceedings of the European Wind Energy Association Conference and Exhibition*, 1986, pp. 407–410.

- [10] P. M. O. Gebraad, "Data-driven wind plant control," Ph.D. dissertation, Delft University of Technology, 2014.
- [11] M. Bastankhah and F. Porté-Agel, "Experimental and theoretical study of wind turbine wakes in yawed conditions," *Journal of Fluid Mechanics*, vol. 806, pp. 506–541, 2016.
- [12] S. Boersma, M. Vali, M. Kühn, and J.-W. van Wingerden, "Quasi linear parameter varying modeling for wind farm control using the 2D Navier-Stokes equations," in *Proceedings of the American Control Conference (ACC)*, 2016.
- [13] C. R. Shapiro, J. Meyers, C. Meneveau, and D. F. Gayme, "Dynamic wake modeling and state estimation for improved model-based receding horizon control of wind farms," in *Proceedings of the American Control Conference (ACC)*, 2017, pp. 709–716.
- [14] S. Kapp and M. Kühn, "A five-parameter wind field estimation method based on spherical upwind lidar measurements," in *Proceedings of The Science of Making Torque from Wind*, Oldenburg, Germany, 2012.
- [15] P. Towers and B. L. Jones, "Real-time wind field reconstruction from lidar measurements using a dynamic wind model and state estimation," *Wind Energy*, vol. 19, no. 1, pp. 133–150, 2016.
- [16] E. Simley, L. Y. Pao, P. M. O. Gebraad, and M. Churchfield, "Investigation of the impact of the upstream induction zone on lidar measurement accuracy for wind turbine control applications using large-eddy simulation," *Journal of Physics: Conference Series*, vol. 524, no. 1, p. 012003, 2014.
- [17] S. Raach, D. Schlipf, F. Haizmann, and P. W. Cheng, "Three dimensional dynamic model based wind field reconstruction from lidar data," *Journal of Physics: Conference Series*, vol. 524, no. 1, p. 012005, 2014.
- [18] P. M. O. Gebraad, F. W. Teeuwisse, J.-W. van Wingerden, P. A. Fleming, S. D. Ruben, J. R. Marden, and L. Y. Pao, "Wind plant power optimization through yaw control using a parametric model for wake effects - a CFD simulation study," *Wind Energy*, vol. 19, no. 1, pp. 95–114, 2014.
- [19] P. M. O. Gebraad and J.-W. van Wingerden, "Maximum power-point tracking control for wind farms," *Wind Energy*, vol. 18, no. 3, pp. 429–447, 2015.

- [20] Z. Dar, K. Kar, O. Sahni, and J. H. Chow, "Windfarm power optimization using yaw angle control," *IEEE Transactions on Sustainable Energy*, vol. 8, no. 1, pp. 104–116, 2017.
- [21] M. Vali, V. Petrović, S. Boersma, J.-W. van Wingerden, and M. Kühn, "Adjoint-based model predictive control of wind farms: Beyond the quasi steady-state power maximization," in *Proceedings of the 20th World Congress of the International Federation of Automatic Control (IFAC)*, 2017, pp. 4510–4515.
- [22] M. T. van Dijk, J.-W. van Wingerden, T. Ashuri, and Y. Li, "Wind farm multi-objective wake redirection for optimizing power production and loads," *Energy*, vol. 121, pp. 561–569, 2017.
- [23] J.-W. van Wingerden, L. Y. Pao, J. Aho, and P. A. Fleming, "Active power control of waked wind farms," in *Proceedings of the 20th World Congress of the International Federation of Automatic Control (IFAC)*, no. 1, 2017, pp. 4484–4491.
- [24] T. Burton, N. Jenkins, D. Sharpe, and E. Bossanyi, *Wind Energy Handbook*. Chichester, United Kingdom: John Wiley & Sons, Ltd, 2011.
- [25] J. Marshall, L. Buhl, "A new empirical relationship between thrust coefficient and induction factor for the turbulent windmill state," National Renewable Energy Laboratory, Tech. Rep., 2005.
- [26] D. Schlipf, "Lidar-assisted control concepts for wind turbines," Ph.D. dissertation, University of Stuttgart, 2016.
- [27] A. Borraccino, D. Schlipf, F. Haizmann, and R. Wagner, "Wind field reconstruction from nacelle-mounted lidar short-range measurements," *Wind Energy Science*, vol. 2, no. 1, pp. 269–283, 2017.
- [28] S. B. Pope, *Turbulent flows*. Cambridge, UK: Cambridge University Press, 2013.
- [29] M. Churchfield and S. Lee, "NWTC design codes-SOWFA," 2012. [Online]. Available: <http://wind.nrel.gov/designcodes/simulators/SOWFA>
- [30] D. Allaerts and J. Meyers, "Large eddy simulation of a large wind-turbine array in a conventionally neutral atmospheric boundary layer," *Physics of Fluids*, vol. 27, no. 6, p. 065108, 2015.

- [31] B. Maronga, M. Gryschka, R. Heinze, F. Hoffmann, F. Kanani-Sühring, M. Keck, K. Ketelsen, M. O. Letzel, M. Sühring, and S. Raasch, “The Parallelized Large-Eddy Simulation Model (PALM) version 4.0 for atmospheric and oceanic flows: model formulation, recent developments, and future perspectives,” *Geoscientific Model Development*, vol. 8, no. 8, p. 2515, 2015.
- [32] J. Jonkman and M. Buhl Jr., “FAST User’s Guide,” National Renewable Energy Laboratory, Golden (Colorado), USA, Tech. Rep. EL-500-38230, 2005.
- [33] DNV GL. (2018) Bladed. [Online]. Available: <https://www.dnvgl.com/energy/generation/software/bladed/index.html>
- [34] M. Dörenkämper, B. Witha, G. Steinfeld, D. Heinemann, and M. Kühn, “The impact of stable atmospheric boundary layers on wind-turbine wakes within offshore wind farms,” *Journal of Wind Engineering and Industrial Aerodynamics*, vol. 144, pp. 146–153, 2015.
- [35] J. Jonkman, S. Butterfield, W. Musial, and G. Scott, “Definition of a 5-MW Reference Wind Turbine for Offshore System Development,” National Renewable Energy Laboratory, Tech. Rep. TP-500-38060, 2009.
- [36] R. F. Mikkelsen and J. N. Sørensen, “Actuator disc methods applied to wind turbines,” Ph.D. dissertation, Technical University of Denmark, Denmark, 2004.
- [37] P. A. Fleming, P. M. O. Gebraad, J.-W. van Wingerden, S. Lee, M. Churchfield, A. K. Scholbrock, J. Michalakes, K. Johnson, and P. Moriarty, “The SOWFA super-controller: A high-fidelity tool for evaluating wind plant control approaches,” NREL, Tech. Rep. CP-5000-57175, 2013.
- [38] M. Churchfield, S. Lee, and P. Moriarty, “Overview of the Simulator for Offshore Wind Farm Application (SOWFA),” 2012. [Online]. Available: https://nwtc.nrel.gov/system/files/SOWFA_webinar_05-03-2012.pdf
- [39] S. Frandsen, R. Barthelmie, S. Pryor, O. Rathmann, and S. Larsen, “Analytical modelling of wind speed deficit in large offshore wind farms,” *Wind Energy*, vol. 9, no. 1, pp. 39–53, 2006.
- [40] A. Niayifar and F. Porté-Agel, “Analytical modeling of wind farms: A new approach for power prediction,” *Energies*, vol. 9, no. 9, p. 741, 2016.

- [41] J. D. Grunnet, M. Soltani, T. Knudsen, M. Kragelund, and T. Bak, "Aeolus toolbox for dynamic wind farm model, simulation and control," in *Proceedings of the European Wind Energy Association Conference and Exhibition*, 2010.
- [42] J. R. Marden, S. D. Ruben, and L. Y. Pao, "A model-free approach to wind farm control using game theoretic methods," *IEEE Transactions on Control Systems Technology*, vol. 21, no. 4, pp. 1207–1214, 2013.
- [43] K. E. Johnson and G. Fritsch, "Assessment of extremum seeking control for wind farm energy production," *Wind Engineering*, vol. 36, no. 6, pp. 701–715, 2012.
- [44] J. Annoni, P. M. O. Gebraad, A. K. Scholbrock, P. A. Fleming, and J.-W. van Wingerden, "Analysis of axial-induction-based wind plant control using an engineering and a high-order wind plant model," *Wind Energy*, vol. 19, no. 6, pp. 1135–1150, 2016, we.1891.
- [45] S. Boersma, B. M. Doekemeijer, M. Vali, J. Meyers, and J.-W. van Wingerden, "A control-oriented dynamic wind farm model: WFSim," *Wind Energy Science*, vol. 1, pp. 1–34, 2018.
- [46] Á. Jiménez, A. Crespo, and E. Migoya, "Application of a LES technique to characterize the wake deflection of a wind turbine in yaw," *Wind Energy*, vol. 13, no. 6, pp. 559–572, 2010.
- [47] V. A. Banakh and I. N. Smalikho, "Estimation of the turbulence energy dissipation rate from the pulsed doppler lidar data," *Atmospheric and Oceanic Optics*, vol. 10, pp. 957–965, 1997.
- [48] C. Weitkamp, *Lidar: Range-Resolved Optical Remote Sensing of the Atmosphere*, ser. Springer Series in Optical Sciences. Springer, 2005.
- [49] P. Lindelöw, "Fiber based coherent lidars for remote wind sensing," Ph.D. dissertation, Technical University of Denmark, 2008.
- [50] J.-P. Cariou, "Pulsed lidars," in *Remote Sensing for Wind Energy, DTU Wind Energy-E-Report-0029(EN)*, June 2013, ch. 5, pp. 104–121.
- [51] J. Gottschall, H. Lilov, G. Wolken-Möhlmann, and B. Lange, "Lidars on floating offshore platforms," in *European Wind Energy Association annual event*, Copenhagen, Denmark, 2012.

- [52] K. A. Kragh, M. H. Hansen, and T. Mikkelsen, "Improving yaw alignment using spinner based LIDAR," in *Proceedings of the 49th AIAA Aerospace Sciences Meeting Including the New Horizons Forum and Aerospace Exposition*, Orlando, USA, 2011.
- [53] K. A. Kragh, M. H. Hansen, and T. Mikkelsen, "Precision and shortcomings of yaw error estimation using spinner-based light detection and ranging," *Wind Energy*, vol. 16, no. 3, pp. 353–366, 2013.
- [54] P. A. Fleming, A. K. Scholbrock, A. Jehu, S. Davoust, E. Osler, A. D. Wright, and A. Clifton, "Field-test results using a nacelle-mounted lidar for improving wind turbine power capture by reducing yaw misalignment," *Journal of Physics: Conference Series*, vol. 524, no. 1, p. 012002, 2014.
- [55] S. K. Kanev and F. J. Savenije, "Active wake control: loads trends," Tech. Rep. ECN-E-15-004, 2015.
- [56] M. Abkar and F. Porté-Agel, "Influence of atmospheric stability on wind-turbine wakes: A large-eddy simulation study," *Physics of Fluids*, vol. 27, no. 3, p. 035104, 2015.
- [57] P. A. Fleming, P. M. O. Gebraad, S. Lee, J.-W. van Wingerden, K. Johnson, M. Churchfield, J. Michalakes, P. Spalart, and P. Moriarty, "Evaluating techniques for redirecting turbine wakes using SOWFA," *Renewable Energy*, vol. 70, pp. 211–218, 2014.
- [58] P. A. Fleming, A. Ning, P. M. O. Gebraad, and K. Dykes, "Wind plant system engineering through optimization of layout and yaw control," *Wind Energy*, vol. 19, no. 2, pp. 329–344, 2016.
- [59] F. Campagnolo, V. Petrović, J. Schreiber, E. M. Nanos, A. Croce, and C. L. Bottasso, "Wind tunnel testing of a closed-loop wake deflection controller for wind farm power maximization," *Journal of Physics: Conference Series*, vol. 753, no. 3, p. 032006, 2016.
- [60] J. Schottler, F. Mühle, J. Bartl, J. Peinke, M. S. Adaramola, L. Sætran, and M. Hölling, "Comparative study on the wake deflection behind yawed wind turbine models," in *Journal of Physics: Conference Series*, vol. 854, no. 1. IOP Publishing, 2017, p. 012032.
- [61] M. F. Howland, J. Bossuyt, L. A. Martinez-Tossas, J. Meyers, and C. Meneveau, "Wake structure in actuator disk models of wind turbines in yaw under uniform inflow conditions," *Journal of Renewable Sustainable Energy*, 2016.

- [62] P. A. Fleming, J. Annoni, A. Scholbrock, E. Quon, S. Dana, S. Schreck, S. Raach, F. Haizmann, and D. Schlipf, "Full-scale field test of wake steering," in *Journal of Physics: Conference Series*, vol. 854, no. 1. IOP Publishing, 2017, p. 012013.
- [63] J. Annoni, P. A. Fleming, A. K. Scholbrock, J. Roadman, S. Dana, C. Adcock, F. Porte-Agel, S. Raach, F. Haizmann, and D. Schlipf, "Analysis of control-oriented wake modeling tools using lidar field results," *Wind Energy Science Discussions*, vol. 2018, pp. 1–17, 2018.
- [64] A. Rettenmeier, J. Anger, O. Bischoff, M. Hofsäß, D. Schlipf, and I. Würth, "Nacelle-based lidar systems," in *Remote Sensing for Wind Energy, DTU Wind Energy-E-Report-0029(EN)*, June 2013, ch. 8, pp. 157–170.
- [65] D. Schlipf and P. W. Cheng, "Adaptive feed forward control for wind turbines," *at - Automatisierungstechnik*, vol. 61, no. 5, pp. 329–338, 2013.
- [66] D. Schlipf, P. Fleming, S. Kapp, A. Scholbrock, F. Haizmann, F. Belen, A. Wright, and P. W. Cheng, "Direct speed control using lidar and turbine data," in *Proceedings of the American Control Conference*, Washington, USA, 2013.
- [67] D. Schlipf, J. Mann, and P. W. Cheng, "Model of the correlation between lidar systems and wind turbines for lidar assisted control," *Journal of Atmospheric and Oceanic Technology*, vol. 30, no. 10, pp. 2233–2240, 2013.
- [68] D. Schlipf, P. A. Fleming, F. Haizmann, A. K. Scholbrock, M. Hofsäß, A. Wright, and P. W. Cheng, "Field testing of feedforward collective pitch control on the CART2 using a nacelle-based lidar scanner," *Journal of Physics: Conference Series*, vol. 555, no. 1, p. 012090, 2014.
- [69] A. Rettenmeier, O. Bischoff, D. Schlipf, J. Anger, M. Hofsäß, P. W. Cheng, R. Wagner, M. Courtney, and J. Mann, "Turbulence and wind speed investigations using a nacelle-based lidar scanner and a met mast," in *European Wind Energy Association Conference and Exhibition*, 2012.
- [70] D. Schlipf, A. Rettenmeier, F. Haizmann, M. Hofsäß, M. Courtney, and P. W. Cheng, "Model based wind vector field reconstruction from lidar data," in *Proceedings of the German Wind Energy Conference DEWEK*, Bremen, Germany, 2012.

- [71] P. M. O. Gebraad, M. J. Churchfield, and P. A. Fleming, "Incorporating atmospheric stability effects into the FLORIS engineering model of wakes in wind farms," in *Journal of Physics: Conference Series*, vol. 753, no. 5. IOP Publishing, 2016, p. 052004.
- [72] S. Raach, D. Schlipf, and P. W. Cheng, "Lidar-based wake tracking for closed-loop wind farm control," *Wind Energy Science*, vol. 2, no. 1, pp. 257–267, 2017.
- [73] S. Raach, D. Schlipf, F. Borisade, and P. W. Cheng, "Wake redirecting using feedback control to improve the power output of wind farms," in *Proceedings of the American Control Conference (ACC)*, Boston, USA, July 2016.
- [74] L. Vollmer, G. Steinfeld, D. Heinemann, and M. Kühn, "Estimating the wake deflection downstream of a wind turbine in different atmospheric stabilities: an LES study," *Wind Energy Science*, vol. 1, no. 2, pp. 129–141, 2016.
- [75] E. Simley and L. Y. Pao, "Correlation between rotating LIDAR measurements and blade effective wind speed," in *Proceedings of the 51st AIAA Aerospace Sciences Meeting Including the New Horizons Forum and Aerospace Exposition*, Dallas, USA, 2013.
- [76] G. I. Taylor, "The spectrum of turbulence," *Proceedings of the Royal Society of London. Series A - Mathematical and Physical Sciences*, vol. 164, no. 919, pp. 476–490, 1938.
- [77] J. Katz and A. Plotkin, *Low-speed aerodynamics*. Cambridge University Press, 2001, vol. 13.
- [78] P. Torres, J.-W. van Wingerden, and M. Verhaegen, "Modeling of the flow in wind farms for total power optimization," in *Proceedings of the 9th IEEE International Conference on Control and Automation (ICCA)*. IEEE, 2011, pp. 963–968.
- [79] S. Raach, J.-W. van Wingerden, S. Boersma, D. Schlipf, and P. W. Cheng, " \mathcal{H}_∞ controller design for closed-loop wake redirection," in *Proceedings of the American Control Conference (ACC)*, Seattle, USA, 2017, pp. 703–708.
- [80] S. Raach, S. Boersma, J.-W. van Wingerden, D. Schlipf, and P. W. Cheng, "Robust lidar-based closed-loop wake redirection for wind farm control," in *Proceedings of the 20th World Congress of the International Federation of Automatic Control (IFAC)*, Toulouse, France, 2017.
- [81] L. Ljung, Ed., *System Identification (2nd Ed.): Theory for the User*. Upper Saddle River, NJ, USA: Prentice Hall PTR, 1999.

- [82] R. Tóth, *Modeling and identification of linear parameter-varying systems*. Springer, 2010, vol. 403.
- [83] S. Skogestad and I. Postlethwaite, *Multivariable Feedback Control: Analysis and Design*. John Wiley & Sons, 2005.
- [84] B. D. Hirth, J. L. Schroeder, W. S. Gunter, and J. G. Guynes, “Measuring a utility-scale turbine wake using the TTUKa mobile research radars,” *Journal of Atmospheric and Oceanic Technology*, vol. 29, no. 6, pp. 765–771, 2012.
- [85] P.-J. Trombe, P. Pinson, C. Vincent, T. Bøvith, N. A. Cutululis, C. Draxl, G. Giebel, A. N. Hahmann, N. E. Jensen, B. P. Jensen, N. F. Le, H. Madsen, L. B. Pedersen, and A. Sommer, “Weather radars - the new eyes for offshore wind farms?” *Wind Energy*, vol. 17, no. 11, pp. 1767–1787, 2014.
- [86] J.-J. Trujillo, F. Bingöl, G. C. Larsen, J. Mann, and M. Kühn, “Light detection and ranging measurements of wake dynamics. Part II: two-dimensional scanning,” *Wind Energy*, vol. 14, no. 1, pp. 61–75, 2011.
- [87] B. M. Doekemeijer, J.-W. van Wingerden, S. Boersma, and L. Y. Pao, “Enhanced Kalman filtering for a 2D CFD Navier-Stokes wind farm flow model,” in *Journal of Physics: Conference Series*, vol. 753, no. 5. IOP Publishing, 2016, p. 052015.
- [88] B. M. Doekemeijer, S. Boersma, L. Y. Pao, and J.-W. van Wingerden, “Ensemble Kalman filtering for wind field estimation in wind farms,” in *Proceedings of the American Control Conference (ACC)*, Seattle, USA, 2017, pp. 19–24.
- [89] M. Morari and E. Zafiriou, *Robust process control*. Prentice Hall Englewood Cliffs, NJ, 1989.

Curriculum vitae

Steffen Raach was born on January 19th, 1987 in Reutlingen, Germany. In 2007 he started studies of Engineering Cybernetics (Technische Kybernetik) at University of Stuttgart. With a DAAD scholarship he spent a semester in Tampere, Finland, to write his mid-studies thesis with Prof. Erno Keskinen and Prof. Peter Eberhard. In the second half of his studies he specialized on Mechatronics and took courses on different fields of control theory like nonlinear systems and control, robust control, model-predictive control and multi-agent systems. 2013 he finalized his studies with his diploma thesis about “Model Predictive Control of a Floating Wind Turbine with Individual Pitch Control” at Stuttgart Wind Energy (SWE) with David Schlipf, Frank Lemmer and Prof. Po Wen Cheng.



After his studies he continued at University of Stuttgart as researcher at SWE and PhD candidate. His main research interests have been in control applications in wind energy with and without the use of lidar system. He was first in charge of managing the national funded Lidar II project which focused on lidar-assisted control of wind turbines. After that he specialized on wind farm control applications and introduced the concept of lidar-based closed-loop wake redirection. His research interests and his expertise in the field of wind farm control made him a work package leader in the H2020 CL-Windcon project. He supervised several Diploma, B.Sc., and M.Sc. students and carried out teaching activities in the wind energy master and bachelor program at the University of Stuttgart. Several stays at the National Renewable Energy Laboratory (NREL) and at Delft University of Technology have helped him to collaborate with different partners and to develop his knowledge in different fields of wind energy control.

Together with David Schlipf, Frank Lemmer, Florian Haizmann, and Holger Fürst, he founded the startup sowento in 2016. After a first phase in the startup incubator of the university, the sowento GmbH was established in 2018. Since then, he is the Managing Director of sowento and strives for realizing sowento’s vision of a just world with sustainable energy supply for everybody.